Annual Report
Jahresbericht

2001

WALTHER–MEISSNER–INSTITUT
für Tieftemperaturforschung
Bayerische Akademie der Wissenschaften

.

Contact:

Prof. Dr. Rudolf Gross
Walther–Meissner–Institut für Tieftemperaturforschung
Bayerische Akademie der Wissenschaften
and
Lehrstuhl für Technische Physik – E23
Technische Universität München

Address:

Walther–Meissner–Str. 8	Phone:	+49 – (0)89 289 14201
D - 85748 Garching	Fax:	+49 – (0)89 289 14206
GERMANY	e–mail:	Rudolf.Gross@wmi.badw.de
	WWW–address:	http://www.wmi.badw.de

Secretary's Office:

Jutta Laaser	Phone:	+49 – (0)89 289 14202
	Fax:	+49 – (0)89 289 14206
	e–mail:	Jutta.Laaser@wmi.badw.de
Emel Dönertas	Phone:	+49 – (0)89 289 14205
	Fax:	+49 – (0)89 289 14206
	e–mail:	Emel.Doenertas@wmi.badw.de

Preface

The Walther–Meissner–Institut for Low Temperature Research (WMI) of the Bavarian Academy of Sciences carries out research projects at low and ultra–low temperatures and supplies liquid helium to both universities in Munich. The research program of the WMI is devoted to **fundamental** and **applied research** in the field of **low temperature solid state physics** with the main focus on

- superconductivity and superfluidity as well as superconducting devices,
- magnetism and magneto–electronics,
- mesoscopic systems and quantum effect devices,
- and the general properties of metallic systems at low and very low temperatures.

The WMI also conducts applied research into methods and techniques for generating and using low temperatures. With respect to materials the research program is focused on

- superconducting and magnetic materials, both in bulk and thin film form,
- and the heteroepitaxy of oxide materials.

The year 2001 has been a year of change with a lot of reconstruction activities going on at the WMI. In particular, a new clean room (about 50 m^2) with all the required technical infrastructure has been set up. Meanwhile, the clean room is operated and both the electron beam lithography and the optical lithography have been successfully installed. Furthermore, the new thin film laboratory (about 80 m^2) has been put into operation and most of the thin film equipment (Laser Molecular Beam Epitaxy, magnetron sputtering system, ion beam sputtering system, ion beam etching system, e–beam evaporation system) has been reinstalled. Beyond the clean room and thin film laboratories a new x–ray laboratory with both a two–circle and high resolution four–circle diffractometer, a high field laboratory with a 8/10 and 15/17 Tesla magnet unit, a SQUID magnetometer for the measurement of magnetic sample properties between 1.5 and 700 K, a new chemical laboratory, as well as a new laboratory for the synthesis of bulk materials and single crystal growth have been put into operation. That is, the year 2001 was highly important for preparing the infrastructure and experimental basis for the future years.

Despite the disturbing reconstruction activities, the research at the WMI has been very successful in 2001 as demonstrated by more than 35 scientific papers and many invited presentations at international conferences. The ongoing research projects have been successfully continued and new projects have been started. Throughout 2001, an average of 15 scientific staff members, 18 members of the administrative and technical staff, 10 doctorate candidates, 4 diploma candidates and more than 10 short and long–term guests belonged to the institute. Of course, the scientific productivity of the WMI would not be possible without the collaborative atmosphere, the high motivation of our research groups and the support of various funding agencies. This Annual Report gives an overview on the scientific results which in many cases have been obtained in collaboration with international guests. We are very pleased that within this year the international collaboration again has been extended and that the WMI could host many international guest researchers.

Our 2001 Annual Report is intended to provide an overview of our work to our friends and partners in research and industry and thereby to intensify our numerous collaborations. I would be particularly pleased if the report would stimulate new collaborations. In order to be useful also for our numerous international partners, especially within EU projects, the report is written in English.

I finally would like to thank all the colleagues, guests, students, post–docs and cooperating partners, who contributed to the success of our work within the last year, and last but not least all our friends and sponsors for their interest, trust and continuous support.

Garching, December 2001

Rudolf Gross

Contents

The Walther–Meissner–Institut

The Walther–Meissner–Institut for Low Temperature Research is operated by the Commission for Low Temperature Physics of the Bavarian Academy of Science. The Commissions (Research Groups) of the Bavarian Academy are set up in order to carry out long–term projects which are too ambitious for the lifetime or capacity of any single researcher, or which require the collaboration of specialists in various disciplines. At present there are 36 Commissions with more than 300 employees.

The research at the Walther–Meissner–Institut is focused on low temperature physics and also the techniques for low and ultra–low temperature experiments. The individual research groups of the WMI offer attractive research opportunities for diploma (graduate) students, PhD students and postdocal fellows. The WMI ist equipped with state of the art facilities for the preparation and characterization of superconducting and magnetic materials as well as for various low and ultra–low temperature experiments. The main resources are listed in the following:

Materials Preparation and Fabrication of Nanostructures

- Laser Molecular Beam Epitaxy machine for oxide heterostructures (equipped with in–situ RHEED, AFM/STM system, atomic oxygen source, metallization)
- magnetron sputtering system for oxide heteroepitaxiy (equipped with four sputtering guns an an oxygen ion gun)
- ion beam sputtering system
- metallization system (equipped with e–gun and thermal evaporators)
- ion beam etching system
- polishing machine for substrate preparation
- ultrasonic bonding machine
- 50 m^2 class 1000 clean room facility
- optical lithography (Süss maskaligner MJB 3, projection lithography)
- electron beam lithography (based on Philips XL 30 SFEG scanning electron microscope and Raith Elphy Plus lithography system including a laser stage)

Characterization

- 2–circle x–ray diffractometer (Bruker D8 Advance, up to 1.600°C)
- high resolution 4–circle x–ray diffractometer (Bruker D8 Discover)
- scanning electron microscopy with EDX analysis
- AFM/STM system
- Raman spectroscopy (1.5 to 300 K)
- SQUID magnetometer (1.5 to 700 K, up to 7 Tesla)
- several high field magnet systems (up to 17 Tesla)
- several ^{3}He/^{4}He dilution refrigerators for temperatures down to 10 mK
- ultra–low temperature facility for temperatures down to below 100 μK
- experimental set–ups for the measurement of specific heat, magnetization, thermal expansion as well as electrical and thermal transport properties as a function of temperature, magnetic field and pressure
- experimental set–up for the measurement of noise including low noise SQUID amplifiers and signal analyzers

- high frequency network analyzer (up to 40 GHz) for the determination of high frequency parameters

Acoustic Attenuation in Unconventional Superconductors

Dietrich Einzel

This contribution is devoted to a calculation of the hydrodynamic sound attenuation for a large class of unconventional pair–correlated Fermi systems. Possible applications include gap–anisotropic systems as different as the superfluid phases of liquid ^{3}He, heavy Fermion superconductors, (hole–doped) cuprates and Sr_2RuO_4. We give a general expression for the sound attenuation coefficient which is valid for arbitrary orientations of the sound propagation ($\hat{\mathbf{q}}$) *and polarization* ($\hat{\mathbf{u}}$) *direction with respect to each other and the gap anisotropy axis* ($\hat{\mathbf{n}}$). *Special emphasis is to the behavior in the low temperature limit where low energy thermal excitations (the so–called nodal Bogoliubov quasiparticles) are known to dominate the transport processes. Analytical results for the low temperature power laws are derived for certain models for quasiparticle scattering.*

We consider Fermi systems with pairing correlations described by an energy gap $\Delta_{\mathbf{p}} = \Delta_0 f_{\mathbf{p}}$, and quasiparticle excitation energies

$$E_{\mathbf{p}} = \sqrt{\xi_{\mathbf{p}}^2 + |\Delta_{\mathbf{p}}|^2} \tag{1}$$

In global thermodynamic equilibrium the quasiparticle excitations have a momentum distribution function $\nu_{\mathbf{p}}$

$$\nu_{\mathbf{p}} = \frac{1}{\exp\left(\frac{E_{\mathbf{p}}}{k_{\rm B}T}\right) + 1} \tag{2}$$

with energy derivative

$$\varphi_{\mathbf{p}} = -\frac{\partial \nu_{\mathbf{p}}}{\partial E_{\mathbf{p}}} = \frac{1}{4k_{\rm B}T\cosh^2\left(\frac{E_{\mathbf{p}}}{k_{\rm B}T}\right)} \tag{3}$$

The electronic contribution to the viscous hydrodynamic sound attenuation in unconventional superconductors in spatial dimension d is governed by the electronic viscosity, a fourth rank tensor, which reads within the relaxation time approximation:

$$\eta_{ij}^{\mu\nu}(T) = \frac{1}{V}\sum_{\mathbf{p}\sigma} \varphi_{\mathbf{p}} \tau_{\mathbf{p}}^{\rm s} \bar{\sigma}_{\mathbf{p}}^{i\mu} \bar{\sigma}_{\mathbf{p}}^{j\nu} \tag{4}$$

Here $\tau_{\mathbf{p}}^{\rm s}$ denotes the superconducting quasiparticle relaxation time. In spatial dimension $d, \bar{\sigma}_{\mathbf{p}}^{\alpha\beta}$ is the traceless tensor $\bar{\sigma}_{\mathbf{p}}^{\alpha\beta} = p_\alpha V_{\mathbf{p}\beta} - \mathbf{p}\cdot\mathbf{V}_{\mathbf{p}}/d\ \delta_{\alpha\beta} = p_{\rm F} v_{\rm F}(\xi_{\mathbf{p}}/E_{\mathbf{p}})\sigma_{\mathbf{p}}^{\alpha\beta}$, $\sigma_{\mathbf{p}}^{\alpha\beta} = \hat{\mathbf{p}}_\alpha\hat{\mathbf{p}}_\beta - \delta_{\alpha\beta}/d$ and $\mathbf{V}_{\mathbf{p}} = \partial E_{\mathbf{p}}/\partial\mathbf{p} = (\xi_{\mathbf{p}}/E_{\mathbf{p}})\mathbf{v}_{\mathbf{p}}$ denotes the Bogoliubov quasiparticle group velocity. Converting the momentum sum into an integral one has

$$\eta_{ij}^{\mu\nu} = n p_{\rm F} v_{\rm F}\ d\int \frac{d^{d-1}\Omega_{\mathbf{p}}}{S_d}\int_{-\mu}^{\infty} d\xi_{\mathbf{p}} \varphi_{\mathbf{p}} \tau_{\mathbf{p}}^{\rm s} \frac{\xi_{\mathbf{p}}^2}{E_{\mathbf{p}}^2} \sigma_{\mathbf{p}}^{i\mu}\sigma_{\mathbf{p}}^{j\nu} \tag{5}$$

Here $S_d = \int d^{d-1}\Omega_{\mathbf{p}} = 2\pi^{d/2}\Gamma(d/2)$ is the surface of the d–dimensional hypercube with Γ denoting Euler's (factorial) function. In 3–dimensional superconductors with uniaxial gap anisotropies, characterized by the anisotropy axis $\hat{\mathbf{n}}$ and an angle $x = \hat{\mathbf{p}}\cdot\hat{\mathbf{n}}$ one may write

$$\begin{aligned} \eta_{ij}^{\mu\nu}(T) &= n p_{\rm F} v_{\rm F}\ 3\int_0^1 dx\ b_{ij}^{\mu\nu}(x)\int_{-\mu}^{\infty} d\xi_{\mathbf{p}}\varphi_{\mathbf{p}}\tau_{\mathbf{p}}^{\rm s}\frac{\xi_{\mathbf{p}}^2}{E_{\mathbf{p}}^2} \\ b_{ij}^{\mu\nu}(x) &= \int_0^{2\pi}\frac{d\varphi}{2\pi}\sigma_{\mathbf{p}}^{i\mu}\sigma_{\mathbf{p}}^{j\nu} \end{aligned} \tag{6}$$

For 2–dimensional tetragonal superconductors the tensor structure of $\eta_j^{\mu\nu}$ is less complex:

$$\begin{aligned} \eta_{ij}^{\mu\nu}(T) &= np_{\rm F}v_{\rm F}\,2\int_0^{2\pi}\frac{d\phi}{2\pi}\,b_{ij}^{\mu\nu}(\phi)\int_{-\mu}^{\infty}d\xi_{\mathbf{p}}\varphi_{\mathbf{p}}\tau_{\mathbf{p}}^{\rm s}\frac{\xi_{\mathbf{p}}^2}{E_{\mathbf{p}}^2} \\ b_{ij}^{\mu\nu}(\phi) &= \begin{pmatrix} \frac{\cos 2\phi}{2} & \frac{\sin 2\phi}{2} \\ \frac{\sin 2\phi}{2} & -\frac{\cos 2\phi}{2} \end{pmatrix}_{i\mu}\otimes\begin{pmatrix} \frac{\cos 2\phi}{2} & \frac{\sin 2\phi}{2} \\ \frac{\sin 2\phi}{2} & -\frac{\cos 2\phi}{2} \end{pmatrix}_{j\nu} \end{aligned} \tag{7}$$

Eqs. (6) and (7) are believed to be applicable to a large class of unconventional 3–d (with uniaxial gap anisotropies) and quasi–2–d pair–correlated Fermi systems. The expressions for $b_j^{\mu\nu}(x)$ and $b_{ij}^{\mu\nu}(\phi)$ must be omitted here for lack of space, they can be found in ref. [1]. The experimental observability of the electronic viscosity manifests itself in the electronic contribution to the hydrodynamic sound attenuation $\alpha_{\rm B}(T) = (\omega^2/\rho c^3)\bar{\eta}(T)$:

$$\bar{\eta}(T) = \hat{\mathbf{q}}_i\hat{\mathbf{q}}_j\hat{\mathbf{u}}_\mu\hat{\mathbf{u}}_\nu\eta_{ij}^{\mu\nu} = np_{\rm F}v_{\rm F}\,d\int\frac{d^{d-1}\Omega_{\mathbf{p}}}{S_d}\left[\hat{\mathbf{q}}\cdot\sigma_{\mathbf{p}}\cdot\hat{\mathbf{u}}\right]^2\int d\xi_{\mathbf{p}}\varphi_{\mathbf{p}}\tau_{\mathbf{p}}^{\rm s}\frac{\xi_{\mathbf{p}}^2}{E_{\mathbf{p}}^2}$$

Here $\hat{\mathbf{q}}$ is the unit vector in the direction of sound propagation, and$\hat{\mathbf{u}}$ denotes the polarization, longitudinal ($\hat{\mathbf{q}}\parallel\hat{\mathbf{u}}$) and transverse ($\hat{\mathbf{q}}\perp\hat{\mathbf{u}}$), respectively.
In 3–dimensional superconductors with uniaxial gap anisotropies one has

$$\begin{aligned} \bar{\eta}(T) &= np_{\rm F}v_{\rm F}\,3\int_0^1 dx\,\bar{b}(x)\int_0^{\infty}d\xi_{\mathbf{p}}\varphi_{\mathbf{p}}\tau_{\mathbf{p}}^{\rm s}\frac{\xi_{\mathbf{p}}^2}{E_{\mathbf{p}}^2} \\ \bar{b}(x) &= \hat{\mathbf{q}}_i\hat{\mathbf{q}}_j\hat{\mathbf{u}}_\mu\hat{\mathbf{u}}_\nu b_{ij}^{\mu\nu} = \int_0^{2\pi}\frac{d\varphi}{2\pi}\left[\hat{\mathbf{q}}\cdot\sigma_{\mathbf{p}}\cdot\hat{\mathbf{u}}\right]^2 \end{aligned} \tag{8}$$

For 2–dimensional tetragonal superconductors one may write

$$\begin{aligned} \bar{\eta}(T) &= \cos^2(\alpha+\beta)\,\bar{\eta}_{\parallel}(T) + \sin^2(\alpha+\beta)\,\bar{\eta}_{\perp}(T) \\ \bar{\eta}_{\parallel,\perp}(T) &= \bar{\eta}_{\rm N}\,2\int_0^{2\pi}d\phi\,\left\{\cos^2 2\phi, \sin^2 2\phi\right\}\int_{-\mu}^{\infty}d\xi_{\mathbf{p}}\varphi_{\mathbf{p}}\frac{\tau_{\mathbf{p}}^{\rm s}}{\tau_{\rm N}}\frac{\xi_{\mathbf{p}}^2}{E_{\mathbf{p}}^2} \end{aligned} \tag{9}$$

Here $\bar{\eta}_{\rm N} = np_{\rm F}v_{\rm F}\tau_{\rm N}/4$ is the normal state viscosity in $d=2$ and we have assumed that$\hat{\mathbf{q}} = \{\cos\alpha, \sin\alpha\}$ and $\hat{\mathbf{u}} = \{\cos\beta, \sin\beta\}$. In the longitudinal case one has $\beta = \alpha$, whereas in the transverse case $\beta = \alpha + \pi/2$.

There is an analogue to the longitudinal and transverse viscosities in $d=2$ to an entirely different physical quantity, namely the electronic Raman effect. It turns out that the normalized sound attenuation or viscosity for 2–dimensional superconductors is identical to that for the normalized quasiparticle Raman intensity $I_{\gamma\gamma}(\omega, T)$ extrapolated to zero frequency:

$$\frac{I_{\gamma\gamma}^{\rm B}(\omega=0,T)}{I_{\gamma\gamma}^{\rm N}(\omega=0,T)} = \frac{1}{\int_0^{2\pi}d\phi\,\delta\gamma_{\mathbf{p}}^2}\int_0^{2\pi}d\phi\,\delta\gamma_{\mathbf{p}}^2\int_{-\mu}^{\infty}d\xi_{\mathbf{p}}\varphi_{\mathbf{p}}\frac{\tau_{\mathbf{p}}^{\rm s}}{\tau_{\rm N}}\frac{\xi_{\mathbf{p}}^2}{E_{\mathbf{p}}^2} \tag{10}$$

This is no surprise, since for quasi–2–dimensional tetragonal superconductors the Raman vertex for longitudinal ($\delta\gamma_{\mathbf{p}}^{B_{1g}} = \cos 2\phi$) and transverse ($\delta\gamma_{\mathbf{p}}^{B_{2g}} = \sin 2\phi$) photon polarizations, corresponds to the longitudinal ($\sigma_{\mathbf{p}}^{xx}$) and transverse ($\sigma_{\mathbf{p}}^{xy}$) components of the stress tensor vertex $\sigma_{\mathbf{p}}^{jj}$ and one may identify for $d=2$:

$$\frac{\eta_{\parallel}}{\eta_{\rm N}} \equiv \frac{I_{B_{1g}}^{\rm B}(\omega=0,T)}{I_{B_{1g}}^{\rm N}(\omega=0,T)} \quad ; \quad \frac{\eta_{\perp}}{\eta_{\rm N}} \equiv \frac{I_{B_{2g}}^{\rm B}(\omega=0,T)}{I_{B_{2g}}^{\rm N}(\omega=0,T)} \tag{11}$$

Therefore the investigation of normalized Raman intensities in the (hydrodynamic) limit $\omega \to 0$ can be correlated to and thus complement the results obtained from quite a distinct experimental method, namely the hydrodynamic electronic sound attenuation.

The details of the further analysis of equations (8) and (9), which can be found in Ref. [1], includes
1. the discussion of various quasiparticle scattering laws $a_{\mathbf{p}}$ which connect the relaxation time of the superconductor $\tau_{\mathbf{p}}^{\mathrm{s}}$ with that of a normal state τ_{N},

$$\frac{1}{\tau_{\mathbf{p}}^{\mathrm{s}}} = \frac{a_{\mathbf{p}}}{\tau_{\mathrm{N}}} \qquad \text{and} \tag{12}$$

2. the discussion of the normalized attenuation $\alpha_{\mathrm{B}}/\alpha_{\mathrm{N}}$ in the low temperature limit, where

$$\frac{\alpha_{\mathrm{B}}(T)}{\alpha_{\mathrm{N}}} = C\{d, \mathbf{q}, \mathbf{u}, \mathbf{n}, f_{\mathbf{p}}, a_{\mathbf{p}}\} \left(\frac{k_{\mathrm{B}}T}{\Delta_0}\right)^{\mu\{d,\mathbf{q},\mathbf{u},\mathbf{n},f_{\mathbf{p}}\}} \tag{13}$$

The coefficient C and the exponent μ depend, besides on propagation an polarization directions of the sound wave, on the gap anisotropy $f_{\mathbf{p}}$ under consideration. It turns out that while C depends particularly on the scattering law $a_{\mathbf{p}}$, μ does not for a fairly large class of different $a_{\mathbf{p}}$. The acoustic attenuation at low temperatures in the form (13) is seen to describe qualitatively correct a surprisingly large set of experimental observations in unconventional pair–correlated Fermi systems [1].

In conclusion the hydrodynamic sound attenuation of many (unconventional) pair–correlated Fermi systems can be described at least qualitatively within a generalized weak coupling BCS model which does not attempt to calculate the energy dispersion of the nodal quasiparticles from some microscopic model but makes certain phenomenological assumptions on the order parameter symmetry. Through the comparatively large number of predicted parameters C and particularly μ, which describe the viscous transport at low temperature, it may serve as to provide conditions for the unambiguous identification the order parameter symmetry for a given superconducting or superfluid Fermi system.

References

[1] Acoustic Attenuation in Unconventional Superconductors,
Dietrich Einzel, *to be published in the J. Low Temp. Phys., 2002*

Evidence for an unconventional metal-insulator transition in Bi2212

F. Venturini, M. Opel, and R. Hackl [1]

Copper-oxygen compounds have a complex phase diagram containing long-range antiferromagnetic order, magnetic fluctuations, charge and spin ordering, pseudogap behaviour, and superconductivity at temperatures up to 160 K. The interrelation of the various phases is one of the keys to understand the materials. As a substantial complication in comparison to more conventional systems, the results from different experiments do normally not yield a unified picture but rather pose new questions. This is particularly true if a wide range of effective doping p is being considered. Here we study $Bi_2Sr_2(Y_{1-x}Ca_x)Cu_2O_{8+\delta}$ (Bi2212) where a major part of the phase diagram can be accessed. In addition, for the perfect surface Bi2212 can be studied very well by angle-resolved photoemission spectroscopy (ARPES) yielding single-particle properties which can be compared to the many-body response being obtained by transport or Raman measurements.

As has been shown recently by ARPES, there is no substantial doping dependence of neither the momentum dependence nor the magnitude of the quasiparticle (qp) relaxation rate $\hbar/\tau(\mathbf{k},\omega) = 2\Sigma''(\mathbf{k},\omega)$ [1]. In contrast, the symmetry dependence of the Raman relaxation rates $\Gamma_\mu(\omega,T,p)$ (with the symmetry index $\mu = B_{1g}, B_{2g}$) being directly related to momentum-dependent properties via the selection rules exhibits a strong variation with p in that $\Gamma_{B_{1g}} \simeq \Gamma_{B_{2g}}$ in overdoped samples and $\Gamma_{B_{1g}} \simeq 3\Gamma_{B_{2g}}$ for small p. [2] Apparently, the symmetry dependence of the Raman relaxation rates cannot be accounted for by qp properties alone. As a solution of this dilemma we propose a generalized metal-insulator (MIT) transition with a momentum and doping dependent gap $\Delta_M(\mathbf{k},p)$ to occur. We show that this scenario allows to describe our results quantitatively and to reconcile a variety of other experiments.

An indication of an MIT was found in copper oxides with relatively low superconducting transition temperatures T_c. The resistivity $\rho(T)$ in magnetic fields high enough to suppress superconductivity exhibits a minimum at $T_0(p)$ which moves to zero temperature with increasing p and disappears close to optimal doping, $p \simeq 0.16$, where T_c is maximal [3]. Since $\rho(T)$ has no characteristic energy scale other than the temperature itself, the MIT has been ascribed to the existence of a nearby quantum-critical point (QCP). As a consequence, the fluctuations expected in the system at $T > 0$ would give rise to the distinctly non Fermi-liquid behaviour as observed in most transport and thermodynamic quantities. Various proposals associated with the development of pre-formed pairs, or incipient spin and/or charge ordering, have been made for the origin of a QCP [4, 5, 6, 7]. Still, there is no picture which has been able to reproduce the complex behaviour of the electron dynamics over a wide range of doping levels.

For the experiments in the crucial doping range, we prepared new samples starting from an extremely homogeneous overdoped single crystal grown by the traveling solvent floating zone (TSFZ) method with a T_c of 78 K and a transition width of only 0.2 K. From this specimen several pieces were cut and annealed at 620 K in oxygen partial pressures of 300 and 1350 bar to obtain transition temperatures of 62 and 56 K, respectively.

Raman spectra $\chi''_\mu(\omega,p)$ for a fixed temperature of approximately 180 K and various doping levels p are plotted in Fig. 1. For B_{2g} symmetry sampling "cold" qp with momenta along the diagonals of the BZ (Fig. 1 (b)) the doping dependence is very weak. For B_{1g} symmetry projecting out "hot" qp propagating along the CuO bonds (Fig. 1 (a)) the response is suppressed strongly with decreasing doping in an energy range of about 2000 cm^{-1} indicating the existence of a gap of this magnitude for the hot qps.

[1] In collaboration with T.P. Devereaux (University of Waterloo, Waterloo, ON N2L 3G1, CANADA), J.K. Freericks (Georgetown University, Washington, D.C. 20057, USA), I. Tüttő (RISPO, H-1525 Budapest), B. Revaz (DPMC, University of Geneva, CH-1121 Geneva). F.V. would like to thank the Gottlieb Daimler and Karl Benz Foundation for financial support.

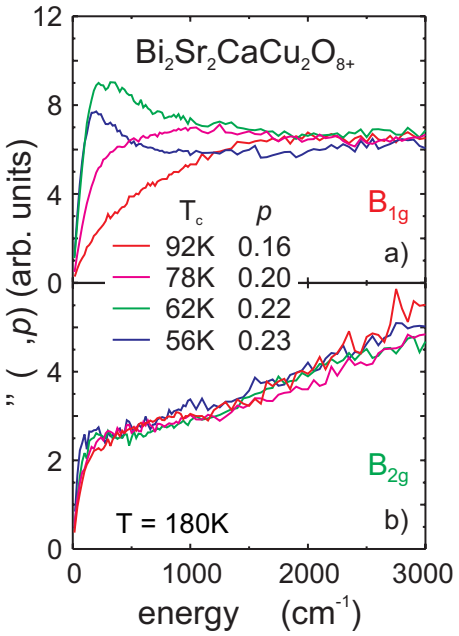

Figure 1: Raman spectra $\chi''_\mu(\omega, p)$ for constant temperature as a function of doping on an extended energy scale. For clarity the contributions from lattice vibrations have been subtracted out. Since the spectral shape at high energies depends only weakly on doping the spectra have been scaled (by factors of about 2 or smaller) to match above 3000 cm^{-1} and to emphasize the changes at low energy.

In order to link the experimental observations to momentum-dependent electron dynamics we analyze the electronic Raman response in the dc limit, $\omega \to 0$. For non-resonant scattering we obtain [9, 10]

$$\chi''_\mu(\omega \to 0) = \omega N_F \times \\ \times \left\langle \gamma_\mu^2(\mathbf{k}) \int d\xi \left(-\frac{\partial f^0}{\partial \xi} \right) \frac{Z_\mathbf{k}^2(\xi, T)}{2\Sigma''_\mathbf{k}(\xi, T)} \right\rangle . \quad (1)$$

Here N_F is the density of electronic levels at the Fermi energy E_F , and $\gamma_\mu(\mathbf{k})$ is the Raman scattering amplitude, dependent upon incident (scattered) photon polarizations $\hat{e}_{I(S)}$ corresponding to different symmetries $\mu = B_{1g}, B_{2g}$. $\Sigma''_\mathbf{k}(\omega, T)$ and $Z_\mathbf{k}(\omega, T)$ are the imaginary part of the single particle self energy and the qp residue, respectively, f^0 is the Fermi distribution function, and $\langle \cdots \rangle$ denotes an average over the Fermi surface. We define the Raman relaxation rate as the inverse slope of the spectra in the dc limit, $\Gamma_\mu(T) \equiv \langle \gamma_\mu^2(\mathbf{k}) \rangle N_F [\partial \chi''_\mu(\omega \to 0, T)/\partial \omega]^{-1}$. In lowest order and in an isotropic metal one obtains $\Gamma_\mu(T) = \hbar[\tau(T)]^{-1}$ [2]. In general, $\Gamma_\mu(T)$ is proportional to many-particle quantities such as the resistivity $\rho(T)$ which resemble variations of both lifetime and carrier density.

$\Gamma_\mu(T)$ can be explicitly extracted from the Raman spectra [2]. In Fig. 2 (a) Raman relaxation rates at a fixed temperature $T = 200$ K obtained in this and previous studies are compiled. The magnitude of $\Gamma_{B_{1g}}(T, p)$ decreases by approximately 70% for $0.09 \leq p \leq 0.22$, while $\Gamma_{B_{2g}}(T, p)$ is almost constant up to $p \simeq 0.20$ and changes by only 30% in the narrow range $0.20 < p < 0.22$. The abrupt crossover for $0.20 < p < 0.22$ is remarkable: the Raman relaxation rates rapidly decrease, and the anisotropy vanishes.

The variations of the relaxation rates with temperature are shown in Fig. 2(b). $\partial \Gamma_{B_{2g}}(T, p)/\partial T$ (cold qps) deviates only little from 2 in the entire doping range. Since $\Gamma_{B_{2g}}(T)$ varies approximately linearly with temperature [2] we have $\Gamma_{B_{2g}}(T) \simeq 2k_B T$. In contrast, $\partial \Gamma_{B_{1g}}(T, p)/\partial T$ (hot qps) is strongly temperature dependent, increases continuously with p and changes sign close to optimum doping. For $p \geq 0.22$ any kind of anisotropy disappears.

It is both the apparent symmetry dependence of the relaxation rates, $\Gamma_{B_{2g}} < \Gamma_{B_{1g}}$, [Fig. 2 (a)] and the characteristic increase of the relaxation rate towards lower temperature, $\partial \Gamma_{B_{1g}}(T, p)/\partial T < 0$ for $p \leq 0.16$ which indicate that there is not only a gap but also a strong anisotropy of the gap with the maxima located around the M-points (see Fig. 2 (a)). Thus the "hot" qps show a crossover from metallic to insulating behaviour near optimal doping while the "cold" qps are metallic for all dopings at the temperatures examined. This is what we call an anisotropic or unconventional metal-insulator transition as opposed to a conventional Mott transition [11] since the charge excitations become gapped only along specific directions of the Fermi surface, and the overall dc transport is still metallic. Therefore, we examine now the effect of an anisotropic Mott gap on the Raman response.

The result can be directly derived from Eq. (1) using the following approximations: (1) the qp residue is constant, $Z_\mathbf{k}(\omega, T) \equiv Z$, and non-zero only for $\Delta_\mathrm{M} \leq |2\omega| \leq E_\mathrm{b}$, e.g., for frequencies located in either part of the correlated subband with a total width E_b separated symmetrically with respect to the chemical

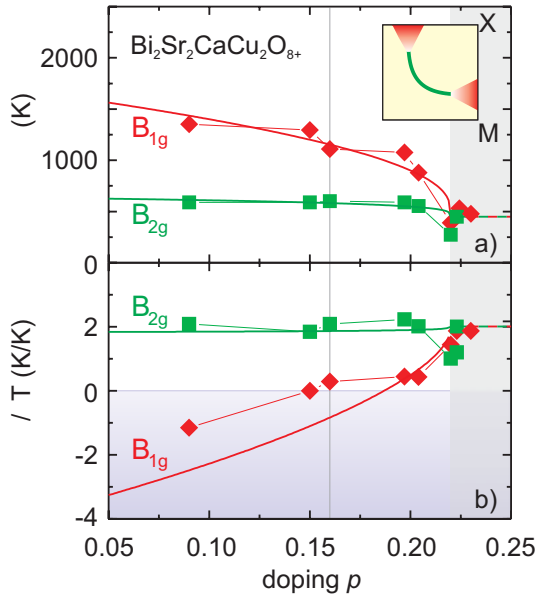

Figure 2: (a) Raman relaxation rates $\Gamma_\mu(p)$ as a function of doping for different symmetries $\mu = B_{1g}, B_{2g}$. The smooth lines are fits to the data employing Eq. (2). The **k**-dependent gap is sketched in the inset. The metallic part above $p_c = 0.22$ is shaded. The vertical line corresponds to optimum doping. (b) Variation with temperature of the relaxation rate, $\partial\Gamma_\mu(T)/\partial T$. The smooth lines are theoretical predictions assuming the single-electron lifetime to vary as $\hbar/\tau = 2k_BT$.

potential by $\pm\Delta_M/2$, (2) $\Sigma''_{\mathbf{k}}(\omega,T) = \Sigma''(T)$, (3) $\Delta_M(p,\varphi) = \Delta^0_M(p)\cos^2(2\varphi)$ with φ the azimuthal angle on a cylindrical Fermi surface, and (4) $\Delta^0_M(p) = \Delta^0_M(1 - p/p_c)^\zeta$ for $p \le p_c$. We obtain for $\Delta_M(p), k_BT \ll E_b$

$$\frac{\Gamma_\mu(T,p)}{2\Sigma''(T)} = \begin{cases} \frac{1}{2}[1+\exp(\frac{\Delta^\mu_M(p)}{2k_BT})] & \text{insulator} \\ 1 & \text{metal} \end{cases} \qquad (2)$$

Here, $\Delta^\mu_M(p)$ is an effective gap originating from the Fermi-surface integration. Eq. (2) shows explicitely that in the presence of a gap the Raman relaxation rate $\Gamma_\mu(T,p)$ does not only depend on the qp scattering rate $\Sigma''(T)$, as would be measured by angle-resolved photoemission (ARPES) for example, but also on the Fermi factor, hence on the thermally available states. We are aware that the approximations for Z, Σ'', and N_F exclude the application of this model in the vicinity of the critical point. However, the doping range in our experiments is much larger than the critical regime.

In Fig. 2 along with the data, we plot theoretical curves calculated from Eq. (2) with $\Sigma''(T) = k_BT$ (compatible with transport or ARPES results in a wide range of doping [12, 13]), $\Delta^0_M = 1100$ K, and $\zeta = 0.25$. For the B_{2g} spectra, the weak influence of the gap causes the temperature dependence to come essentially from $\Sigma''(T)$, hence justifying the assumption $\Sigma''(T) = T$. The general trend of the observed B_{1g} spectra, in particular the sign change, is well reproduced by the phenomenology. At lower doping, $p < 0.16$ there are discrepancies. Most likely $\Sigma''(T) = T$ is not as good an approximation for the scattering rate of anti-nodal qp as for nodal ones below optimal doping (see Ref. [13]). Although the **k**-dependence of the gap is simple, the agreement for both B_{1g} and B_{2g} symmetries is remarkable. This strongly suggests that an underlying QCP for this material lies at a doping of $p_c = 0.22$, on the overdoped side of the phase diagram.

References

[1] A.A. Kordyuk *et al.*, cond-mat/0104294 preprint (2001).
[2] M. Opel *et al.*, Phys. Rev. B **61**, 9752 (2000).
[3] S. Ono *et al.*, Phys. Rev. Lett. **85**, 638 (2000) and references therein.
[4] S.C. Zhang, Science **275**, 1089 (1997).
[5] C.M. Varma, Phys. Rev. B **61**, R3804 (2000)
[6] S. Chakravarty *et al.*, Phys. Rev. B **63**, 094503 (2001).
[7] S. Andergassen, S. Caprara, C. Di Castro, and M. Grilli, Phys. Rev. Lett. **87**, 56401 (2001).
[8] J.L. Tallon and J.W. Loram, Physica C **349**, 53 (2001).
[9] T.P. Devereaux and D. Einzel, Phys. Rev. B **51**, 16336 (1995), *ibid.* **54**, 15547 (1996); D. Einzel and C. Schuster, Czech. J. Phys **46** (Suppl. S2), 993 (1996).
[10] T.P. Devereaux and A.P. Kampf , Phys. Rev. B **59**, 6411 (1999).
[11] N. Mott, *Conduction in Non-Crystalline Materials* (Clarendon Press, Oxford, 1987).
[12] C. Kendziora, M.C. Martin, J. Hartge, L. Mihaly, and L. Forró, Phys. Rev. B **48**, 3531 (1993).
[13] M.R. Norman, M. Randeria, H. Ding, and J.C. Campuzano, Phys. Rev. B **57**, R11093 (1998); T. Valla, A.V. Fedorov, P.D. Johnson, Q. Li, G.D. Gu, and N. Koshizuka, Phys. Rev Lett. **85**, 828 (2000).

Variation of the electronic Raman spectra in Bi-2212 with doping and excitation energy

F. Venturini, M. Opel, R. Hackl [1]

The superconducting state of the cuprates is characterized by a strongly momentum and doping dependent energy gap $\Delta(\mathbf{k}, p) \simeq \Delta_0(p)[\cos(k_x a) - \cos(k_y a)]/2$ which is believed to be a fingerprint of the so far unknown coupling mechanism. However, in spite of extensive studies important details are not clear. For instance, at low energies, $\hbar\omega \ll \Delta_0(p)$, or, equivalently, for electrons propagating along the nodes of the gap at 45° ($k_x = k_y$) in the Brillouin zone (BZ) the gap seems to scale with the superconducting transition temperature T_c while for large energies or along the principal directions ($k_x = 0$ or $k_y = 0$) one finds $\Delta_0(p) \propto (1-p)$. As a consequence, the gap seems to be more isotropic at high doping levels $p > 0.16$ than close to optimal doping $p \simeq 0.16$ [1].

Useful insights into the properties of the gap leading beyond those obtained by angle-resolved photoemission spectroscopy (ARPES), electron tunneling or infrared (ir) spectroscopy could be obtained by Raman scattering in $Bi_2Sr_2(Y_{1-x}Ca_x)Cu_2O_{8+\delta}$ (Bi-2212), $YBa_2Cu_3O_{6+x}$ (Y-123), and $La_{2-x}Sr_xCuO_4$ (LSCO) at various doping levels. [2, 3, 4, 5] Nevertheless, the understanding is still incomplete. As an example, the doping dependence of the gap maximum could not yet be related to one of the other relevant energy scales. It is not clear either to which extent the spectral shape of the response being indicative of the underlying interactions depends on the energy of the incident photons [6]. Therefore, we investigated new samples of very high quality using different photon energies $\hbar\omega_I$ for excitation.

The $Bi_2Sr_2(Y_{1-x}Ca_x)Cu_2O_{8+\delta}$ single crystals were either grown in ZrO_2 crucibles or zone melted and post-annealed (Table 1). p is calculated from T_c via the relation $T_c(p) = T_c^{\max}[1 - 82.6(p-0.16)^2]$ [7].

Table 1: Bi-2212 single crystals studied.

T_c(K)	57	92	92	78	62	56
p	0.09	0.15	0.16	0.20	0.22	0.23

For excitation we used Ar^+ and Kr^+ laser lines at 458, 514, 528, and 647 nm. The measured spectra are divided by the Bose-Einstein factor in order to obtain the Raman response $\chi''_\mu(\omega, T, p)$ with $\mu = B_{1g}, B_{2g}$. Raman-scattering experiments reveal a two-particle response of interacting electrons in a similar way as infrared spectroscopy hence combining advantages of ARPES, by allowing momentum resolution, and of conductivity measurements. Through the choiceof the polarizations vectors of the incident and scattered photons $\hat{\mathbf{e}}_{I(S)}$ different portions of the Fermi surface can be projected out. With $\hat{\mathbf{e}}_I$ and $\hat{\mathbf{e}}_S$ parallel to the x and y crystallographic directions, respectively, the B_{2g} symmetry is projected out, and excitations with momenta along the diagonals of the BZ are probed. With polarizations along $x'y'$ (at 45° to the Cu-O bonds) the B_{1g} symmetry is selected probing electrons with momenta along the BZ axes.

Fig. 1 shows the B_{1g} and B_{2g} electronic Raman spectra in differently doped Bi-2212 samples in the superconducting state at approximately 10 K and in the normal state at approximately 90 K. The data are plotted as a function of energy normalized to the respective transition temperatures of the samples to better visualize the scaling of relevant energies with T_c.

The scaling behavior of the superconductivity-induced features in B_{1g} and B_{2g} symmetry depends in a very different way on the carrier concentration. In B_{1g} symmetry the intensity is strongly suppressed

[1] In collaboration with B. Revaz (DPMC, University of Geneva, CH-1121 Geneva) and H. Berger (EPFL, CH-1025 Lausanne). F.V. would like to thank the Gottlieb Daimler and Karl Benz Foundation for financial support.

upon decreasing doping level. For $p < 0.13$ there is no evidence of superconductivity-induced features (Fig. 1(e)). The energy of the superconductivity-induced pair-breaking feature $\hbar\omega^{\rm peak}$, is also strongly affected by doping, going from $\hbar\omega^{\rm peak}/k_BT_c \sim 4.5$ in the most overdoped sample (Fig. 1(a)) to $\hbar\omega^{\rm peak}/k_BT_c \sim 8.7$ in the slightly underdoped one (Fig. 1(d)). From these observations we conclude that, in the doping range studied, the peak energy is not proportional to k_BT_c but decreases monotonously with increasing doping level (Fig. 1(a)-(e)). It is worth noticing that we observe the same doping dependence in Y-123 samples [8].

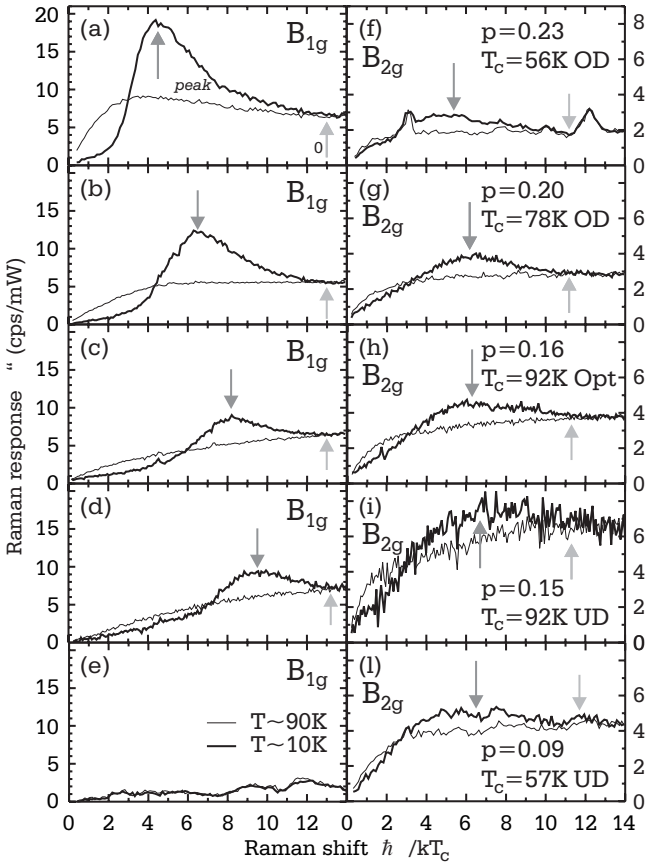

Figure 1: Doping dependence of the Raman spectra in B_{1g} and B_{2g} symmetries in the superconducting and normal state. The arrows mark the $\hbar\omega^{\rm peak}$ and $\hbar\omega_0$ energies.

In contrast to the B_{1g} symmetry, the B_{2g} spectra show a superconductivity-induced feature at all doping levels as it is evident from Fig. 1(f)-(l). In addition, the maxima of the superconducting spectra $\hbar\omega^{\rm peak}/k_BT_c$ are approximately doping independent and between 6 and 6.5, with the exception of the the most overdoped sample (Fig. 1(f)). Both from the analysis of $\hbar\omega^{\rm peak}$ and from the slope of low frequency part of the Raman spectra it is possible to extract the magnitude Δ_0 of the d-wave superconducting energy gap [9]. In B_{2g} symmetry the measured spectra support Δ_0 to scale with T_c.

The effects of superconductivity are observable up to an energy $\hbar\omega_0$, where superconducting and normal spectra merge. $\hbar\omega_0$ again scales with T_c at any doping level studied in both B_{1g} and B_{2g} symmetry .

The scaling of Δ_0 with T_c is consistent with the results for the superconducting energy gap derived from the magnetic penetration depth, electron tunneling for low bias voltages [10, 11], and Andreev reflection measurement [1]. However, if the B_{1g} peak energy $\hbar\omega^{\rm peak}$ is considered, Raman scattering seems to reveal an additional energy scale which increases monotonously with decreasing doping level. On the other hand, the doping dependence of $\hbar\omega^{\rm peak}_{B_{1g}}$ resembles that of the energy scale probed by ARPES and tunneling experiments [12, 13].

It has been suggested that there are two relevant energy scales, namely the single-particle excitation energy, probed by ARPES and tunneling spectroscopies, which increases with decreasing doping, and a coherence energy scale, obtained, e.g., by Andreev reflections or B_{2g} Raman scattering [1]. These two energies merge at high doping levels where BCS-like behavior is believed to be recovered and are increasingly different at low doping levels. More experiments are required to investigate the scaling behavior of $\hbar\omega^{\rm peak}_{B_{1g}}$ in the underdoped side of the phase diagram.

The shape of the spectra can be seriously changed by resonance (matrix element) effects giving further insight into the excitations being probed. In fact, such type of effects on the pair-breaking excitations in B_{1g} symmetry have been reported recently for highly overdoped Bi-2212 samples. It has been argued that they are a signature of an antiferromagnetically correlated Fermi liquid [6]. We analyzed the electronic

contribution for excitation energies 1.6 eV $\leq \hbar\omega \leq$ 2.7 eV corresponding to 647 nm $\geq \lambda \geq$ 458 nm in B_{1g} and B_{2g} scattering geometries. Fig. 2 shows the Raman response in B_{1g} and B_{2g} symmetry for three overdoped Bi-2212 samples. In all cases the spectra at wavelengths $\lambda \neq 458$ nm have been multiplied

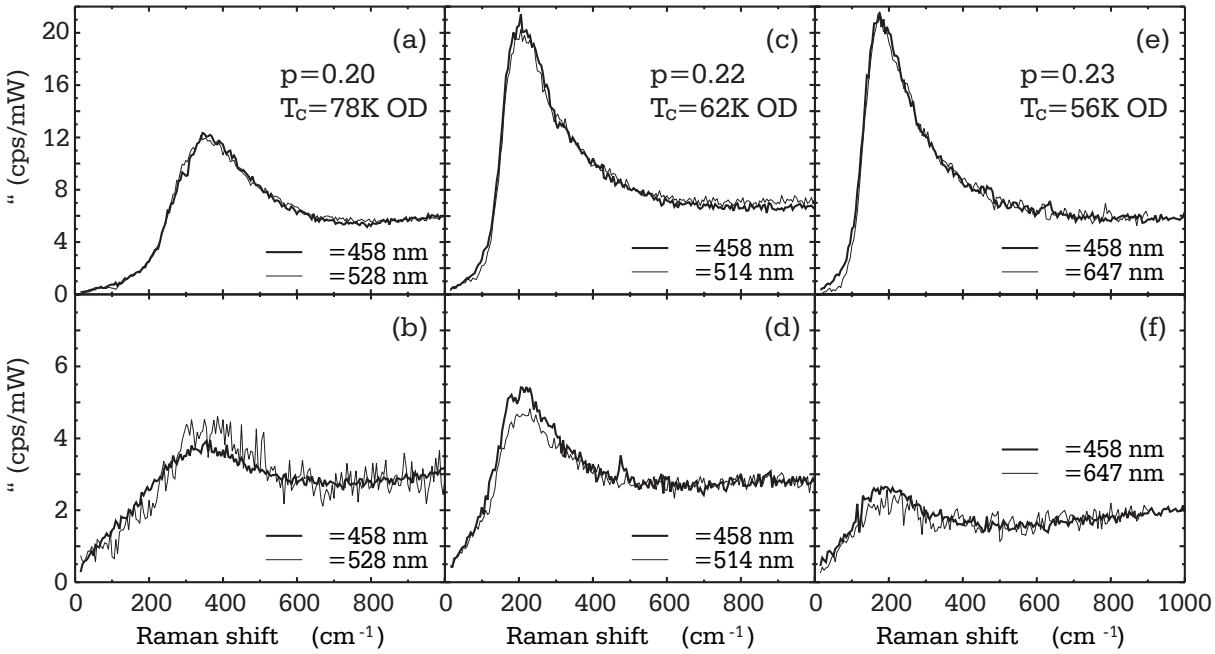

Figure 2: B_{1g} and Raman B_{1g} spectra of overdoped Bi-2212 samples in the superconducting state ($T \sim 10$ K) at different excitation energies as indicated.

by a constant, ranging from 0.7 to 2, to adjust the intensity to the spectra at $\lambda = 458$ nm. In both configurations we do not find any significant variation of the lineshape of the spectra with excitation energy at any doping level. However, we observe a reduction of the overall intensity in the B_{2g} symmetry by a factor of approximately 2 upon decreasing photon energies. Nevertheless, the Raman tensor elements determining the spectral weight and shape of $\chi''_\mu(\omega, T, p, \lambda)$ turn out to depend only weakly on λ in the doping range examined and do not indicate a relationship to magnetic excitations.

In conclusion, we presented electronic Raman-scattering results on Bi-2212 in the superconducting state. The B_{1g} and B_{2g} symmetry spectra are characterized by very different doping dependences of the superconductivity-induced features. The B_{2g} spectra are consistent with a superconducting energy gap with d-wave symmetry and a maximum $\Delta_0(p)$ scaling with $T_c(p)$. The maxima at B_{1g} symmetry seem to obey $\hbar\omega^{\rm peak}_{B_{1g}} = E_0(1 - p/p_0)$ with $E_0 \simeq 1300$ cm^{-1} close to the magnetic exchange energy J and $p_0 \simeq 0.27$ the doping level at which superconductivity disappears.

References

[1] G. Deutscher, Nature **397**, 410 (1999).
[2] C. Kendziora and A. Rosenberg, Phys. Rev. B **52**, 9867 (1995).
[3] M. Opel *et al.*, Phys. Rev. B **61**, 9752 (2000).
[4] S. Sugai and T. Hosokawa, Phys. Rev. Lett. **85**, 1112 (2000).
[5] X.K. Chen *et al.*, Phys. Rev. B **56**, R513 (1997); J. Naeini *et al.*, Phys. Rev. B **59**, 9642 (1999).
[6] M. Rübhausen *et al.*, Phys. Rev. Lett. **82**, 5349 (1999).
[7] J.L. Tallon and J. Loram, Physica C **349**, 53 (2001).
[8] R. Nemetschek *et al.*, Eur. Phys. J. B **5**, 495 (1998).
[9] T.P. Devereaux and D. Einzel, Phys. Rev. B **51**, 16336 (1995).
[10] C. Panapogoulos *et al.*, Phys. Rev. B **57**, 13422 (1998).

[11] C. Renner *et al.*, Phys. Rev. Lett. **80**, 149 (1998).
[12] N. Miyakawa *et al.*, Phys. Rev. Lett. **80**, 157 (1998).
[13] J. Mesot *et al.*, Phys. Rev. Lett. **83**, 840 (1999).

Electronic Raman scattering in $La_{2-x}Sr_xCuO_4$

Qing-ming Zhang, Francesca Venturini, Rudi Hackl [1]

Polarized electronic Raman scattering (ERS) is a powerful tool to determine the symmetry of the energy gap in anisotropic superconductors. In the B_{1g} channel, the pair-breaking peak can be seen at $2\Delta_0$ in $Bi_2Sr_2CaCu_2O_{8+\delta}$ (BSCCO), $YBa_2Cu_3O_{7-\delta}$ (YBCO) *etc.*, and a broad pair-breaking peak appears at $\sim 1.7\Delta_0$ for B_{2g} [1, 2, 3]. These results are consistent with the predictions based on a $d_{x^2-y^2}$-wave theory [1, 4].

But detailed studies on $La_{2-x}Sr_xCuO_4$ (LSCO) indicate that this system is different from BSCCO and YBCO [5, 6]. We performed ERS experiments on two differently doped high-quality single crystals of LSCO with $x = 0.10$ (underdoped) and $x = 0.15$ (optimally doped). The spectra were obtained at various temperatures and excitation energies up to 8000 cm^{-1}. In order to extract the four pure symmetries (A_{1g}, A_{2g}, B_{1g}, and B_{2g}) spectra were also taken using circular light polarizations.

Most of the Raman spectra presented here were obtained with an Ar^+ ion laser at 458 nm. For larger excitation wavelengths, the Kr^+ laser line at 647 nm was used. The measurements were made in a vacuum of 5×10^{-7} mbar at temperatures between 4.2 and 300 K. The increase in temperature in the normal state due to laser heating was calculated from the spectra using the Stokes/Anti-Stokes relation. In the superconducting state, the laser heating was measured by comparing the pair-breaking intensities at different laser powers. In any case, the laser heating was below 7 K/mW. The single crystals of LSCO were prepared by the standard traveling zone floating method. Each sample has a perfect polished (001) plane.

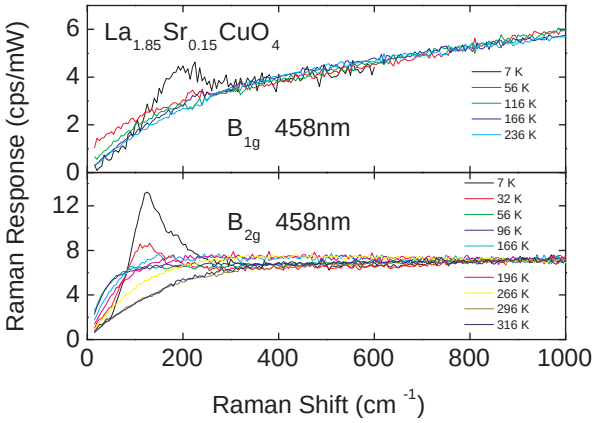

Figure 1: B_{1g} and B_{2g} Raman spectra from optimally doped $La_{1.85}Sr_{0.15}CuO_4$ at different temperatures.

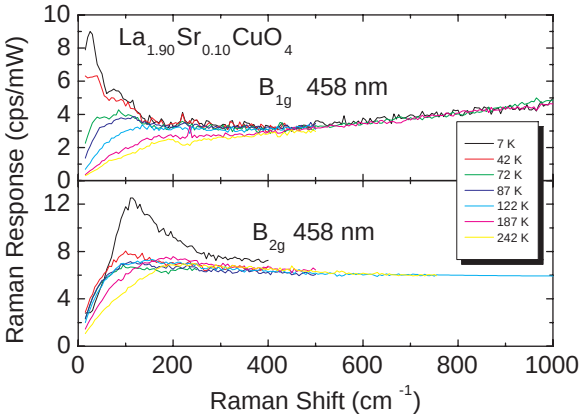

Figure 2: B_{1g} and B_{2g} spectra from underdoped $La_{1.90}Sr_{0.10}CuO_4$ at different temperatures.

Figures 1 and 2 show spectra in B_{1g} and B_{2g} symmetry at 458 nm from optimally doped $La_{1.85}Sr_{0.15}CuO_4$ and underdoped $La_{1.90}Sr_{0.10}CuO_4$, respectively. In the superconducting state, both samples show a well-defined B_{2g} pair-breaking peak compared with B_{1g}. This result is obviously different from that of BSCCO [3]. In addition, for the underdoped sample the B_{1g} spectra at lower energies show an anomalous increase in intensity with decreasing wave numbers.

[1] In collaboration with Jun'ya Hori and Toshizo Fujita (Hiroshima)

Using the memory function approach [7, 2], we calculate dynamical relaxation rates and mass renormalization factors. The results are presented in Figures 3 and 4. For the optimally doped sample, the relaxation rates in the B_{1g} and the B_{2g} channel show an approximate linear frequency dependence at all measured temperatures. A deviation occurs only at lower frequencies. But for the underdoped sample, this linear behavior for B_{1g} changes with temperature. From Figures 3 and 4, extrapolations can be made to obtain the static relaxation rates (Fig. 5). We find that they are different from those of BSCCO and YBCO as well [2, 3].

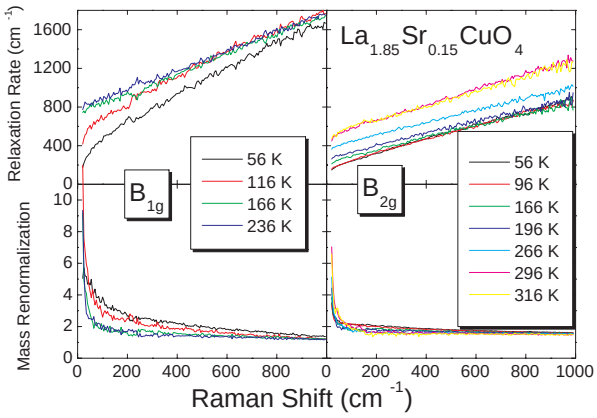

Figure 3: Dynamical relaxation rates and mass renormalization factors of $La_{1.85}Sr_{0.15}CuO_4$.

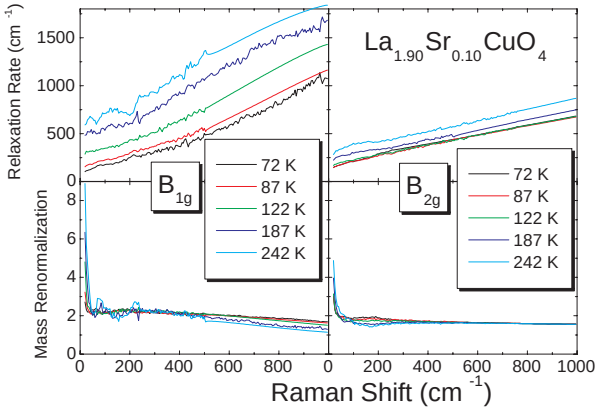

Figure 4: Dynamical relaxation rates and mass renormalization factors of $La_{1.90}Sr_{0.10}CuO_4$.

Figure 6 shows B_{1g} and B_{2g} spectra at three different excitation energies from the optimally doped sample. The intensities in the B_{1g} channel depend only weakly on the excitation energy. But it is striking that the intensities in B_{2g} are dramatically suppressed with increasing excitation wavelength. In contrast, BSCCO does not show such an obvious dependence on excitation energy neither in B_{1g} nor in B_{2g} symmetry [3].

Using a higher resolution, spectra were obtained in the very low energy range of $10 \ldots 100$ cm^{-1} (Fig. 7). The spectral shape of both B_{1g} and B_{2g} symmetry depends weakly on the excitation energy. The B_{1g} spectra show an approximately linear frequency dependence, but there is a crossover from linear to non-linear behavior in the B_{2g} channel. These results are vice versa to those obtained earlier from BSCCO [3].

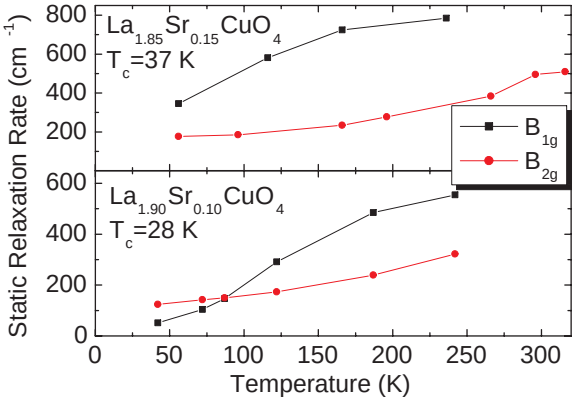

Figure 5: Static relaxation rates.

In combination with circular light polarizations, we can extract the pure A_{1g}, A_{2g}, B_{1g}, and B_{2g} contributions. The results for optimally doped LSCO are shown in Fig. 8. All the four spectra show a quite weak temperature dependence. A_{1g} has a hump around 4000 cm^{-1}. It should be pointed out that this hump cannot be related to the two-magnon process because of its higher energy. The spectra in A_{1g}, B_{1g}, and B_{2g} symmetry approach each other at energies above 7000 cm^{-1}. It is interesting that the A_{2g} contribution which was thought to be negligible in the high-T_c compounds becomes finite with increasing energy.

In summary, polarized ERS experiments were carried out on high-quality single crystals of $La_{2-x}Sr_xCuO_4$ with $x = 0.10$ and $x = 0.15$. Spectra at various temperatures and excitation energies were obtained. A complete symmetry analysis was made to extract the pure contributions of the four symmetries. In the superconducting state, the pair-breaking peak can be observed in both B_{1g} and B_{2g} symmetry. In the B_{2g} channel, the peak intensity depends strongly on the excitation energy, but in B_{1g} symmetry the excitation energy has only a small effect on the peak intensity. The low energy parts ($\hbar\omega < 100$ cm^{-1}) of the B_{1g} spectra show an approximately linear dependence on frequency. The behavior is non-linear in the B_{2g} channel. These results are inconsistent with the predictions based on $d_{x^2-y^2}$ wave pairing in the clean limit.

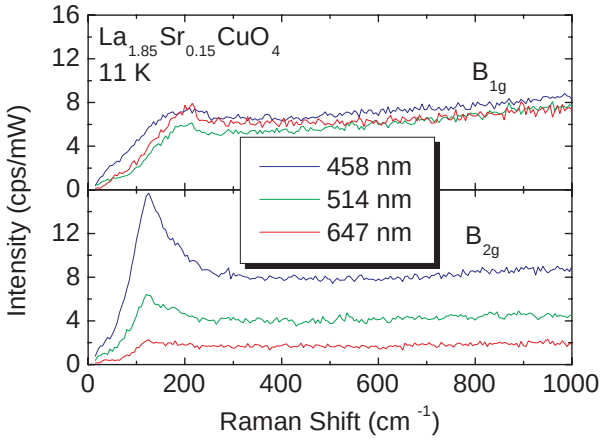

Figure 6: Spectra at different excitation energies from $La_{1.85}Sr_{0.15}CuO_4$.

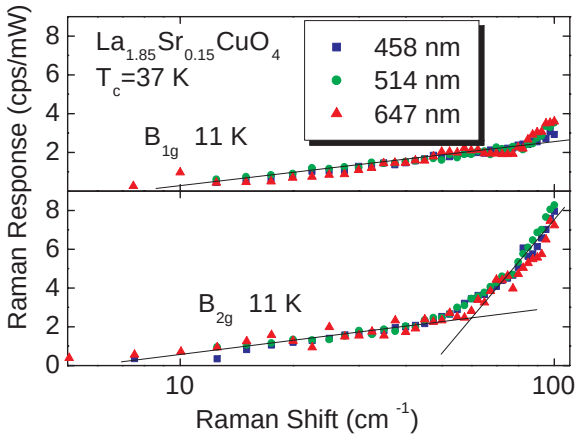

Figure 7: Spectra at low energies from $La_{1.85}Sr_{0.15}CuO_4$.

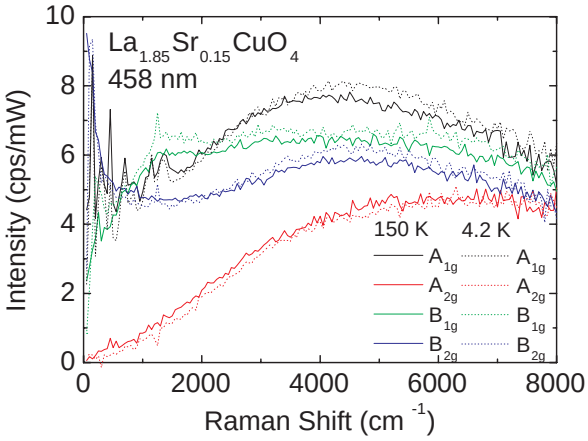

Figure 8: Spectra in pure symmetries from $La_{1.85}Sr_{0.15}CuO_4$ at 150 K (solid) and 4 K (dashed).

References

[1] D. Einzel and R. Hackl, J. Raman Spectroscopy **27**, 307 (1996).

[2] M. Opel, R. Nemetschek, C. Hoffmann, R. Philipp, P. F. Müller, R. Hackl, I. Tüttő, A. Erb, B. Revaz, E. Walker, H. Berger, and L. Forró, Phys. Rev. B **61**, 9752 (2000).

[3] F. Venturini, M. Opel, R. Hackl, to be published in J. Phys. Chem. Solids.

[4] T. Devereaux and D. Einzel, Phys. Rev. B **51**, 16336 (1995).

[5] J. G. Naeini, X. K. Chen, J. C. Irwin, M. Okuya, T. Kimura, and K. Kishio, Phys. Rev. B **59**, 9642 (1999).

[6] X. K. Chen, J. C. Irwin, H. J. Trodahl, T. Kimura, and K. Kishio, Phys. Rev. Lett. **73**, 3290 (1994).

[7] W. Götze and P. Wölfle, Phys. Rev. B **6**, 1226 (1972).

Symmetry of the order parameter in high-temperature superconductors

B. Welter, Y. Krockenberger, M. Schonecke, A. Marx, L. Alff, R. Gross [1]

The symmetry of the order parameter in high-temperature superconductors (HTS) has been an intense field of research in the recent years. For hole doped HTS there is strong evidence that the dominant order parameter is of $d_{x^2-y^2}$-wave type implying a sign change in the phase of the order parameter upon rotation of $\pi/2$ [1]. However, there are still major questions to be solved. The first question of deeper physical interest is the possible existence of a quantum critical point (QCP) at a critical doping concentration [2, 3]. Such a scenario implies violation of time reversal symmetry not only at surfaces but as a bulk property. This can be realised by development of a second superconducting phase with a phase shift of $\pi/2$ with respect to the dominant order parameter. There is currently contradicting experimental evidence for such a second superconducting phase [4, 5]. One experimental method to obtain phase sensitive information on the superconducting order parameter is tunneling and Andreev spectroscopy. We are performing such experiments using grain boundary tunneling junctions [6]. From our experiments, we have *not* obtained evidence for a QCP. To solve this issue, more fundamental understanding of the magnetic field response of the tunneling spectra is definitely needed. Also more doping dependent measurements with a meaningful statistics have to be performed.

The second important question is the electron-hole symmetry of high-temperature superconductivity. Very recently, using field-effect induced charge carriers in infinite layer compounds, it was confirmed that the differences in the phase diagram of hole and electron doped HTS can be reproduced in one system [7]. At present it is unclear, whether electron and hole doping produces different superconducting phases. Experimentally, exactly contradicting experiments have been presented [1, 8]. A possible way out of this exciting, but unsatisfying situation is a doping dependence of the symmetry of the order parameter [9, 10].

$La_{2-x}Ce_xCuO_4$

We have performed detailed experiments at different electron doping in order to clarify this issue. For this study we have used the well known electron doped HTS $Pr_{2-x}Ce_xCuO_4$, but also thin films of the new electron doped HTS $La_{2-x}Ce_xCuO_4$ [11, 12]. This HTS differs from the hole doped HTS only in one ion (Ce instead of for example Sr). A second difference associated with hole

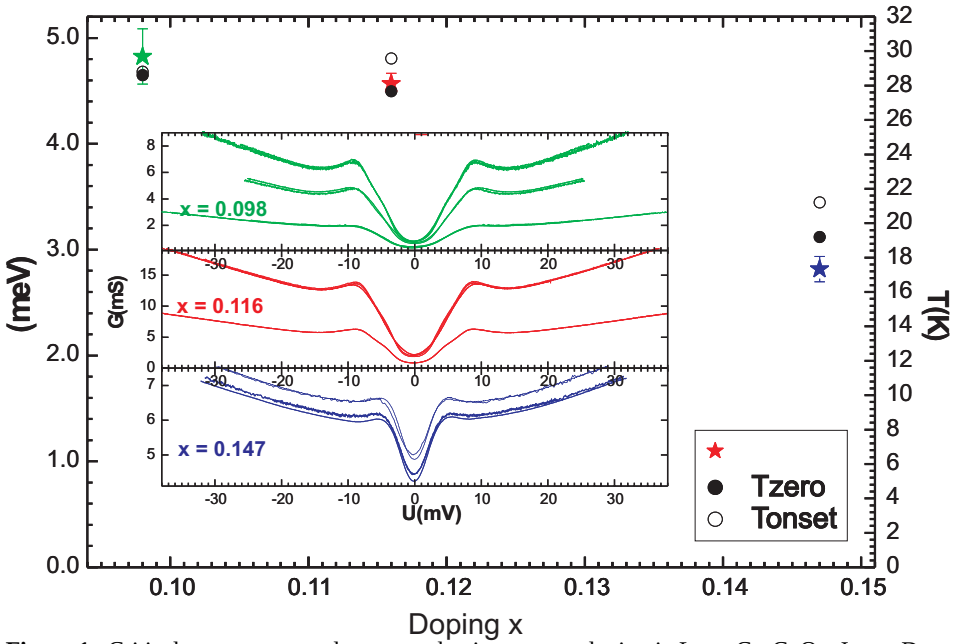

Figure 1: Critical temperature and superconducting gap vs. doping in $La_{2-x}Ce_xCuO_4$. Inset: Doping dependent tunneling spectra measured in grain boundary junctions with a 36.8° misorientation angle.

[1] In collaboration with M. Hepp (Universität zu Köln) and M. Naito, H. Sato (NTT, Japan).

vs. electron doping
in La_2CuO_4 is that electron doped compounds have always T'-structure, hole doped compounds always T-structure. In the figure, we summarize our main experimental results.

Tunneling spectroscopy is phase sensitive with respect to the sign of the phase of the order parameter. It is well known (see for example [6]), that a sign change as occuring in the d-wave pair potential leads to zero-energy states at the Fermi-level. Such states produce a zero-bias anomaly in the tunneling spectra. It is clear from our measurements that such a zero-bias anomaly is absent for the whole doping range we have studied (see figure). This leads to the conclusion that the order parameter symmetry in electron-doped HTS has no sign change as for example in an (anisotropic) s-wave symmetry. Thus, our experiments which are unpublished until now, have not solved but deepend the contradiction in experiments. The most important experiment contradicting our results is a tricrystal experiment [1] also relying on the sign change of the pair potential. It is necessary to repeat this experiment and to design new experiments to solve the issue. We are currently preparing measurements based on the critical current in asymmetric junctions which enable to distinguish clearly between d- and s-wave symmetry of the order parameter [13].

References

[1] C. C. Tsuei and J. R. Kirtley, Rev. Mod. Phys. **72**, 969 (2000).

[2] R. B. Laughlin, Phys. Rev. Lett. **80**, 5188 (1998).

[3] M. Vojta, Y. Zhang, and S. Sachdev, Phys. Rev. Lett. **85**, 4940 (2000).

[4] Y. Dagan, G. Deutscher, Phys. Rev. Lett. **87**, 177004 (2001).

[5] N.-C. Yeh, C.-T. Chen, G. Hammerl, J. Mannhart, A. Schmehl, C. W. Schneider, R. R. Schulz, S. Tajima, K. Yoshida, D. Garrigus, and M. Strasik, Phys. Rev. Lett. **87**, 087003 (2001).

[6] L. Alff and R. Gross, Superlattices and Microstructures **25**, 1041 (1999).

[7] J. H. Schön, M. Dorget, F. C. Beuran, X. Z. Zu, E. Arushanov, C. Deville Cavellin, and M. Languës, Nature **414**, 434 (2001).

[8] L. Alff, S. Meyer, S. Kleefisch, U. Schoop, A. Marx, H. Sato, M. Naito, and R. Gross, Phys. Rev. Lett. **83**, 2644 (1999).

[9] L. Alff, B. Welter, S. Kleefisch, A. Marx, and R. Gross, Physica C **357-360**, 309 (2001).

[10] L. Alff, S. Kleefisch, B. Welter, K. Sengebusch, S. Meyer, U. Schoop, F. Herbstritt, A. Marx, R. Gross, M. Naito, H. Sato, Physica C **341-348**, 1659 (2000).

[11] M. Naito and M. Hepp, Jpn. J. Appl. Phys. 39, L485 (2000).

[12] M. Hepp, Diploma thesis, University of Cologne (2000).

[13] J. Mannhart, H. Hilgenkamp, B. Mayer, Ch. Gerber, J. R. Kirtley, K. A. Moler, and M. Sigrist, Phys. Rev. Lett. 77, 2782 (1996).

Pseudogap in electron-doped high-temperature superconductors

B. Welter, Y. Krockenberger, M. Schonecke, A. Marx, L. Alff, R. Gross [1]

The pseudogap phenomen still belongs to the unsettled questions in high-temperature superconductivity [1]. One of the promising candidates to solve the quest for the origin of the pseudogap is the so-called precursor scenario [2]. Within this scenario one believes that Cooper-pairs are formed at a certain temperature T^* and condense into the superconducting phase at a much lower temperature $T_C < T^*$ into the coherent superconducting state. Some experimental evidence indicates a common origin of the superconducting gap and the pseudogap by showing that the pseudogap evolves smoothly from the superconducting gap when temperature is increased above T_C [3, 4, 5]. However, there is also experimental evidence that in some high-temperature superconductors (HTS) pseudogap and superconducting gap do not coincide [6].

For electron doped HTS, the search for a pseudogap has begun only recently. From angle resolved photoemission spectroscopy [8] and optical spectroscopy [9] there is some evidence for a gap like feature at energies (around 50 meV) much larger than the energy of the superconducting gap (around 10 meV). In addition there is evidence for a normal state gap at the same energy scale than the superconducting gap [10, 11].

$Pr_{2-x}Ce_xCuO_4$

To investigate further the origin of the low-energy, normal-state gap in the tunneling spectra of electron doped HTS, we have studied the doping and magnetic field dependence. In the figure we show data measured in the Grenoble High Magnetic Field Facility (supported by the "Training and mobility of researchers" programme of the European Community). $Pr_{2-x}Ce_xCuO_4$ tunneling spectra of 3 differently doped thin film grain boundary junctions for 20 T and 6 K are shown.

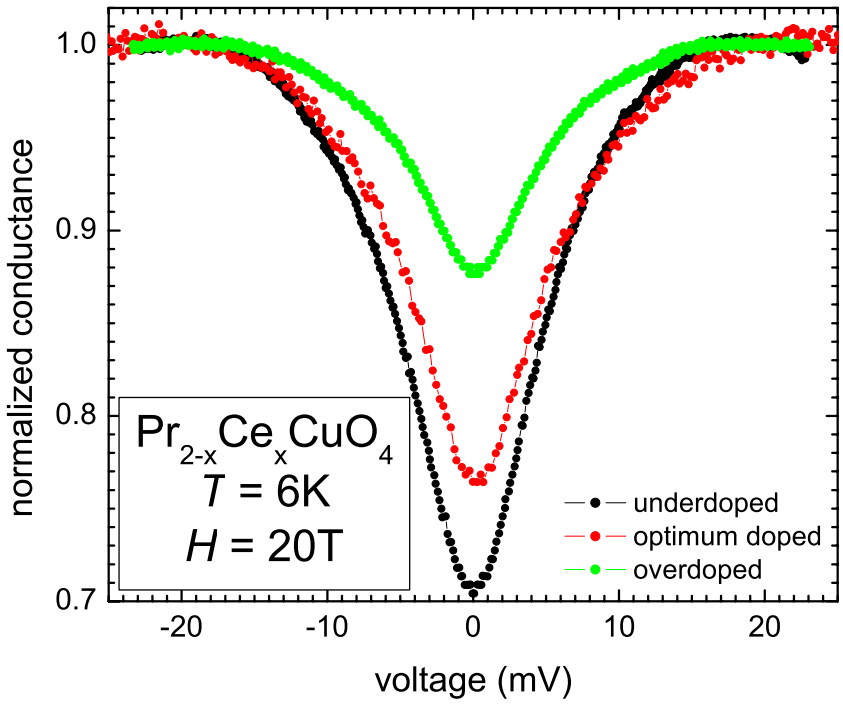

Figure 1: Normalized tunneling spectra for different doping at 6 K and 20 T (measurement performed in Grenoble). As electron doped HTS $Pr_{2-x}Ce_xCuO_4$ was used [12].

[1] In collaboration with M. Hepp (Universität zu Köln) and M. Naito, H. Sato (NTT, Japan).

The measurements show that there clearly is a gap far above the upper critical field of the superconductor which is around 5-6 T. The measurements in the high-field laboratory have proven that the gap feature indeed is a normal-state phenomenon. In a recent paper we have suggested that this gap is a pseudogap related to superconductivity since the energy scale of both gaps conincide [10]. In our new measurements we have additionally investigated the doping dependence. From the figure, it seems that the both the modulation and the size of the gap vary with doping. It is however difficult to extract a gap value from the measurements without theoretical refinement. There are different possible explanations for the observed gap feature: Since the gap and the modulation become smaller for overdoped samples where the material is closer to a normal metal than in the underdoped region where correlation effects dominate the physics, the gap could be interpreted as electron correlation gap. On the other hand, it is predicted that the precursor pseudogap is largest for underdoping and vanishes around optimum doping which also is consistent with our doping dependent measurements. Still further measurements with focus on more extreme doping (for both strongly under and over doped samples) are required to establish the doping dependence of the pseudogap.

References

[1] T. Timusk and B. Statt, Rep. Prog. Phys. **62**, 61 (1999).

[2] V. J. Emery and S. A. Kivelson, Nature **374**, 434 (1995); V. J. Emery, S. A. Kivelson, and O. Zachar, Phys. Rev. B **56**, 6120 (1997).

[3] Ch. Renner, B. Revaz, J.-Y. Genoud, K. Kadowaki, and Ø. Fischer, Phys. Rev. Lett. **80**, 149 (1998).

[4] Y. DeWilde, N. Miyakawa, P. Guptasarma, M. Iavarone, L. Ozyuzer, J. F. Zasadzinski, P. Romano, D. G. Hinks, C. Kendziora, G. W. Crabtree, and K. E. Gray, Phys. Rev. Lett. **80**, 153 (1998).

[5] N. Miyakawa, P. Guptasarma, J. F. Zasadzinski, D. G. Hinks, and K. E. Gray, Phys. Rev. Lett. **80**, 157 (1998).

[6] T. Sato, T. Yokoya, Y. Naitoh, T. Takahashi, K. Yamada, and Y. Endoh, Phys. Rev. Lett. **83**, 2254 (1999).

[7] T. Startseva, T. Timusk, A. V. Puchkov, D. N. Basov, H. A. Mook, M. Okuya, T. Kimura, and K. Kishio, Phys. Rev. B **59**, 7184 (1999).

[8] N. P. Armitage, D. H. Lu, C. Kim, A. Damascelli, K. M. Shen, F. Ronning, D. L. Feng, P. Bogdanov, and Z.-X. Shen, Y. Onose, Y. Taguchi, and Y. Tokura, P. K. Mang, N. Kaneko, and M. Greven, Phys. Rev. Lett. **87**, 147003 (2001).

[9] E. J. Singley, D. N. Basov, K. Kurahashi, T. Uefuji, and K. Yamada, Phys. Rev. B **64**, 224503 (2001).

[10] S. Kleefisch, B. Welter, A. Marx, L. Alff, R. Gross, and M. Naito, Phys. Rev. B **63**, R100507 (2001).

[11] A. Biswas, P. Fournier, V. N. Smolyaninova, R. C. Budhani, J. S. Higgins, and R. L. Greene, Phys. Rev. B **64**, 104519 (2001).

[12] M. Naito and H. Sato, Appl. Phys. Lett. **67**, 2557 (1995); H. Yamamoto, M. Naito, and H. Sato, Phys. Rev. B **56**, 2852 (1997).

Time reversal symmetry breaking in superconductor-normal metal tunneling junctions

M.Schonecke, B. Welter, A. Marx, L. Alff, R. Gross

In the recent years we have developed the so-called ramp-type technology [1, 2]. Using this junction geometry, it is possible to realize a manifold of different contacts between a variety of materials. While there are ongoing research activities in the field of junctions between high-temperature superconductors (HTS) and ferromagnetic doped manganites [3], in this year we realized normal metal - HTS tunneling junctions. A simplified scheme of the junction is shown in Fig. 1. After etching a ramp into a HTS thin film ($YBa_2Cu_3O_{7-\delta}$) by ion beam etching, we have deposited a thin $SrTiO_3$ layer as insulating barrier on top of the ramp. This layer is only about 5 nm thick. After deposition of the barrier we evaporated *in-situ* a gold electrode as the normal-metal side of the junction. Such superconductor - insulator - normal metal (SIN) junctions can be used to investigate the local density of states at the interface.

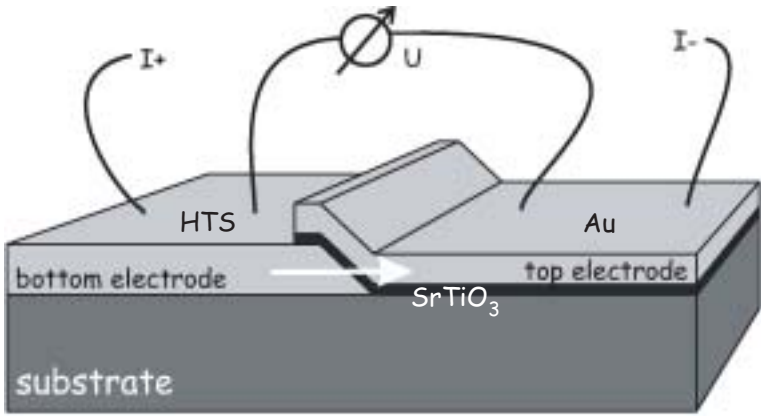

Figure 1: Geometry of a ramp-type junction.

It is well known that for HTS with $d_{x^2-y^2}$-wave symmetry of the order parameter at a (110) interface zero-energy states are formed due to Andreev bound states [4]. If a second superconducting phase is present having a phase shift with respect to the dominant order parameter, time reversal symmetry can be broken leading to split of the zero-energy state in zero magnetic field [5, 6]. In our SIS grain boundary junctions such a splitting was never observed even in applied fields [7]. Since all experiments observing a possible splitting of the zero-energy states were performed using SIN junctions, we investigated also SIN junctions in order to obtain an insight in the formation mechanism of the splitting.

As shown in Fig. 2 we observe a complex response of the junction to an applied magnetic field. We highlight three observations:

1. The first important observation is that indeed a splitting of the zero-bias anomaly exists in zero applied magnetic field. We note that this splitting is strongly sample dependent. We observed it in only a few percent of the junctions.

2. The second observation is that the splitting increases on applying magnetic field. This increase is in agreement with the experiments in other junction types [5].

3. The most striking observation however is, that at high fields (above 8 T) a third peak develops exactly at zero energy (marked by an arrow in Fig. 2). Such a peak is not predicted within the existing theory [6]. We note that in the original paper that first reports the observation of zero-field splitting such a third peak at zero energy was also present in the data but not further commented on in the paper [5].

At the present moment we cannot provide a model to explain our experimental results. However, these observations challenge the until now developed theory of the magnetic field response of Andreev bound states.

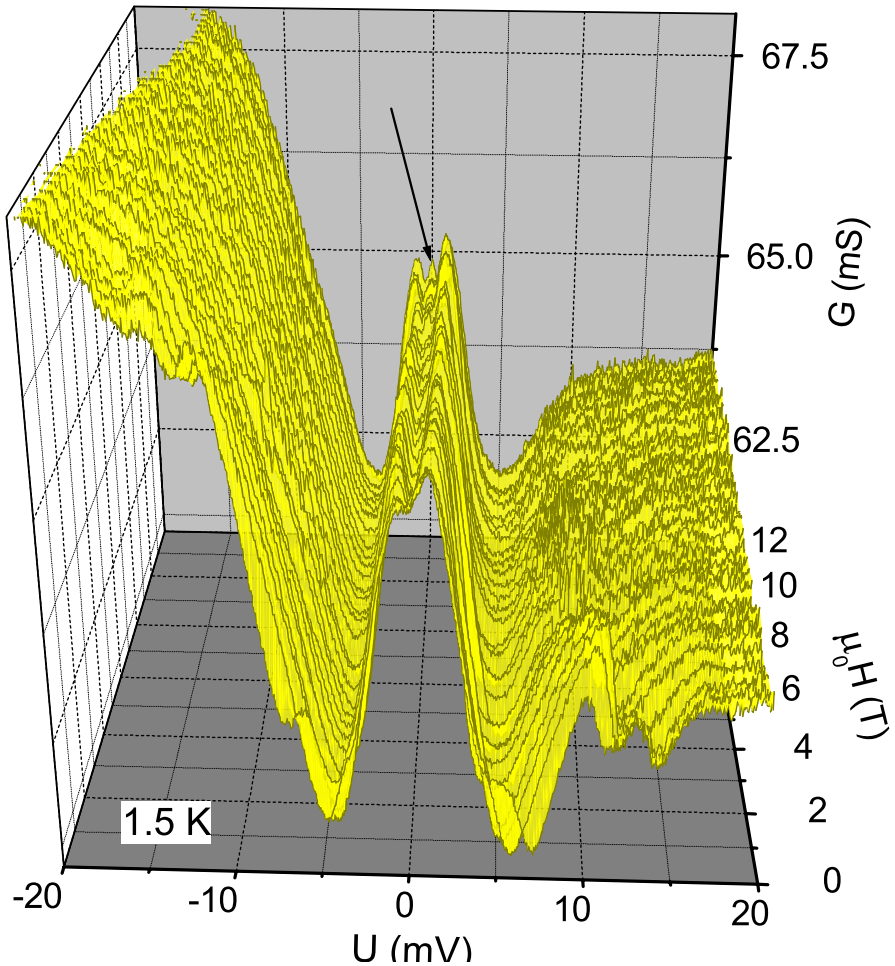

Figure 2: Tunneling spectra for different magnetic fields at 1.5 K. The junction is formed between $YBa_2Cu_3O_{7-\delta}$ and Au devided by $SrTiO_3$.

References

[1] L. Alff, U. Schoop, R. Gross, R. Gerber, A. Beck, Physica C **271**, 339 (1996).

[2] U. Schoop, M. Schonecke, S. Thienhaus, S. Schymon, L. Alff, R. Gross, Physica C **351**, 200 (2001).

[3] U. Schoop, M. Schonecke, S. Thienhaus, F. Herbstritt, J. Klein, L. Alff, R. Gross, Physica C **350**, 237 (2001).

[4] C. R. Hu, Phys. Rev. Lett. **72**, 1526 (1994); C. Yang and C. R. Hu, Phys. Rev. B **50**, 16766 (1994).

[5] M. Covington, M. Aprili, E. Paraoanu, L. H. Greene, F. Xu, J. Zhu, and C. A. Mirkin, Phys. Rev. Lett. **79**, 277 (1997).

[6] M. Fogelström, D. Rainer, and J. A. Sauls, Phys. Rev. Lett. **79**, 281 (1997).

[7] L. Alff, A. Beck, R. Gross, A. Marx, S. Kleefisch, Th. Bauch, H. Sato, M. Naito, and G. Koren, Phys. Rev. B **58**, 11197 (1998).

Charge-density waves and superconductivity in the organic metal α-(BEDT-TTF)$_2$KHg(SCN)$_4$

D. Andres, M. Kartsovnik, W. Biberacher, K. Neumaier

The family of organic metals based on the molecule bis(ethylenedithio)-tetrathiafulvalene (BEDT-TTF) commonly possess a layered crystal structure, consisting of conducting BEDT-TTF sheets, which are separated by insulating anion layers [1]. This leads to a reduction in dimensionality of the electron system. The Fermi surface of the organic compound α-(BEDT-TTF)$_2$KHg(SCN)$_4$ consists of slightly warped cylinders and open sheets, representing quasi-two-(Q2D) and quasi-one-dimensional (Q1D) electronic bands, respectively. In recent years, the title compound attracted a lot of attention due to its transition into an unconventional ground state below 8 K, exhibiting numerous anomalies in magnetic field. To the moment there are strong arguments that this transition is caused by the formation of a density wave [2, 3, 4]. Basically, a density wave adds an additional periodic potential to the system that leads to a reconstruction of the Fermi surface. The Q1D sheets of the Fermi surface nest on each other, the electrons become gapped and the system gains energy.

The fact that this density wave transition is suppressed by magnetic field [4] and that at 24 Tesla a first order transition into a high field state occurs, strongly suggests a charge-density wave (CDW) rather than a spin-density wave (SDW) to be the nature of this low temperature state. Indeed, in a CDW system the paramagnetic Pauli effect leads to a gradual suppression of the transition temperature. At the paramagnetic limit there is then a first order transition into a CDW$_x$ state, a hybrid of charge and spin-density waves (SDW), which remains present up to much higher fields [5]. Last year our group observed that with quasi-hydrostatic pressure the density wave gets gradually suppressed . This can be explained by a stronger overlap of the molecular orbitals under pressure that should enhance the dimensionality of the Q1D part of the Fermi surface, resulting in less perfect nesting conditions. However, in a magnetic field applied perpendicular to the conducting crystal layers it turned out that the CDW state becomes restored [6]. This is due to the so-called orbital effect: the dimensionality of the electrons moving perpendicular to the field on the corrugated open sheets effectively decreases that enhances the nesting instability. Fig 1 shows the measured phase lines at different pressures [6]. For clarity the high-field first order transition is not shown: to the left of each line there exists a CDW state while to the right there is a normal metal.

Based on these observations, the main interest of the present study was focused on the pressure range where the density wave transition at zero-field vanishes, i.e. between 2.5 and 3.5 kbar. In this range, theory [5] expects a new quantum phenomenon of field induced charge-density wave (FICDW) transitions. These transitions are analogous to field induced spin-density waves, which have been (and still are) a topic of intense interest in the field of Q1D organic metals (for a review see e.g. [1, 7]). When the nesting of the Fermi surface is imperfect, not all Q1D electrons become gapped and small pockets (of electrons and holes) remain on the reconstructed Fermi surface. A series of first order transitions then appear at low enough temperature due to abrupt changes of the wave vector of the density wave in order

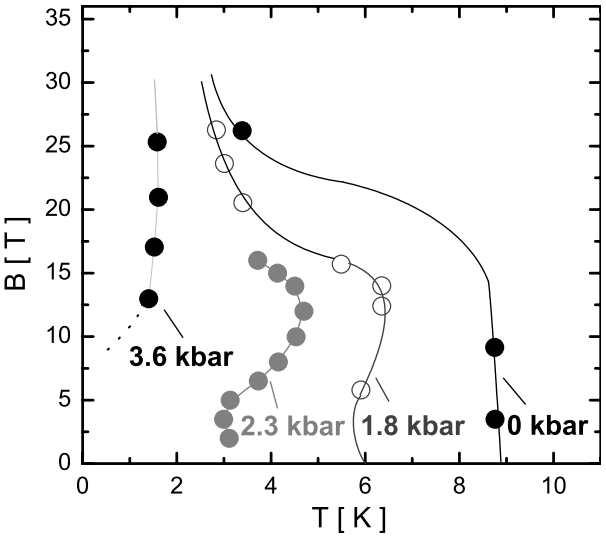

Figure 1: Measured phase lines at different pressure values.

to keep the Fermi surface in between the Landau levels [7].

All experiments under pressure were performed measuring the interlayer resistance with a magnetic field applied perpendicular to the conducting layers. In Fig. 2 field sweeps at several temperatures down to 50 mK and at two different pressures are depicted. The curves at ambient pressure show the already well-known behaviour in the density wave state of this compound: with field the resistance strongly increases, comes to a maximum and further shows a negative slope until it reaches the high field state (not shown in this picture). The fast Shubnikov-de Haas (SdH) oscillations originate from the Q2D part of the electronic system, which remains present after the reconstruction of the Fermi surface in the CDW state.

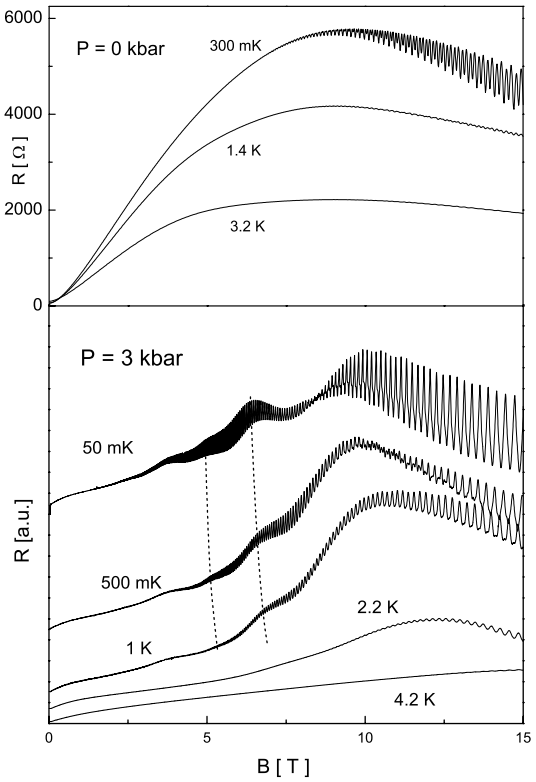

Figure 2: Interlayer resistance vs. field at different temperatures for two different pressure values. The curves at 3 kbar are shifted with respect to each other. The dashed lines (see text) are guides for the eye.

The behaviour dramatically changes upon increasing the pressure to 3 kbar, where the density wave is supposed to be already completely suppressed at zero-field. While at 2.2 K the enhancement of the resistance starting from $\approx$ 6 T can be explained by entering the CDW state, in good agreement with the phase diagrams, the situation becomes rather complex below 2 K. A strong modulation of the background resistance appears, becoming more pronounced at lower temperatures. In principle, one could expect a quantum oscillation arising from small closed orbits on the partially gapped Q1D Fermi surface, so that a low SdH frequency might appear with lowering the temperature. However, there is no clear periodicity found in the inverted field dependence of the curves plotted in Fig. 2. Moreover, the phase of the SdH oscillations should not change with temperature as it obviously does in the present case (as indicated by the dashed lines in Fig. 2). Therefore, the observed anomalies definitely cannot be attributed to a normal SdH oscillation of low frequency. On the other hand, the aperiodicity is more consistent with a series of FICDW transitions. However, we could not detect any hysteresis or sharp features expected for first order transitions, which should appear according to the theory at very low temperatures. Although we still cannot claim an unambiguous detection of FICDW, the observed non-monotonic behaviour makes us believe that this phenomenon is present in this organic compound.

Another very interesting observation is illustrated in Fig 3. For the first time it could be shown that under quasi-hydrostatic pressure α-(BEDT-TTF)$_2$KHg(SCN)$_4$ becomes superconducting. At 3 kbar, where we expect the density wave to be suppressed at zero-field, the resistance sharply drops to zero on cooling below 160 mK. Remarkably, the transition temperature T_c is found not to coincide for two different samples measured, implying a dependence on the crystal quality. At lower pressure, where the CDW is established at zero-field, the behaviour becomes different: On cooling, already above T_c(3kbar) the resistance slowly starts to decrease, showing several anomalies until at the lowest achievable temperature one sample becomes superconducting while the other clearly remains resistive. Altogether, these

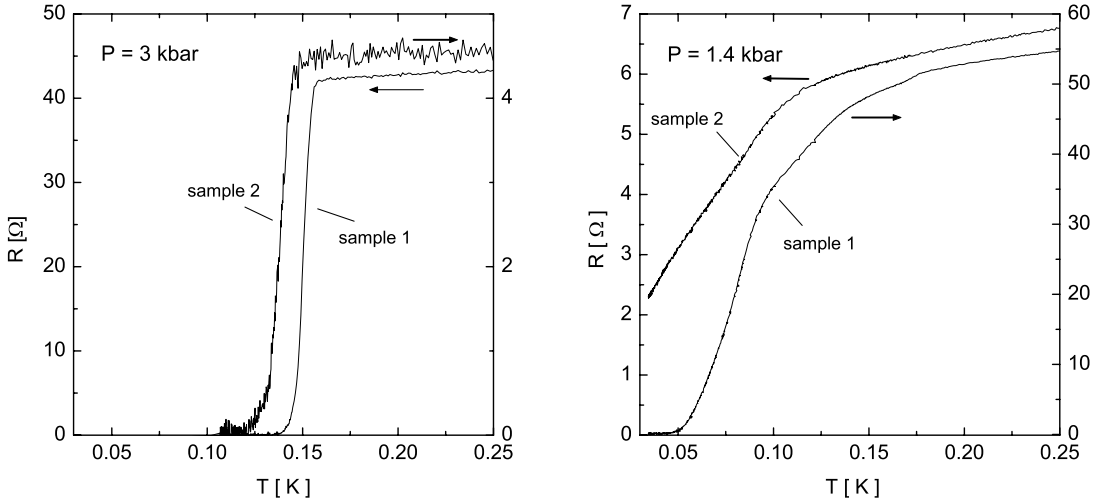

Figure 3: Superconducting transition for two different samples at two pressure values.

observations might be similar to the behaviour found in the SDW ground state of the Q1D organic metal $(TMTSF)_2PF_6$. There, with the suppression of the SDW state by pressure a superconducting state is induced [1], which to the moment is suggested to be formed by a triplet pairing mechanism [8]. Moreover, it has been shown that the SDW and superconducting states coexist at a certain pressure range. It would be interesting to find out, whether such a coexistence can also occur in CDW systems.

References

[1] T. Ishiguro, K. Yamaji, and G.Saito, Organic superconductors, 2^{nd} edition, Springer-Verlag Berlin Heidelberg (1998).
[2] M. V. Kartsovnik, A. E. Kovalev, and N. D. Kushch, J. Phys. I France **3**, 1187 (1993).
[3] M. Basletić, B. Korin-Hamzić, M. V. Kartsovnik, and H. Müller. Synth. Met. **120**, 1021 (2001).
[4] P. Christ, W. Biberacher, M. V. Kartsovnik, E. Steeb, E. Balthes, H. Weiss, and H. Müller, JETP Lett. **71**, 303 (2000).
[5] D. Zanchi, A. Bjelis, and G. Montambaux, Phys. Rev. B **53**, 1240 (1996).
[6] D. Andres, M. Kartsovnik, W. Biberacher, H. Weiss, E. Balthes, H. Müller, and N Kushch, Phys. Rev. B **64**, 161104(R) (2001).
[7] P. M. Chaikin, J. Phys. I France **6**, 1875 (1996).
[8] I. J. Lee, M. J. Naughton, P. M. Chaikin, Physica B **294-295**, 413 (2001).

Anomalous beating phase of the oscillating magnetoresistance in layered metals

M. Kartsovnik, W. Biberacher, and P. Grigoriev

The magnetic quantum oscillations have been extensively used in the last decade for studying quasi-two-dimensional (Q2D) organic metals [1]. It is well known that, due to extremely high anisotropies of these materials, the amplitudes of the oscillations and their harmonic contents are often strongly enhanced and cannot be described by the standard Lifshitz-Kosevich (LK) theory [2]. Moreover, recent results [3, 4] suggest that substantial deviations from the LK theory may take place even when the oscillations are weak and represented by only the first harmonic. This is reflected in an anomalous beating behaviour of the oscillations observed on organic metals κ-(BEDT-TTF)$_2$Cu[N(CN)$_2$]Br [3] and (BEDT-TTF)$_4$[Ni(dto)$_2$] [4].

Generally, beats of the Shubnikov–de Haas (SdH) and de Haas–van Alphen (dHvA) oscillations in Q2D metals originate from a slight warping of their Fermi surfaces in the direction normal to the 2D plane. The superposition of the contributions from the maximum and minimum cyclotron orbits is expected to lead to an amplitude modulation of the k-th harmonic by the factor $\cos(2\pi k\Delta F/2B-\pi/4)$, where B is the magnetic field and $\Delta F=(c\bar{h}/2\pi e)(A_{\max}-A_{\min})$ is the difference between the oscillation frequencies caused by the extremal orbits with the k-space areas $A_{\max}$ and $A_{\min}$, respectively [2]. From the beat frequency one can readily evaluate the warping of the Fermi surface (FS) and hence the interlayer transfer integral, $4t_\perp \approx \varepsilon_F \Delta F/F$. The situation becomes less clear when the warping is so weak that less than one half of the beat period can be observed experimentally. In principle, an observation of one single node would already be quite informative [3], provided the phase offset (i.e. the phase of the beat at $1/B\to 0$) is known. The latter, in the standard LK theory is strictly determined by geometrical reasons to be equal to $-\pi/4$ for both SdH and dHvA effects [2]. By contrast, the experiments [3, 4] have revealed a significant difference in the node positions of beating dHvA and SdH signals. The respective phase shift in the latter compound was estimated to be as big as $\pi/2$. However, the nature of the shift has not been understood due to relatively complicated FSs and limited set of experimental data.

In order to clarify the problem, we have carried out comparative studies of the oscillating magnetization (dHvA effect) and interlayer resistivity (SdH effect) of the radical cation salt β-(BEDT-TTF)$_2$IBr$_2$. This material exhibits a simple metallic behavior down to lowest temperatures. Its electronic properties are determined by a single cylindrical FS slightly (by $\simeq 1\%$) warped in the direction perpendicular to the highly conducting BEDT-TTF layers [5]. The experiment was done on a high-quality single crystal at $T\approx 0.6$ K in magnetic field up to 16 T. To assure exactly the same conditions for the dHvA and SdH effects (in particular, identical field orientations are of crucial importance!) the measurements were performed in a set-up providing a simultaneous registration of the magnetic torque and resistance.

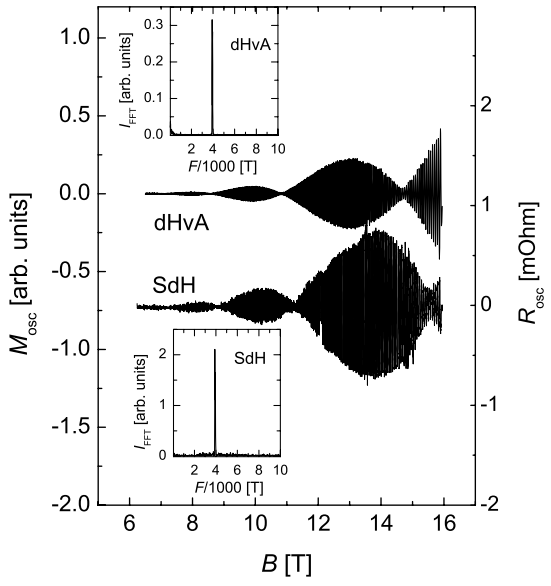

Figure 1: dHvA (left scale) and SdH (right scale) oscillations in β-(BEDT-TTF)$_2$IBr$_2$ at $\theta\approx 14.8°$. Insets: corresponding FFT spectra.

Fig. 1 shows the oscillating parts of the magnetization and interlayer magnetoresistance in the normal state of β-(BEDT-TTF)$_2$IBr$_2$ at magnetic field tilted by $\theta\approx 14.8°$ from the normal to the BEDT-TTF layers. The

curves have been obtained by subtracting slowly varying backgrounds from the measured magnetic torque $\tau(B)$ and resistance $R(B)$ and (for the magnetization oscillations, $\tilde{M} \propto \tilde{\tau}/B$) subsequent dividing by B. The fast Fourier transformation (FFT) spectra shown in the insets reveal the fundamental frequency of ≈ 3930 T in agreement with previous works [5]. The second harmonic contribution is about 1% of that from the fundamental one at the highest field.

Clear beats with four nodes are seen in both the dHvA and SdH curves. The positions of the nodes determined as midpoints of narrow field intervals at which the oscillations inverse the phase are plotted on Fig. 2. The straight line is a linear fit of the magnetization data revealing the beat frequency $\Delta F = 40.9$ T that, according to Eq.(6), corresponds to $4t_\perp/\varepsilon_F = \Delta F/F = 1/96$.

From Figs. 1 and 2 one can see that the nodes of the SdH oscillations are considerably shifted to higher fields with respect to those of the dHvA oscillations. The shift grows with increasing the field.

This result can be understood by taking into account oscillations of both the density of states (DOS) and interlayer Fermi velocity contributing to the SdH effect in Q2D metals.

In a magnetic field perpendicular to the conducting layers the electron dispersion takes the form

$$\varepsilon_{n,k_z} = \hbar\omega_c\,(n+1/2) - 2t_\perp \cos(k_z d), \qquad (1)$$

where $t_\perp$ is the interlayer transfer integral, k_z is the wavevector perpendicular to the layers, d is the interlayer distance, $\omega_c = eB/m^*c$ is the cyclotron frequency. Both $\hbar\omega_c$ and $t_\perp$ are assumed to be much smaller than the Fermi energy.

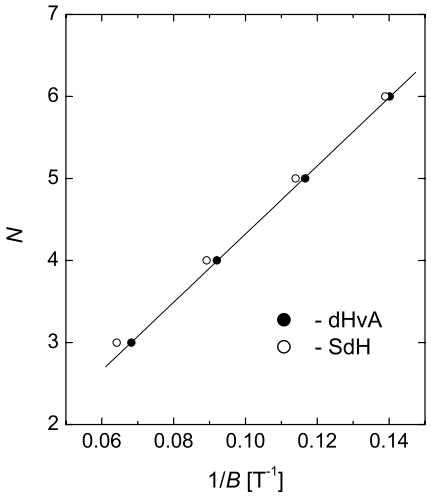

Figure 2: The positions of the nodes in the oscillating magnetization (filled symbols) and magnetoresistance (open symbols) vs. inverse field. The straight line is the linear fit to the magnetization data.

The interlayer conductivity σ_{zz} can be approximately evaluated from the Boltzmann transport equation [6]:

$$\sigma_{zz} = e^2 \sum_{m\equiv\{n,k_z,k_x\}} v_z^2(k_z)\,\delta(\varepsilon(n,k_z)-\mu)\cdot\tau(\mu) \equiv e^2 I(\mu)\tau(\mu) \qquad (2)$$

where v_z is the z-component of the electron velocity and $\tau(\mu)$ the momentum relaxation time at the Fermi level (since the oscillation amplitude is small in our case, the oscillations of the chemical potential μ can be neglected). The relaxation time, in Born approximation, is inversely proportional to the DoS: $1/\tau(\mu) \propto g(\mu)$ and oscillates in magnetic field [7]:

$$g(\mu) \propto 1 + 2\sum_{k=1}^{\infty}(-1)^k \cos\left(\frac{2\pi k\mu}{\hbar\omega_c}\right) J_0\left(\frac{4\pi k t_\perp}{\hbar\omega_c}\right) \qquad (3)$$

with the amplitude modulated by the 0-th order Bessel function $J_0(4\pi k t_\perp/\hbar\omega_c)$. In three-dimensional metals the oscillations of $g(\mu)$ are responsible for both the dHvA and SdH effects. However, in Q2D metals, when $t_\perp$ approaches the cyclotron energy $\hbar\omega_c$, oscillations of the factor $I(\mu) = \sum_{\varepsilon=\mu}|v_z|^2$ in Eq.(2) become also important. The latter are determined by the oscillating interlayer velocity and can be expressed as [8]

$$I(\mu) = 1 + \frac{2\hbar\omega_c}{\pi t_\perp}\sum_{k=1}^{\infty}\frac{(-1)^k}{2k}\cos\left(\frac{2\pi k\mu}{\hbar\omega_c}\right) J_1\left(\frac{4\pi k t_\perp}{\hbar\omega_c}\right) \qquad (4)$$

where the 1-st order Bessel function $J_1(4\pi k t_\perp/\hbar\omega_c)$ also describes beatings but with a phase different from that of the DOS beatings given by $J_0(4\pi k t_\perp/\hbar\omega_c)$ in Eq.(3).

We further consider the limit of strong harmonic damping, neglecting all the harmonics with $k > 1$ in Eqs.(3,4), and sufficiently large $t_\perp > \hbar\omega_c/4\pi$ so that the beats can be observed. Then, using the large argument expansions of the Bessel functions, one can obtain [8]

$$\tilde{\sigma}_{zz} \propto \cos\left(\frac{2\pi\mu}{\hbar\omega_c}\right)\cos\left(\frac{4\pi t_\perp}{\hbar\omega_c} - \frac{\pi}{4} + \phi\right), \quad \phi = \arctan(\hbar\omega_c/2\pi t_\perp) \tag{5}$$

On the other hand, the oscillations of the magnetization, being determined solely by the DOS oscillations, have the form similar to that obtained in the LK theory [7]:

$$\tilde{M} \propto \sin\left(\frac{2\pi\mu}{\hbar\omega_c}\right)\cos\left(\frac{4\pi t_\perp}{\hbar\omega_c} - \frac{\pi}{4}\right). \tag{6}$$

Comparing Eqs.(5) and (6), we see that the beats in the SdH oscillations shift to higher fields with respect to those in the dHvA oscillations as the cyclotron energy approaches the value of the interlayer transfer integral. This is exactly what we observe in the experiment (see Figs. 1,2).

In order to further verify the applicability of the above model, we have studied the dependence of the phase shift ϕ on the tilt angle θ. The interlayer bandwidth effectively decreases as θ approaches Yamaji's angle [9]; thus, one should expect the phase shift to gradually increase. Indeed, we have observed a rapid increase of ϕ in the vicinity of the first Yamaji's angle ($\simeq 30^\circ$). However, at $\theta > 24^\circ$ the shift is found to exceed the theoretically predicted maximum value of $\pi/2$. A more explicit theoretical analysis aimed to explain this result is in progress.

Summarizing, the beats of the SdH oscillations in β-(BEDT-TTF)$_2$IBr$_2$ are found to be shifted towards higher fields with respect to those of the dHvA signal. We attribute this effect to interfering contributions from oscillating DoS and Fermi velocity to the interlayer conductivity of this layered compound. The observed behavior appears to be a general feature of Q2D metals which should be taken into account whenever the cyclotron energy becomes comparable to the interlayer transfer energy. Of a particular importance is the dependence of the beat phase on the magnetic field strength. Ignorance of this fact may lead to considerable errors in estimations of the FS warping from the beat frequency when $2t_\perp \simeq \hbar\omega_c$.

References

[1] J. Wosnitza, *Fermi Surfaces of Low-Dimensional Organic Metals and Superconductors* (Springer-Verlag, Berlin, 1996); M. V. Kartsovnik and V. N. Laukhin, J. Phys. I France **6**, 1753 (1996); J. Singleton, Rep. Prog. Phys. **63**, 1111 (2000).

[2] D. Shoenberg, *Magnetic oscillations in metals* (Cambridge University Press, Cambridge, 1984).

[3] H. Weiss, M. V. Kartsovnik, W. Biberacher, E. Balthes, A. G. M. Jansen, and N. D. Kushch, Phys. Rev. B **60**, R16259 (1999).

[4] M. Schiller, W. Schmidt, E. Balthes, D. Schweitzer, H.-J. Koo, M. H. Whangbo, I. Heinen, T. Klausa, P. Kircher and W. Strunz, Europhys. Lett. **51**, 82 (2000).

[5] M. V. Kartsovnik, V. N. Laukhin, S. I. Pesotskii, I. F. Schegolev and V. M. Yakovenko, J. Phys. I France **2**, 89 (1992); J. Wosnitza, G. Goll, D. Beckmann, S. Wanka, D. Schweitzer and W. Strunz, J. Phys. I France **6**, 1597 (1996).

[6] G. Mahan *Many-Particle Physics*, 2nd ed. (Plenum Press, New York, 1990).

[7] T. Champel and V. P. Mineev, Phil. Magazine B **81**, 55 (2001).

[8] P. D. Grigoriev, M. V. Kartsovnik, W. Biberacher, N. D. Kushch and P. Wyder, Phys. Rev. B **65**, in press.

[9] K. Yamaji, J. Phys. Soc. Jpn. **58**, 1520 (1989).

Effect of Biaxial Strain on Doped Manganites

J. Klein†, *Yafeng Lu*†, *J. B. Philipp, A. Marx, L. Alff, R. Gross* [1]

It is well known that the physics of the hole doped perovskite manganites is determined by a complex interplay of structural, magnetic, electronic, and orbital degrees of freedom. While the classical double exchange model can qualitatively explain the transition from a paramagnetic insulating state to a ferromagnetic metallic state [1], for a more complete understanding of the physics of the manganites electron-lattice coupling has to be included [2]. Depending on the valence state of the manganese ion, Jahn-Teller distortion of the oxygen octahedron and coupling to a breathing mode of the lattice plays an important role, leading to electron localization in a polaron like state. The resulting strong pressure dependence of the electronic properties of the doped manganites has been studied in detail for bulk material [3]. Recently, Millis *et al.* have pointed out that uniform compression, as realized by hydrostatic pressure on single crystals, increases the electron hopping amplitude leading to a more cubic metallic state [4]. In contrast, biaxial strain, as realized in lattice mismatched epitaxial thin films, tends to enhance the Jahn-Teller distortion resulting in more insulating behavior [4, 5]. Therefore, the investigation of the structural, electronic, and magnetic properties of manganite thin films and heterostructures is of great interest to understand the fundamental physics of these materials and their dependence on biaxial strain. Since possible spintronic devices using doped manganites would of course be based on thin film heterostructures, the topic is of great relevance also for potential applications. A simple device structure is shown in Fig. 1.

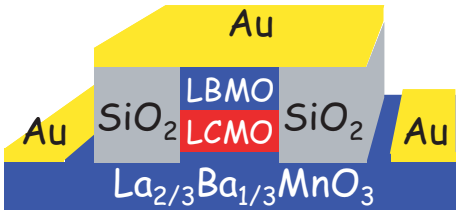

Figure 1: Mesa structure of a tunneling magneto resistance device.

It has been shown recently that doped manganite thin films grown under large compressive lattice mismatch may be structurally, magnetically, and electronically nonuniform [6, 7]. This nonuniformity has been explained with a nonuniform strain distribution due to island formation in the Stranski-Krastinov growth mode. However, even if the films are grown in a layer-by-layer growth mode resulting in homogeneous, coherently strained thin films, both individual thin films and complex superlattices of the doped manganites display novel interesting properties [5, 8, 10, 9, 11, 12, 14, 15]. By high-resolution electron microscopy (HREM) it was shown that ultrathin films of $La_{0.73}Ca_{0.27}MnO_3$ on $SrTiO_3$ substrates form a crystal structure, different from the bulk, having a ferromagnetic insulating ground state [9]. Inhomogeneous transport properties were found in $La_{0.7}Ca_{0.3}MnO_3/SrTiO_3$ heterostructures interpreted as arising from magnetic interface disorder [12].

In our studies with coherently strained superlattices we systematically investigated the effect of biaxial strain on the Curie temperature of the doped manganites [5]. By using the superlattice structures the strain in the manganite layers could be varied over a wide range. Our measurements show that there is a clear correlation between the biaxial strain $\varepsilon_{\mathbf{bi}}$ and the temperature T_p corresponding to the maximum in the resistivity versus temperature curves as well as the measured magnetoresistance. By varying the strain we could derive the quantity $\Delta = (T_p/T_p^{\mathrm{bulk}})(d^2T_p/d\varepsilon_{\mathbf{bi}}{}^2)$ giving the sensitivity of the materials properties to biaxial strain. Our data provide evidence for the relevance of the Jahn-Teller electron-phonon coupling in the doped manganites as predicted by Millis *et al.* [4].

We have carefully studied the structural, electronic, and magnetic properties of strongly strained $La_{2/3}Ca_{1/3}MnO_3$ (LCMO) thin films and LCMO/$La_{2/3}Ba_{1/3}MnO_3$ (LBMO) heterostructures on $SrTiO_3$

[1] In collaboration with G. Carbone and A. Vigliante (MPI Stuttgart).

† II. Physikalisches Institut, Universität zu Köln.

This work is supported by the Deutsche Forschungsgemeinschaft.

grown on substrates [13]. X-ray diffraction (XRD) and reflectivity, HR-TEM, reflection high energy electron diffraction (RHEED), and atomic force microscopy (AFM) show that the investigated epitaxial thin films grow coherently strained in a layer-by-layer growth mode. One of the most important results of this study is that strong enough biaxial strain can induce a metal-insulator-transition only in one direction: Perpendicular to the biaxially strained plane (parallel to the c axis of the LCMO films), insulating behavior associated with non-linear electrical transport is observed, while the in-plane transport remains metallic below the Curie temperature T_C. It is shown that this behavior is not due to interface or surface effects between different layers [16, 17], but is an *intrinsic* property of the highly strained LCMO thin films. The magnetization of the LCMO thin films is strongly reduced compared to the bulk material or less strained LBMO thin films. We propose the existence of an anisotropic ground state with strain induced orbital order. However, the precise determination of the details of the crystal structure as well as the electronic and magnetic properties of the strained thin films has to be elucidated in further experiments.

Our results on strain effects in doped manganites demonstrate that in biaxially strained thin films the interplay of the structural, electronic, and magnetic degrees of freedom leads to a rich variety of novel properties such as a strain induced uni-axial metal-insulator transition [18, 19].

Strain induced orbital order

The main evidence for a strain induced orbital ordering is shown in Fig. 2. In the main panel it is shown that the out-of-plane resistance increases with decreasing temperature even for temperatures below the Curie temperature T_c of the strained thin film. In the inset, the in-plane resistance is shown which shows the typical metal-insulator transition around T_c.

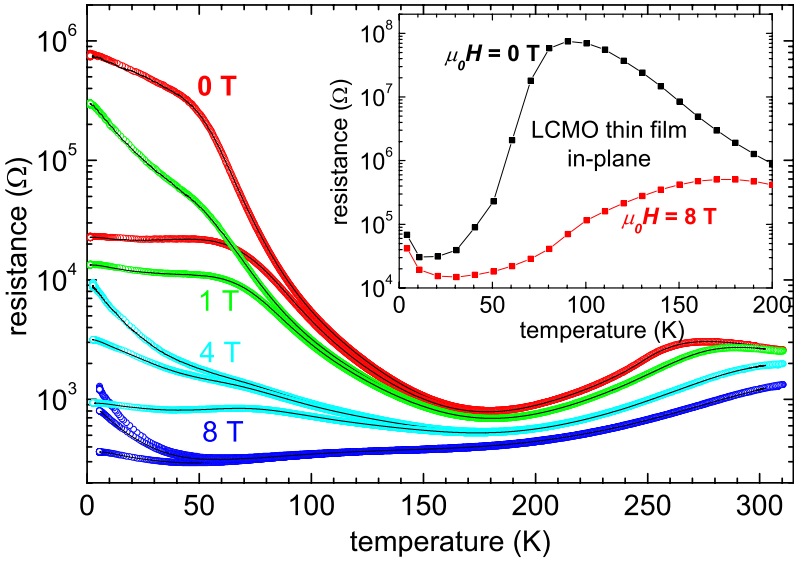

Figure 2: Resistance vs temperature for different magnetic fields and currents. The symbols (full lines) represent data measured during cooling (heating). The inset shows the resistance behavior of a LCMO thin film for in-plane direction.

Recently, the phase diagram of the doped manganites has been analyzed as a function of a tetragonal lattice distortion. Such distortion is present in our biaxially strained LCMO films ($c/a \simeq 0.985$). It has been shown that biaxial strain can induce orbital ordering resulting in different spin structures, such as ferromagnetic (F), layer-type antiferromagnetic (A) and chain-type antiferromagnetic (C) states and, hence, different magnetotransport characteristics [14, 20]. For tensile strain ($c/a < 1$, as present in our samples), a transition from the conventional double exchange mediated, orbital disordered ferromagnetic (F) state to the orbital ordered antiferromagnetic (A) state, which is composed mainly by $d_{x^2-y^2}$ states, is expected. Whereas in the F state the spins are aligned parallel in adjacent planes, in the A state a anti-parallel orientation of the ferromagnetically ordered planes is present. That is, the gradual transition from the F to the A state is accompanied by a strong reduction of saturation magnetization in agreement with the strongly reduced value obtained in our experiments. Furthermore, the A-type antiferromagnetic state can be metallic only within the ferromagnetically ordered plane, but is insulating in perpendicular direction. This again is in agreement with our experimental observation. That is our data can be interpreted naturally by a strain induced orbital ordering at fixed doping.

Our results are important also with respect to artificial magnetic heterostructures composed of doped manganites for spintronic devices. It shows that beyond interface and phase separation effects, the substrate induced strain can induce insulating phases. Such insulating phases of the doped manganites may be used as tunneling barriers in ferromagnetic tunnel junctions employing electrodes of ferromagnetic (metallic) doped manganites.

References

[1] C. Zener, Phys. Rev. **82**, 403 (1951); P. W. Anderson and H. Hasegawa, Phys. Rev. **100**, 675 (1955).
[2] A. J. Millis, P. B. Littlewood, and B. I. Shraiman, Phys. Rev. Lett. **74**, 5144 (1995); A. J. Millis, B. I. Shraiman, and R. Mueller, Phys. Rev. Lett. **77**, 175 (1996).
[3] H. Y. Hwang, T. T. M. Palstra, S.-W. Cheong, and B. Batlogg, Phys. Rev. B **52**, 15046 (1995).
[4] A. J. Millis, T. Darling, and A. Migliori, J. Appl. Phys. **83**, 1588 (1998).
[5] Yafeng Lu, J. Klein, C. Höfener, B. Wiedenhorst, J. B. Philipp, F. Herbstritt, L. Alff, and R. Gross, Phys. Rev **B 62**, 15806 (2000).
[6] Amlan Biswas, M. Rajeswari, R. C. Srivastava, Y. H. Li, T. Venkatesan, R. L. Greene, and A. J. Millis, Phys. Rev. B **61**, 9665 (2000).
[7] Amlan Biswas, M. Rajeswari, R. C. Srivastava, T. Venkatesan, R. L. Greene, Q. Lu, A. L. de Lozanne, and A. J. Millis, Phys. Rev. B **63**, 184424 (2001).
[8] H. L. Ju, Kannan M. Krishnan, and D. Lederman, J. Appl. Phys. **83**, 1588 (1998).
[9] H. W. Zandbergen, S. Freisem, T. Nojima, and J. Aarts, Phys. Rev. B **60**, 10259 (1999).
[10] J. Z. Sun, D. W. Abraham, R. A. Rao, and C. B. Eom, Appl. Phys. Lett. **74**, 3017 (1999).
[11] M. G. Blamire, B.-S. Teo, J. H. Durrell, N. D. Mathur, Z. H. Barber, J. L. McManus Driscoll, L. F. Cohen, and J. E. Evetts, J. Magn. Magn. Mater. **191**, 359 (1999).
[12] Moon-Ho Jo, N. D. Mathur, J. E. Evetts, M. G. Blamire, M. Bibes, and J. Fontcuberta, Appl. Phys. Lett. **75**, 3689 (1999).
[13] J. Klein, C. Höfener, L. Alff, and R. Gross, J. Magn. Magn. Mater. **211**, 9 (2000); see also Supercond. Sci. Technol. **12**, 1023 (1999).
[14] Y. Konishi, Z. Fong, M. Izumi, T. Manako, M. Kasai, H. Kuwahara, M. Kawasaki, K. Terakura, and Y. Tokura, J. Phys. Soc. Jpn. **68**, 3790 (1999).
[15] K. Dörr, J. M. De Teresa, K.-H. Müller, D. Eckert, T. Walter, E. Vlakhov, K. Nenkov, and L. Schultz, J. Phys.: Condens. Matter **12**, 7099 (2000).
[16] J.-H. Park, E. Vescovo, H.-J. Kim, C. Kwon, R. Ramesh, and T. Venkatesan, Phys. Rev. Lett. **81**, 1953 (1998).
[17] M. J. Calderón, L. Brey, and F. Guinea, Phys. Rev. B **60**, 6698 (1999).
[18] J. Klein, J. B. Philipp, G. Carbone, A. Vigliante, L. Alff, R. Gross, submitted to Phys. Rev. Lett.
[19] J. Klein, J. B. Philipp, D. Reisinger, L. Alff, and R. Gross, to appear in phys. stat. sol. (a) **189** (2002).
[20] Z. Fang, I. V. Solovyev, and K. Terakura, Phys. Rev. Lett. **84**, 3169 (2000).

Calorimetric Study ($0.025 < T < 2$ K, $0 < B < 1$ T) of the Non-Liquid-Fermi System $YbRh_2(Si_{1-x}Ge_x)_2$ for $x = 0$ and 0.05

Ch. Langhammer, MPI für CPfS Dresden, and K. Neumaier, WMI

The study of quantum critical phenomena in f-electron-based systems attracts currently considerable attention since pronounced deviations from the properties of a Landau Fermi-liquid (LFL) were observed, mostly in Ce-based heavy-fermion (HF) metals, close to an antiferromagnetic quantum critical point (QCP). Generally, a control parameter such as the degree of alloying or hydrostatic pressure is used to tune these materials through a magnetic instability at which the ordering temperature $T_N \Rightarrow 0$. Up to now, the observation of "non-Fermi-liquid" (NFL) effects in undoped compounds at ambient pressure is restricted to only a few prototypical HF-metals.

$Yb_2Rh_2Si_2$ is the first stoichiometric Yb-based intermetallic compound with pronounced NFL effects already at ambient temperature and zero field with a magnetic phase transition at a very low $T_N \approx 70$ mK ascribed to quasi-2D spin fluctuations. Therefore, $Yb_2Rh_2Si_2$ offers one of the few opportunities to study thermodynamic quantities (such as specific heat) of a HF-metal close to the QCP. A full thermodynamic characterization is indispensable to determine the intrinsic nature of the anomalous behavior observed e.g. in the electrical resistivity. Upon applying hydrostatic pressure T_N increases and allows one – by extrapolating to negative pressures – to define a critical pressure $p_c \approx -0.3$ GPa, which correspond to a tiny volume expansion of only $\Delta V \approx +0.3\%$. This low value of ΔV suggests that T_N can be suppressed to $T \Rightarrow 0$ by expanding the crystal lattice, e.g. by alloying the Si-sites with isoelectronic Ge. The evolution of the unit-cell volume of $YbRh_2(Si_{1-x}Ge_x)_2$ with increasing x indicates that ΔV correspond to a critical Ge-concentration of only $x_c = 0.06$. Thus slightly doping $Yb_2Rh_2Si_2$ with Ge is expected to tune this material to its QCP without affecting its electronic properties and, due the low value of x_c, without introducing significant disorder to the lattice. The $\rho(T)$ data of $YbRh_2(Si_{0.95}Ge_{0.05})_2$, i.e. for x very close to x_c, exhibit a linear temperature dependence above 10 mK over a surprising large temperature range of three decades. The ac-magnetic susceptibility of $YbRh_2(Si_{0.95}Ge_{0.05})_2$ shows no phase transition down to 10 mK indicating that it is close to the QCP. The value of the residual resistivity of this compound is only by a factor of three larger than that of the undoped $Yb_2Rh_2Si_2$, strongly suggesting that the extended linear behavior of $\rho(T)$ is due the proximity of $YbRh_2(Si_{0.95}Ge_{0.05})_2$ to the QCP and not an effect of disorder introduced by Ge-doping.

The specific heat of a $Yb_2Rh_2Si_2$ sample weighing 3.6 mg and of two $YbRh_2(Si_{0.95}Ge_{0.05})_2$ samples weighing 21 and 74 mg, respectively, has been measured using the quasi-adiabatic heat pulse method with a computer-controlled setup in the temperature range from 25 mK to 2 K and in magnetic fields up to 1 T.

For $B = 0$ and $T > 200$ mK the results of the pure and doped samples agree within the experimental error and show for the specific heat coefficient γ a nearly logarithmic dependence $C/T \propto -\ln T$ as expected for NFL systems. Below 200 mK an additional upturn appears in C/T. The pure sample shows a large λ-like anomaly with a peak value of $C/T = 3.46$ J/molK^2 for $T = 75$ mK due to the expected antiferromagnetic (AF) transition. Below 40 mK, C/T levels off in a constant value of 2.0 J/molK^2. For the doped samples the upturn continues down to the lowest temperatures, indicating an antiferromagnetic transition at a finite temperature below the temperature range of our calorimeter. The difference in the experimental results below 60 mK for the two doped samples may be due to different sample qualities or experimental difficulties. Application of magnetic fields $B \| c$ shift the AF-transition to lower temperatures and for $B = 0.3$ T the transition is completely suppressed. Fields $B > 0.3$ T for $Yb_2Rh_2Si_2$ and $B > 0.1$ T for $YbRh_2(Si_{0.95}Ge_{0.05})_2$ lead to a field induced LFL state below some cross-over temperature which increases with B.

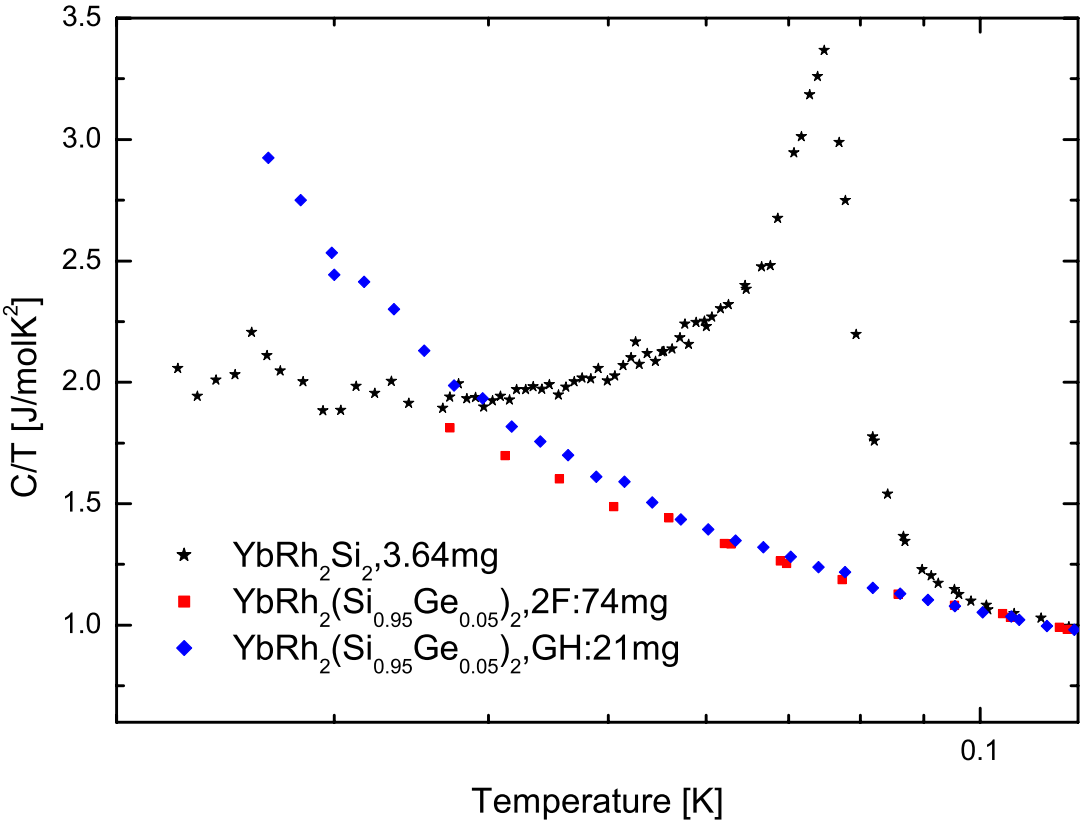

Figure 1: Specific heat versus temperature for three samples.

The specific heat results confirm that $YbRh_2(Si_{0.95}Ge_{0.05})_2$ is located close the QCP, but further measurements with an improved experimental setup (thermometer, thermal contact and a lower base temperature) are required to determine the exact transition temperature.

Nuclear Magnetic Resonance on ^{3}He Nano-Clusters and Solid ^{3}He in a Silver Sinter

Erwin A. Schuberth[1], Frank Deppe[1],Carmen Millan[1], Naoki Matsunaga [2], and E. Dwight Adams[2 1]

Simultaneous measurements of magnetic susceptibility and pressure have been done in ^{3}He nano-clusters embedded in a ^{4}He matrix and in solid ^{3}He in a silver sinter. Pressures ranged from 2.88 MPa to 3.54 MPa, the latter well above the melting curve at T=0. Even at the lowest pressure which is below the melting curve the clusters have a solid fraction of about 25 %. At intermediate pressures we find a peak in χ near 1.1 mK, but with no discontinuity as in bulk ^{3}He. Thus the nuclear magnetic ordering in nanoclusters is different than the U2D2 phase of the bulk material. Solid ^{3}He in a silver sinter of 700 Å particle size has been cooled to 2.5 mK. A very strong nmr signal has been detected, but temperatures were not low enough, to see if a single crystal can be formed in the sinter pores.

Recent studies of solid and liquid clusters have shown that their properties are quite different from those of bulk condensed matter. For example, metal nanoclusters have discrete electronic spectrum structures, which indicate that the magnetic and thermodynamic properties of nano-sized particles with even and odd number of conduction electrons are quite different from each other and from the bulk metal. Nuclear magnetism of 2D films of ^{3}He on a Grafoil substrate is quite different from that in bulk bcc ^{3}He . Direct particle exchange is responsible for exotic phases in the 2D films, where a competition between multi-particle exchange processes leads to frustration [1]. Pure bulk bcc ^{3}He orders antiferromagnetically at 0 .9 mK in a so called U2D2 magnetic structure in low magnetic fields wit a second ordered phase, thought to be a canted antiferromagnet, above 0.45 T.

The best available model up to now is direct multi-particle exchange in the bcc lattice [2] which leads to a similar phase diagram as is observed experimentally, although with extra phase lines and quantitatively different. This shows that even the ”simplest Heisenberg magnet of the world” nuclear magnetism in solid ^{3}He is not fully understood and more experiments in different magnetic fields, at different pressures, and in different geometries are necessary. ^{3}He nano-clusters can be formed in metallic sinters of small pore sizes (700 Å) from a mixture of a small concentration (1%) ^{3}He in ^{4}He where the size and the state depends on the initial ^{3}He concentration and the external pressure. For small ^{3}He concentrations all solid, partially liquid, or totally liquid nano-clusters are produced at various growth pressures. The experiment is described in more detail by Naoki Matsunaga et al. [3].

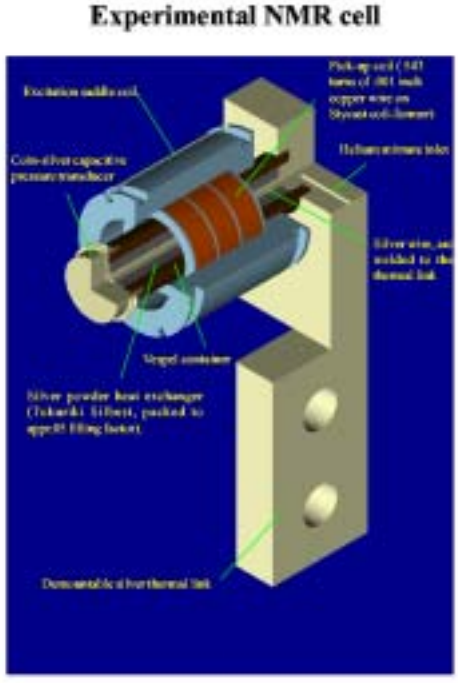

Fig.1: Experimental cell to study nano-sized solid ^{3}He particles embedded in a ^{4}He matrix cooled in a 700 Å silver sinter.

In cooperation with the microKelvin group in Gainesville, Florida, we have studied the magnetic

[1]Walther-Meissner-Institut, Garching, [2]University of Florida

susceptibility of ^{3}He nano-clusters at pressures ranging from 2.88 to 3.54 MPa. The experimental cell used to cool the mixtures is shown in Fig. 1. It contains a sinter of the above mentioned pore size in which the clusters assume an average size of 20 nm. They are embedded in the solid ^{4}He matrix rather than attached to the metal surface.

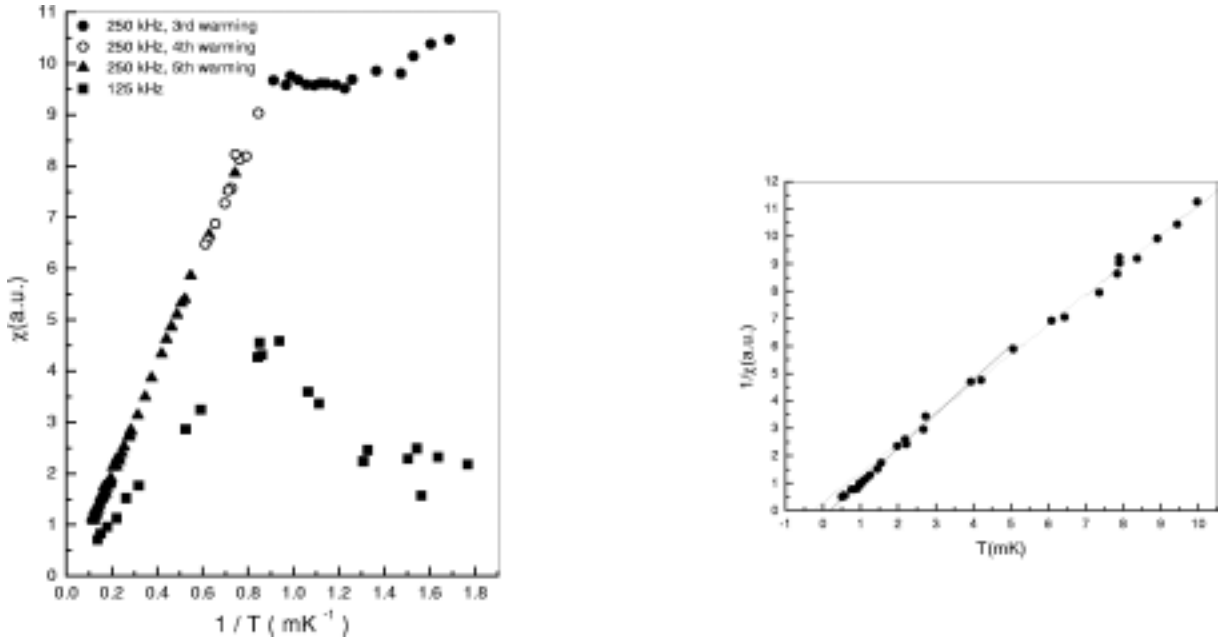

Fig.2 shows the NMR signal intensities after Fourier Transformation of the free induction decay, 3.54 MPa sample. They are proportional to the magnetization of the ^{3}He nano-clusters and have a kink at the solid ordering at 0.9 mK, quite different from the bulk transition, which points to a novel type of magnetism in this restricted geometry. The right part shows inverse χ vs temperature indicating a slightly positive Weiss Θ, also different from the bulk behavior.

Fig. 3: Experimental cell used to cool solid ^{3}He in a silver sinter with an internal NMR coil.

Fig. 3 gives a view on the silver cell with an internal nmr coil used in the Walther Meissner Institut to cool solid ^{3}He, again in a sinter of 700 Å pore size. Up to now a lowest temperature of 2.5 mK has been achieved. The purpose of the experiment is to produce a single crystal inside the sinter and demonstrate its existence by the occurrence of unique nmr lines in the U2D2 phase. A single crystalline sample shall be used for neutron scattering studies of the ordered phases which are under way in cooperation with the Hahn-Meitner Institut, Berlin and 5 other European and US members of a Research and Training Network financed by the European community.

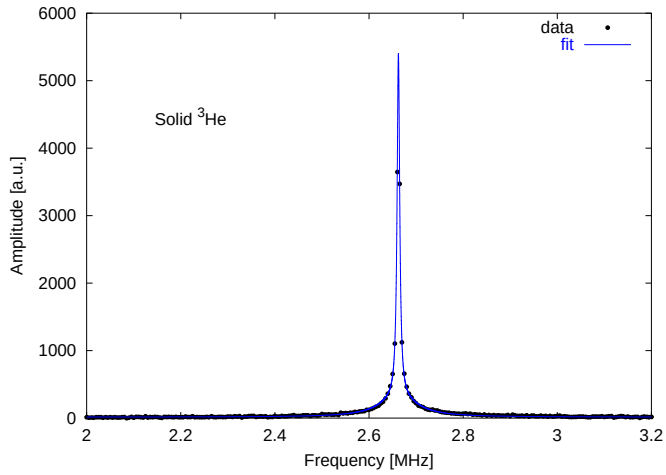

Fig.4: NMR spectrum of solid ^{3}He in a 700 Å silver sinter at T= 3mK

Very recently we obtained the first NMR spectrum from solid ^{3}He in our silver cell at the presently lowest temperature of 3 mK reached 20 hours after the demagetization of the nuclear stage. The experiments are continuing.

We gratefully acknowledge financial support by EU and DAAD

References

[1] M.Roger, C.Bärle, Yu.M.Bunkov, A.S. Chen, and Henri Godfrin, Phys. Rev. Lett. **80**, 1308 (1998)
[2] M. Roger, Review of Modern Physics, **55**, 1 (1983)
[3] N. Matsunaga, V.A. Shvarts, E.D. Adams, J.S. Xia, and E.A. Schuberth, Phys. Rev. Lett. **86**, 2365 (2001)

Electronic Transport in Submircon HTS Grain Boundary Junctions

F. Herbstritt, T. Kemen, A. Marx, R. Gross [1]

HTS grain boundary junctions (GBJ) show a high level of $1/f$ noise. To elucidate the origin of these low frequency fluctuations we have fabricated $YBa_2Cu_3O_{7-\delta}$ (YBCO) grain boundary junctions with cross-sectional areas down to $0.002\,\mu m^2$. The quasiparticle transport characteristics of these junctions display a crossover from Andreev reflection dominated transport for low misorientation angle to tunneling-like behavior for large angles [1]. In the current voltage characteristics we observed a novel reproducible step-like feature in the vicinity of the critical current. This feature is due to the special geometry of the nanosized junctions resulting in large values of the kinetic inductance of the electrodes inversely proportional to the junction cross section area [2].

Sample preparation

The junctions have been fabricated by patterning 20 to 30 nm thick YBCO films on $SrTiO_3$ bicrystal substrates using a multistep combined photo- and electron beam lithography process [3] (cf. figure 1). The patterning process usually resulted in a severe decrease of T_c and I_c as well as an increase of the junction resistance due to the high sensibility of the cuprate material to structural damage and oxygen loss. By applying an ultra-violet light assisted post oxygenation process at 160° C the transport properties could be almost restored to the values of the unpatterned films. The effeciency of this oxidation process becomes evident in the current voltage characteristics of a 280 nm wide and 22 nm thick GBJ depicted in fig. 2. By thoroughly optimizing the patterning process we were able to fabricate superconducting grain boundary Josephson junctions with lateral dimensions down to 100 nm [3, 4]. These are to our knowledge the junctions with the smallest area ever reported.

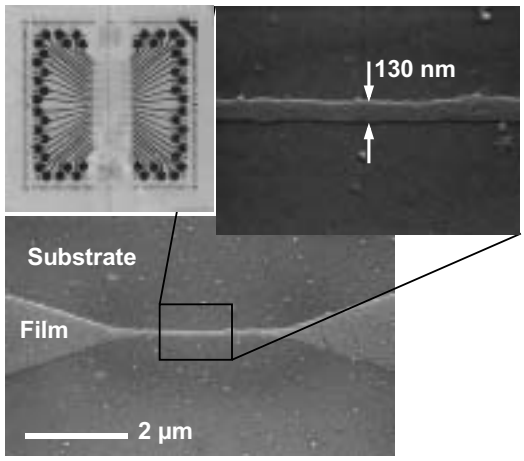

Figure 1: Scanning electron micrograph of a 130 nm wide grain boundary junction.

Current Voltage Characteristics

A characteristic and very reproducible feature of the current voltage characteristics (IVC) of the submicron sized junction is the step-like structure depicted in figs. 2 and 3. Extensive characterizations of this effect give strong evidence that the structure is due to a *LC* resonance which in turn is caused by the large kinetic inductance of the narrow electrodes and the relatively high junction capacitance due to stray field contributions of the substrate material with its high dielectric constant

An important signature of the submicron sized GBJs is the large kinetic inductance of the electrodes which can be estimated to $L_{kin} = \mu_0 \lambda^2 l/A$ where λ is the London penetration depth and l is the electrode length. The inverse dependence on the junction area A immediately shows the importance of I_{kin} for the small junctions. If this large kinetic inductance is capacitively shunted in parallel to the the junction (cf. fig. 4) the dynamics of the Josephson junction is strongly modified [5, 6, 2]. Both simple estimates based on the sample geometry and numerical simulations of its frequency response showed that the capacity of the leads effectively shorts the junction in the relevant frequency range. The impedance Z_p and L_{kin} (cf. fig. 4) form together with the capacity C of the junction a parallel resonant circuit which is excited by the

[1] In collaboration with B. Chesca and R. Kleiner, University of Tübingen, Germany.

This work is supported by the Deutsche Forschungsgemeinschaft.

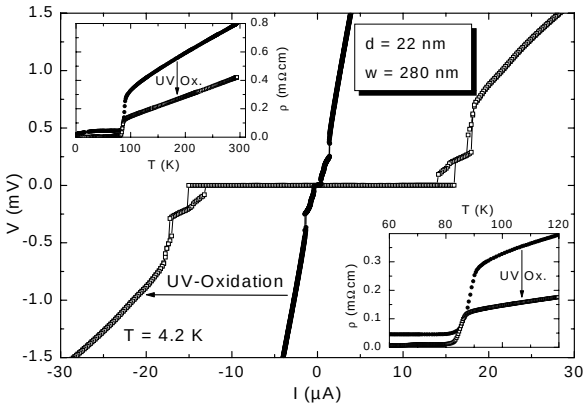

Figure 2: Current voltage characteristics of a 280 nm wide 66° GBJ before and after the ultra-violet light assisted annealing step. The inset shows the resistive transition.

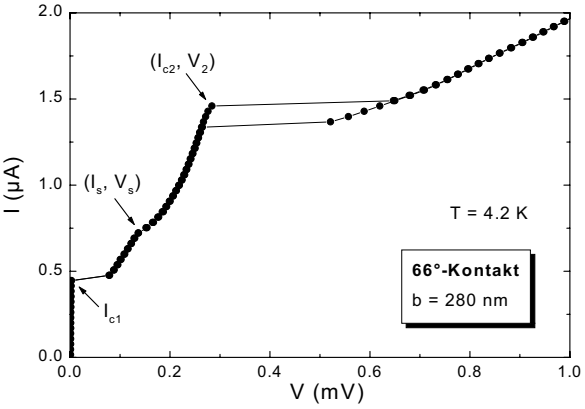

Figure 3: Current voltage characteristics of a 280 nm wide 66° GBJ in the vicinity of the critical current showing a characteristic step-like structure.

ac-Josephson current. In the resistive state the junction acts as an oscillator which couples microwave power into the LC resonator. Close to the resonance frequency $\omega_r = (1/(L_{kin}C) - 1/(2R_nC)^2)^{1/2}$ the resonator re-acts on the junction with a phase shift of $\pi/2$. The interplay of the Josephson oscillations and the *LC* resonator results in an additional dc component of the supercurrent [5, 6] (in the case of external microwave radiation the appearance of Shapiro steps is well known). The amplitude of the dc Josephson current depends on the amplitude of the ac voltage across the junction and on the phase difference between this ac voltage and the ac component of the supercurrent. A model calculation for the appearance of the step structure in the IVCs based on the *LC* resonance model taking into account the critical current and the instability of the resonant branch is depicted in fig. 5 [4]. For voltages above the the resonance voltage V_r the solutions for the additional dc supercurrent become unstable and the junction escapes from the resonant state to the normal conducting branch of the IVC for increasing current. For decreasing current the normal branch is traced back until point C is reached where the junction crosses over to the resonant state. The model of self-induced *LC* resonances provides a good qualitative and quantitative description of the experimentally observed features in the submicron junctions [4].

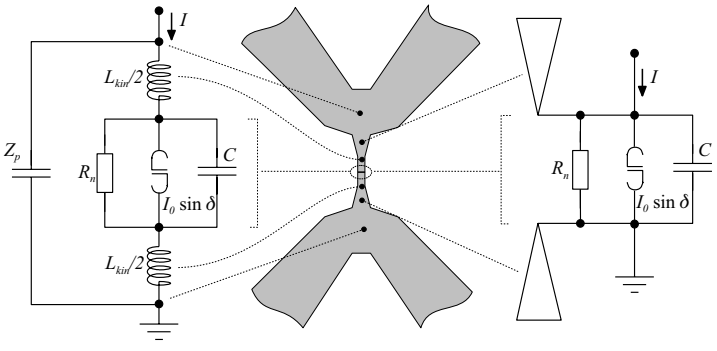

Figure 4: LC resonance model for submicron sized junctions. The junction is shorted by the impedance and inductance of the leads (left). Alternatively, the leads and electrodes can be regarded as antennas (right).

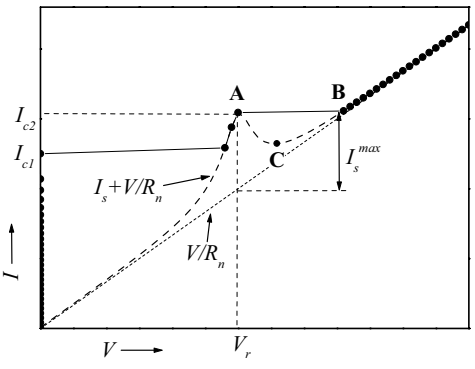

Figure 5: Modeling the step-structure in the LC resonance model. The circles indicate the IVC taking into account the junction critical current and the instability of the resonant branch between points A and B.

Low Frequency Noise

The low frequency voltage fluctuations of the small junctions are dominated by individual switching processes between pairs of discrete conductance levels with an exponential distribution of lifetimes (TLF:

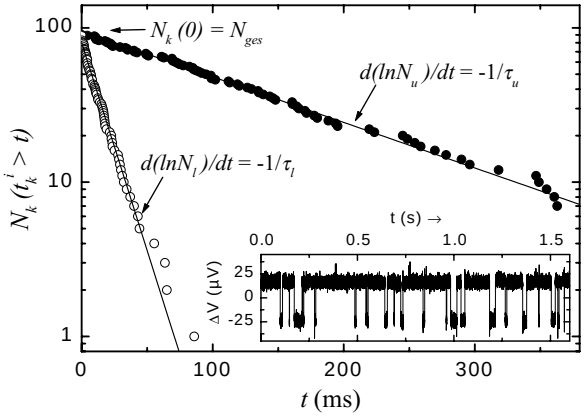

Figure 6: Two level switching of the junction voltage (inset). The individual lifetimes in the upper and lower state are exponentially distributed.

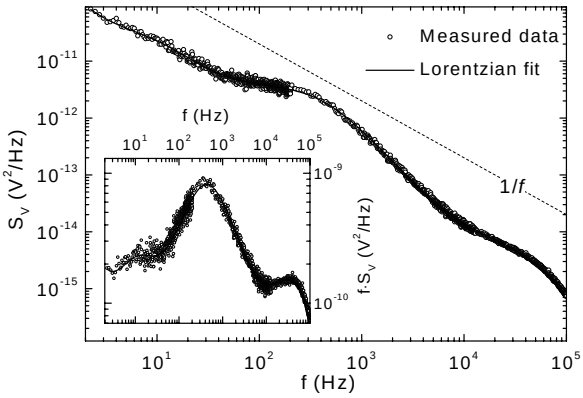

Figure 7: The noise spectrum of the small junctions consists of a few Lorentzian contributions from single two level fluctuators.

two level fluctuators, cf. fig. 6). Therefore, the noise spectra essentially consist of a superposition of a few Lorentzian contributions, each caused by an individual TLF (cf. fig. 7). The avearge transition rates between the levels increase exponentially with applied bias voltage (cf. fig. 8) and show a thermally activated behavior above a transition temperature around 5 - 15 K. Below this temperature the rates are temperature independent (cf. fig. 9). The voltage dependence of the rates decreases with increasing temperature. In some cases interactions between the fluctuators are observed within narrow ranges of the parameter space (V, T).

This behavior of the resistance fluctuations can be well understood as being caused by the trapping and releasing of single charge carriers at defect states within the grain boundary region. A model for such trapping sites, originally developed by Rogers and Buhrman [7] gives a good quantitative agreement with the data, assuming reasonable values for the parameters describing the barrier. Discrepancies of the model concerning the amplitude of the observed conductance fluctuations may be attributed to a considerable inhomogeneity of the barrier transmissivity on a length scale of a few nanometers.

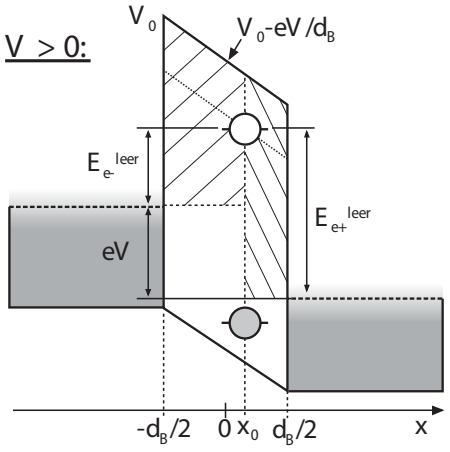

Figure 8: Voltage dependence of the mean lifetimes in the upper and lower voltage state.

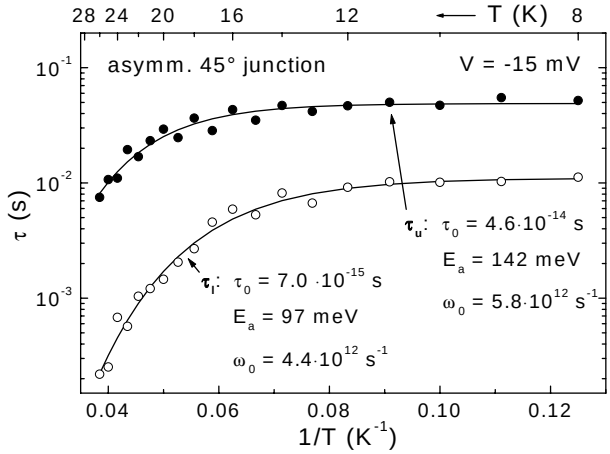

Figure 9: Temperature dependence of the mean lifetimes in an Arrhenius graph. At ~ 18 K the switching changes from tunnelling-like to thermally activated.

References

[1] F. Herbstritt, T. Kemen, L. Alff, A. Marx, and R. Gross, Appl. Phys. Lett. **78**, 955 (2001).

[2] B. Chesca, in preparation (2002).
[3] F. Herbstritt, T. Kemen, A. Marx, and R. Gross, submitted to J. Appl. Phys. (2001).
[4] F. Herbstritt, Ph.D. thesis, Univesity of Cologne (2002).
[5] N. R. Werthammer, Phys. Rev. **146**, 255 (1966).
[6] K. K. Likharev, *Dynamics of Josephson Junctions and Circuits*, Gordon and Breach, New York (1986).
[7] C. T. Rogers, PhD Thesis, Cornell University (1987)

Electronic Transport in Normal Metal–Superconductor Systems

T. Kemen, A. Marx, R. Gross [1]

Phase coherence of the charge carriers in mesoscopic systems gives rise to various quantum interference effects. Universal conductance fluctuations (UCF) are a prominent realization of this quantum interference. These fluctuations are of the order of $\delta G \sim e^2/h$ and are manifested by reproducible aperiodic magnetoconductance patterns (magnetic fingerprint). The presence of a superconducting electrode strongly modifies the quantum interference in the normal conductor. The *proximity effect* describes superconducting-like properties of a mesoscopic normal metal (N) placed in electrical contact with a superconductor (S). The proximity effect is the result of an interplay between the process of Andreev reflection at the NS interface and long-range phase coherence in the normal metal. The phase coherence length L_φ defines the characteristic length scale of the proximity effect which results in a strong modification of the electronic transport properties of the normal metal. Although the proximity effect has been known for many years its impact on a mesoscopic length scale has only recently become the focus of a large number of theoretical and experimental studies [1]. An important consequence of the long-range proximity effect is the reentrance of the normal state conductance at low energies [2, 10]. Furthermore, since the process of Andreev reflection generates additional intereference effects between electrons and retro-reflected holes in N the amplitude of the UCF changes (increase or decrease depending on the sample geometry) [3, 4, 5]. Usually the transparency of the NS interface in real samples is smaller than the optimal value of one. Then, the process of reflectionless tunneling [6, 7] becomes of increasing importance.

The spectral conductance of the NS samples we have investigated show all signatures of the proximity effect: reentrant behavior at low energies and reflectionless tunneling due to specular reflection at the sample surface. Furthermore, in addition to the previously shown increase of the UCF amplitude in samples with a 2-contact geometry [5] we could for the first time find experimental evidence for a *decrease* of the fluctuation amplitude in samples with 4-contact geometry [4].

Sample preparation and experimental techniques

The N-S samples have been fabricated in a multistep process using standard thin film deposition techniques (sputtering and electron beam evaporation) and electron beam lithogragphy (EBL). We have investigated two processes with different sequences of the deposited films. In an *in-situ* process the niobium electrode was sputter deposited and immediately covered by a thin gold film. After the definition of a lift-off mask by EBL the mesoscopic gold wire was deposited. In the *ex-situ* process the Au wire was fabricated first. After an ion beam cleaning process the niobium electrode was prepared in a second deposition step. The in-situ process resulted in smaller interface resistances whereas the fringes along the border of the Nb film which are observable in the scanning eletron micrograph did not pose any problems in the ex-situ process. For samples with 3- and 4-contact geometry (cf. insets of figs. 3 and 4) there is

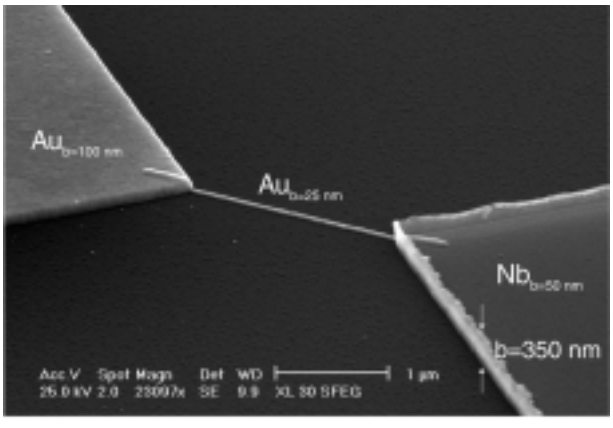

Figure 1: Scanning electron micrograph of a mesoscopic gold nanowire with Au and Nb electrodes. The fringes along the border of the Nb eletrode are due to the sputter deposition process.

[1] In collaboration with T. Bauch, University of Cologne, Germany, and F. Wilhelm, LMU Munich, Germany.
This work has been supported by the Deutsche Forschungsgemeinschaft.

no current flow across the interface. Therefore, the interface resistance does not influence the quantum interference.

Spectral conductance

The spectral conductance of the in-situ NS sample in fig. 2 shows the reentrance behavior for voltages below 200 μV. The fit also depicted in fig. 2 based on the one-dimensional quasiclassical nonlinear Usadel equation [8, 9, 10] gives a good agreement with the experimental data yielding reasonable values for the transparency T and Thouless energy E_{Th}. Deviations from the quasi-classical theory often showed up for samples in 2-contact geometry. We could demonstrate by means of extensive numerical simulations based on a semiclassical model that these deviations are due to the process of reflectionless tunneling caused by specular reflections at the surface and Andreev reflection at the NS interface in the quasi-ballistic overlap region of the mesoscopic wire and the superconducting electrode.

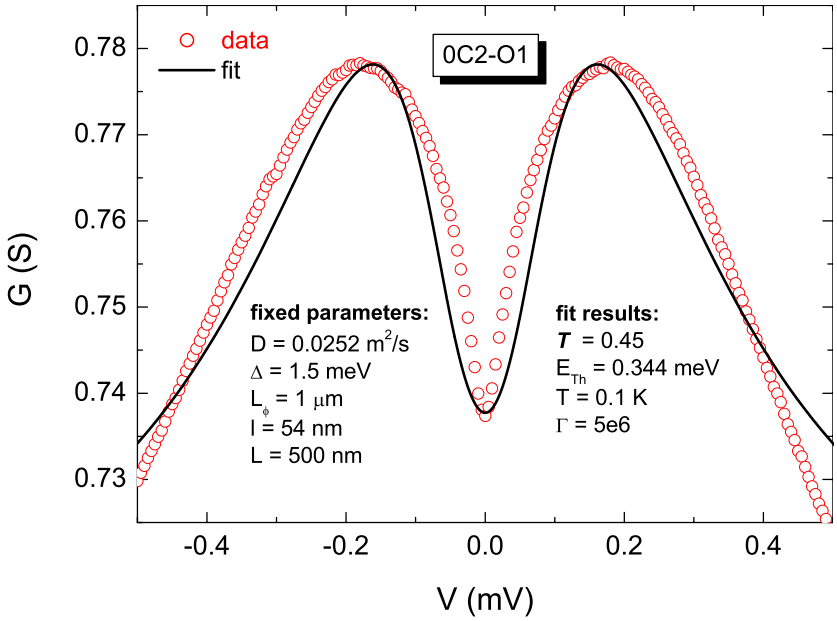

Figure 2: Differential conductance of an in-situ prepared NS sample together with a fit of the one-dimensional quasiclassical theory.

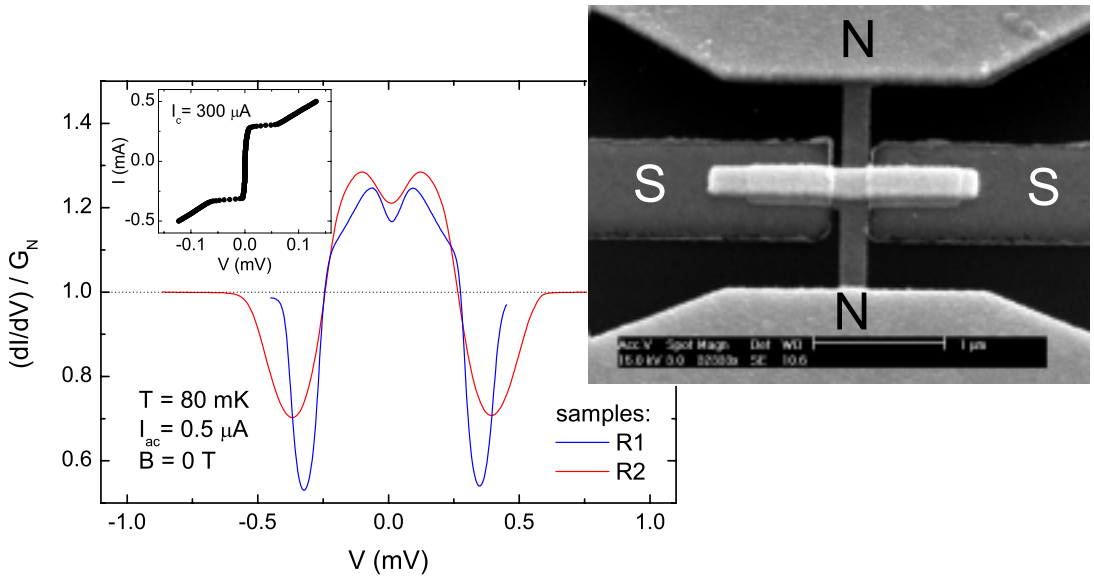

Figure 3: Normalized differential conductance of two samples in four-contact geometry. The inset shows the current voltage characteristics measured between the two superconducting electrodes.

The normalized differential conductance for two samples in 4-contact geometry shown in fig. 3 (the geometry of one of the samples is displayed in the scanning electron micrograph) also depicts the typical spectral conductance for voltages $V < 200\,\mu$V. The inset shows the SNS-type current voltage charac-

teristics following the behavior of the resistively shunted junction (RSJ) model measured between the superconducting electrodes.

Universal conductance fluctuations

The deviations $\Delta G = G(B) - \langle G \rangle$ of the conductance $G(B)$ from the mean value $\langle G \rangle$ measured as a function of an applied magnetic field B in a mesoscopic conductor have a magnitude of the order $\mathrm{rms}(G) = \langle (G - \langle G \rangle)^2 \rangle^{1/2} \simeq e^2/h$ (UCF). In the presence of a superconductor the amplitude of the UCF is modified [3, 4, 5]. By applying a magnetic field larger than the upper critical field of the superconductor B_{c2}^{Nb} the system is driven normal conducting and displays the UCF of the corresponding normal system. Thus it is possible to investigate the influence of the superconductivity on the UCF in *a single sample*. Figure 4 displays the magnetoconductance fluctuations of two 3-contact samples after subtraction of the mean conductance. The rms amplitude of these data has been evaluated in the NS and in the N state. The ratio of the normalized fluctuations $\mathrm{rms}(G_{NS})/\mathrm{rms}(G_N)$ for several samples with 3- and 4-contact geometry are depicted in fig. 5. The horizontal line illustrates the theoretically predicted reduction for the 4-contact geometry [4]. The experimental data for the 4-contact samples are in good agreement with the theoretical prediction whereas the experimentally observed increase of the fluctuation amplitude for the 3-contact samples is in contradiction with theory.

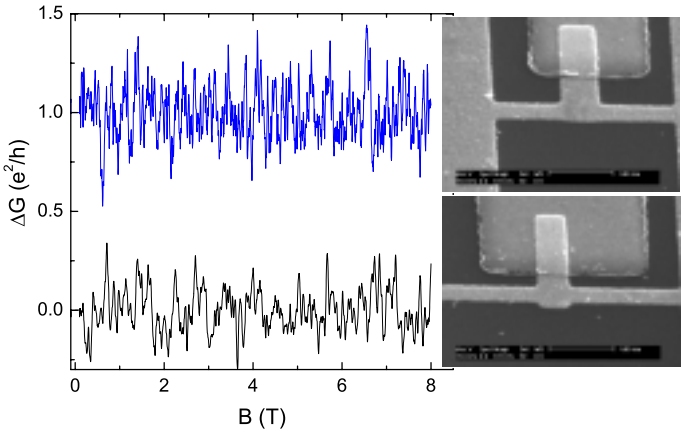

Figure 4: Magnetoconductance fluctuations for two samples in three-contact geometry. The upper curve has been displaced by e^2/h.

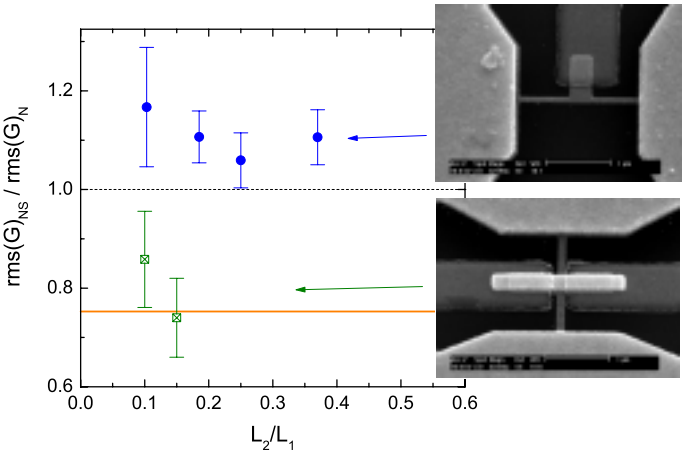

Figure 5: Amplitude of the normalized magnetoconductance fluctuations for different samples with three- and four-contact geometry.

References

[1] S. Gueron, H. Pothier, N. O. Birge, D. Esteve, M. H. Devoret, Phys. Rev. Lett. **77**, 3025 (1996).
[2] P. Charlat, H. Courtois, P. Gandit, D. Mailly, A. F. Volkov, and B. Pannetier, Phys. Rev. Lett. **77**, 4950 (1996).
[3] A. Altland and M. R. Zirnbauer, Phys. Rev. B **55**, 1142 (1997).
[4] T. T. Heikkilae, M. M. Salomaa, and C. J. Lambert, Phys. Rev. B **60**, 9291 (1999).
[5] K. Hecker, H. Hegger, A. Altland, and K. Fiegle, Phys. Rev. Lett. **79**, 1547 (1997).
[6] B. J. van Wees, P. de Vries, P. Magnee, T. M. Klapwijk, Phys. Rev. Lett. **69**, 510 (1992).
[7] I. K. Marmorkos and C. Beenakker, Phys. Rev. B **48**, 2811 (1993).
[8] K. D. Usadel, Phys. Rev. Lett. **25**, 507 (1970).
[9] W. Belzig, F. K. Wilhelm, C. Bruder, G. Schön, and A. D. Zaikin, Superlatt. Microstruct. **25**, 1251 (1999).
[10] H. Courtois, P. Charlat, P. Gandit, D. Mailly, and B. Pannetier, J. Low Temp. Phys. **116**, 187 (1999).

Single Electron Charging Effects in Metallic Nanostructures

J. Schuler, C. Probst, A. Marx, R. Gross

In our technological world electronic devices which are based on quantum effects attain increasing importance. Due to the ongoing reduction of lateral dimensions in the field of semiconductor technology quantum effects must be taken into account in advanced future designs. Apart from the technological constraint they pose a rich field of very interesting scientific aspects and very promising possible applications.

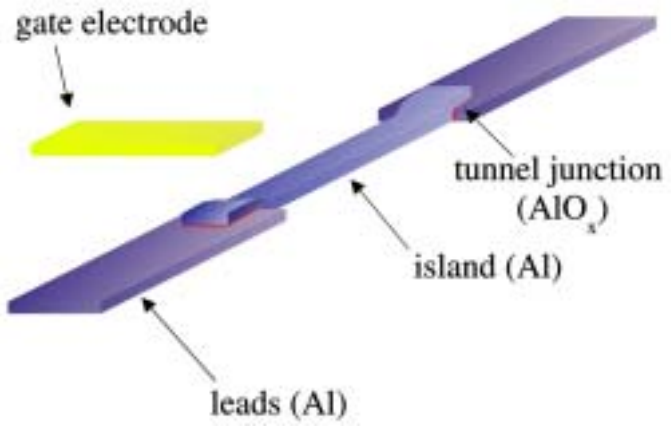

Figure 1: Sketch of a typical Single Electron Transistor (SET).

One of the most promising devices based on quantum effects is the single electron transistor (SET), which exploits the discreteness of the elementary charge. It consists of two tunnel junctions and a capacitively coupled gate electrode. As the region between the two tunnel junctions is only weakly connected to the rest of the electrical circuit, it is usually referred to as the *island* of the SET. The number of excess charge carriers on the island n (additional or missing electrons) always is an integer number. Apart from – almost always undesirable – parasitic effects, the electrical transport through the SET can only be established by electrons tunneling through both junctions separately [1]. Therefore, the number of electrons on the island n is continuously changed during the transport process. By applying a voltage to the gate electrode the energy levels of the electronic states on the island can be changed, and thus the transport of electrons through the device can be drastically influenced. For sufficiently low voltages applied across the two junctions tunneling of electrons across the device can be blocked due to the charging energy of the electron(s) on the island (*Coulomb blockade*).

To observe charging effects of single electrons the involved energy scale of the charging effects has to be sufficiently large compared to rivaling effects such as thermal excitations. The underlying energy scale for single charging effects is the Coulomb energy E_C, so that

$$E_C = \frac{e^2}{2C} \gg k_B T \quad , \tag{1}$$

where e is the electron charge, C the total SET capacitance, k_B the Boltzmann constant and T the temperature. For an Al/AlO$_x$/Al-tunnel junction with total capacitance in the range of 1 fF, the charging energy corresponds to a temperature of 1 K, so that, in oder to satisfy eq. (1) and to minimize the effects of thermal excitations, it is necessary to investigate SET effects at temperatures in the mK regime and/or to fabricate devices with a very small total capacitance.

Apart from the standard SET there is a great variety of SET-like structures e.g. a SET with ferromagnetic components (island and/or leads), single electron pumps, charge qubits etc.

Sample Preparation

The preparation of SET-structures is obtained by a mix&match electron beam lithography process. In a first process step auxiliary structures (alignment marks, optional bond pads, and the leads) are patterned using a standard optical lithography process with subsequent metallization. After the lithography process, first an optional 5 nm thick Cr layer and a 50 to 100 nm thick Au layer are deposited (sputter-process or electron beam evaporation) on the resist layer. Then, a lift-off process is performed to obtain the metal nanostructure.

After this lift-off step, the sample is spin-coated with a two layer resist system. The bottom layer consists of 670 nm-thick PMMA/MAA which is covered by a top layer of 40 - 70 nm-thick PMMA 950k. Afterwards the SET structure is exposed using electron beam lithography and developed in a two-step process, where the profile of the two-layer resist can be adjusted. The profile of the resist system shows a considerable undercut of up to more than 400 nm on each side of the structure, so that the *shadow evaporation* technique can be applied in the next process step.

Aluminum is used as the basic material for almost all SET structures, as it can be easily evaporated using an electron beam evaporation source and as it forms a homogeneous oxide layer on oxidation, that provides the tunneling barrier. The oxide layer thickness can easily be controlled by adjusting the O_2-pressure of the atmosphere, to which the aluminum is exposed after deposition for a certain period of time. To keep the oxidation process well controlled the SET structure itself has to be fabricated in an *in-situ* process. The shadow evaporation technique offers this possibility. Here, Al or other materials are evaporated using an electron beam evaporation source under different angles with respect to the sample surface. In between the individual evaporation steps the Al can be oxidized.

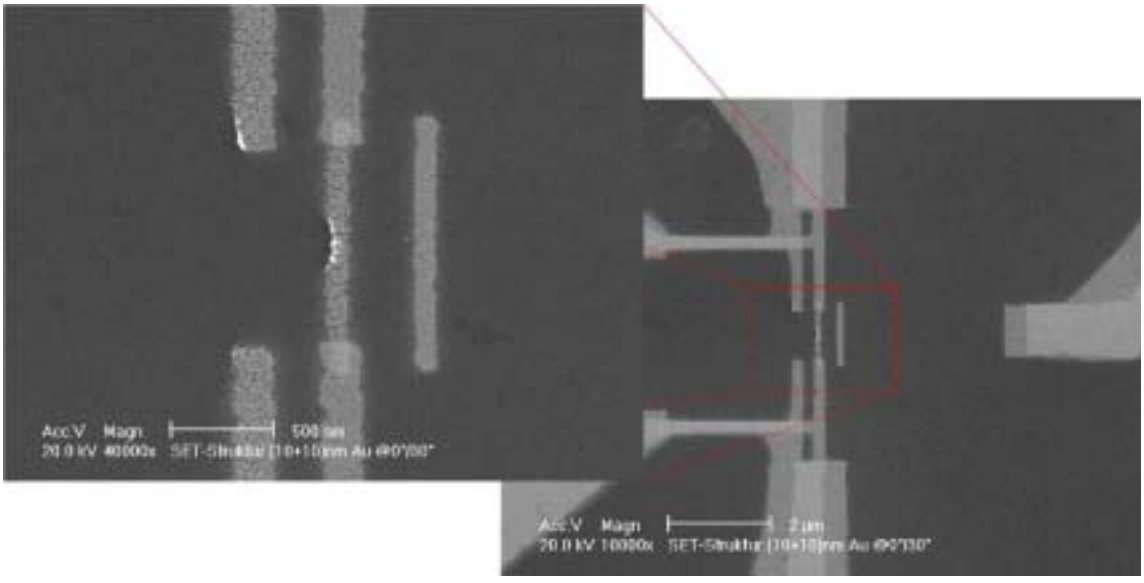

Figure 2: Scanning electron micrograph of a typical SET structure. The leads are 200 nm wide, the island is 100 nm wide and 1.2 μm long. The double structures are caused by the two subsequent evaporation steps under different angles.

After a subsequent lift-off step the sample can once again be patterned using photolithography if required (e.g. leads and bond pads). Figure 2 shows a SET structure.

Experimental Setup

For the experiments in the mK range a dilution refrigerator insert is under construction together with a transportable gas handling system. The insert is built in cooperation with K. Neumaier and fits in any magnet cryostat at the Walther-Meissner-Institute with a free access of 50 mm in diameter. First tests with the new system are scheduled for the beginning of 2002.

The new dilution insert is designed to cool samples within a few hours from room temperature to mK temperatures, an ultimate temperature below 20 mK is expected. The system is equipped with 48 RF-filtered leads and additionally a SQUID-system will be installed for very sensitive measurements. The temperature of the mixing chamber will be controlled and stabilized by two computer controlled instruments, a current source, built by D. Guratzsch, and a very sensitive, automatic ac-resistance bridge, built by J. Höss at the Walther-Meissner-Institute.

References

[1] T. Dittrich, P. Hänggi, G. Ingold, B. Kramer, G. Schön, and W. Zwerger, *Quantum Transport and Dissipation*,VCH-Verlag (1998), chapter 3, *Single Electron Tunneling*.

Layered Manganites with Doping Dependent Intrinsic Tunneling Magnetoresistance

J. B. Philipp, L. Alff, R. Gross [1]

Doped manganites of the form $La_{1-x}A_xMnO_3$ (A = Ca, Sr, Ba) are in the center of intensive research activities, since they show a large variety of magnetic field induced effects as for example the colossal magnetoresistance (CMR). Meanwhile, it has become clear that the physics in this material group cannot be described solely in terms of the classical double-exchange model [1]. It became evident that the complex interplay of the various microscopic (spin, charge, structural, and orbital) degrees of freedom has to be taken into account to describe the rich phenomenology of the doped manganites [2]. Recently, the layered manganites such as the bilayered compound $La_{2-2x}Sr_{1+2x}Mn_2O_7$ in which MnO_2 bilayers and $(La_{1-x}Sr_x)_2O_2$ blocks (see Fig. 1) are stacked along the c-axis direction have attracted particular attention, since they show an extremely rich variety of magnetic structures as a function of doping and since they allow for the study of dimensionality effects on the electronic and magnetic properties in the doped CMR manganites [3, 4, 5, 6, 7, 8]. It has been found that in the layered manganites the quasi-two-dimensional (2D) structure leads to an enhanced CMR effect at the cost of a reduced ferromagnetic transition temperature T_C [9, 10, 11].

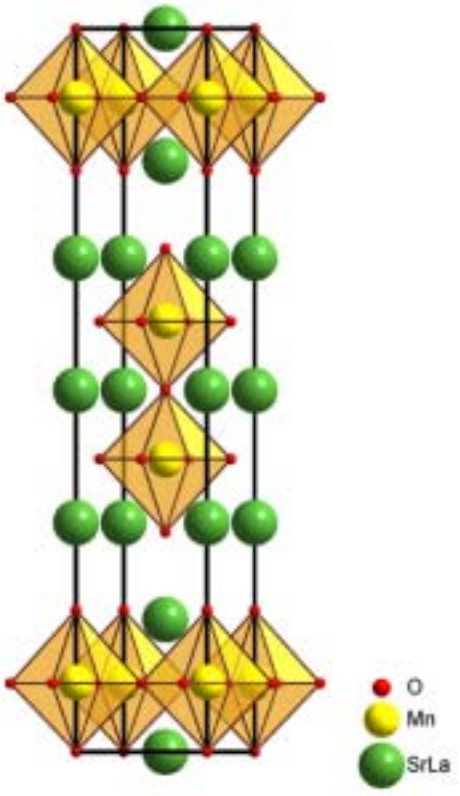

Figure 1: Crystal structure of $La_{2-2x}Sr_{1+2x}Mn_2O_7$ (from reference [13].

The layered manganites can be viewed as an analogon to the cuprate high-temperature superconductors. Both have a strongly anisotropic crystal structure with reduced dimensionality. For the cuprate superconductor $Bi_2Sr_2CaCu_2O_{8-\delta}$ this strong anisotropy has been used to realize intrinsic Josephson junctions by patterning mesa structures into high-quality single crystals and thin films [12]. In order to fabricate similar junctions for TMR (tunneling magnetoresistance) devices based on the intrinsic anisotropy of the layered manganites, the fabrication of high-quality epitaxial thin films is a prerequisite. We have found that for the $x = 0.3$ compound intrinsic ferromagnetic tunnel junctions with non-linear current-voltage characteristics (IVCs) can be realized. At low temperatures (below about 40 K) and independent on doping, the electrical transport behavior of the thin films is dominated by the complex magnetic structure of the layered manganites leading to a possible re-entrant spin glass state due to the competition between super and double exchange interaction that is enhanced by substrate induced strain and disorder [13, 14].

In collaboration with the University of Bonn (Institute of Anorganic Chemistry) we performed high-resolution transmission electron microscopy (HR-TEM) on our thin films revealing a high density of stacking faults due to the formation of competing phases. This high degree of disorder in the thin film samples is most likely the origin of the observed spin-glass like behaviour. A cross-sectional TEM image is shown in Fig. 2. The arrows in Fig. 2 point to a position of the film/substrate interface, where the image contrast is more similar to that of the substrate.

[1] In collaboration with J. Klein and C. Recher, University of Cologne, and T. Walther and W. Mader, University of Bonn. This work is supported by the Deutsche Forschungsgemeinschaft.

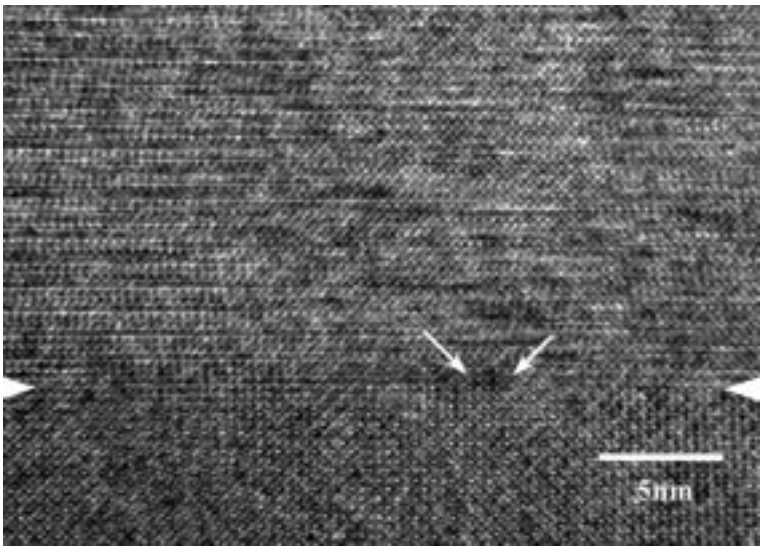

Figure 2: High-resolution transmission electron microscopy image of a $La_{2-2x}Sr_{1+2x}Mn_2O_7$ film grown on NdGa=$_3$.

This indicates a step at the substrate surface. In the film above these arrows, faint horizontal stripes of stronger image contrast are observed. These correspond to monolayers occupied by more strongly scattering cations that have been shifted along [001] with respect to the unit cells of $La_{1.2}Sr_{1.8}Mn_2O_7$. Fourier filtering of the $(001)_f$ reflections shows that at these defects lattice planes have either been inserted or removed from the $La_{1.2}Sr_{1.8}Mn_2O_7$, demonstrating that these defects are stacking faults on (001) planes.

Intrinsic magnetoresistance

In Fig. 3 we show the magnetoresistive (MR) effect in the compound $La_{1.4}Sr_{1.6}Mn_2O_7$ at different temperatures. The observed MR effect for the current flowing in *c*-axis direction is indeed due to the intrinsic ferromagnetic tunnel junctions in the anisotropic manganites. The effect depends on the doping level (it is absent for the compound $La_{1.2}Sr_{1.8}Mn_2O_7$), which is associated with different magnetization directions and coupling schemes between the 2D ferromagnetic layers forming the intrinsic tunnel junctions. The effect is maximum around the critical temperature of the material, but its magnitude is only a few percent (typically 10%). Therefore, from the present state of experiments there is some doubt whether such intrinsic junctions are a good alternative to artificial heterostructures.

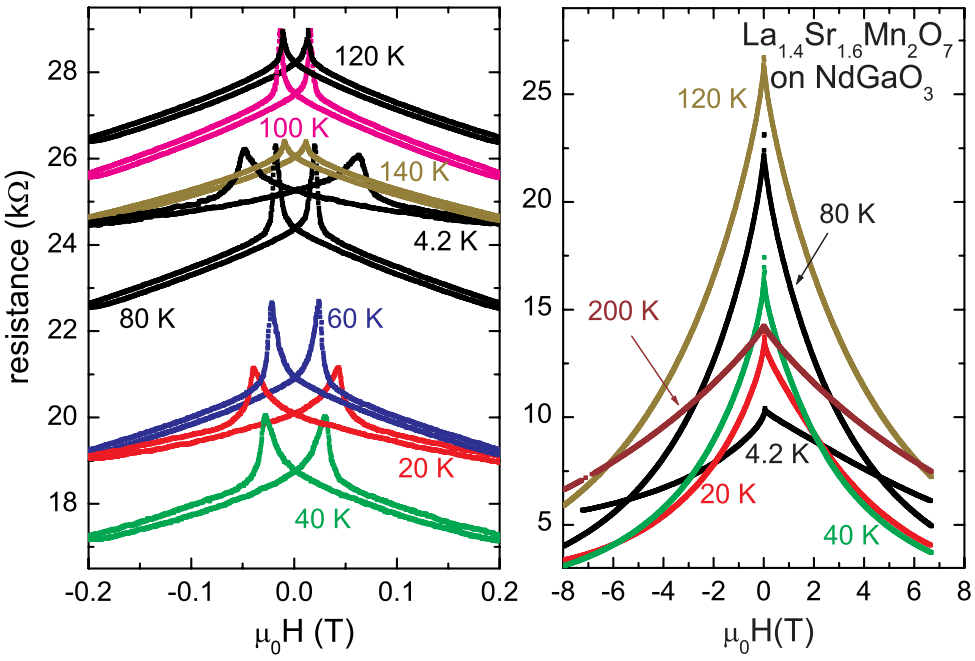

Figure 3: Resistance vs. magnetic field curves at different temperatures for a $La_{1.4}Sr_{1.6}Mn_2O_7$ thin film grown on $NdGaO_3$ for the *c*-axis direction. The left panel shows the low-field effect, the right panel the behavior up to ± 8 T. The field is applied in-plane. [13, 14].

References

[1] C. Zener, Phys. Rev. **82**, 403 (1951).
[2] A. J. Millis, P. B. Littlewood, and B. I. Shraiman, Phys. Rev. Lett. **74**, 5144 (1995).
[3] T. Kimura, A. Asamitsu, Y. Tomioka, and Y. Tokura, Phys. Rev. Lett. **79**, 3720 (1997).
[4] T. Fukumura, H. Sugawara, T. Hasegawa, K. Tanaka, H. Sakaki, T. Kimura, Y. Tokura, Science **284**, 1969 (1999).
[5] Q. Li, K. E. Gray, J. F. Mitchell, A. Berger, R. Osgood, Phys. Rev. **B 61**, 9542 (2000).
[6] U. Welp, A. Berger, V. K. Vlasko-Vlasov, Q. Li, K. E. Gray, J. F. Mitchell, Phys. Rev. **B 62**, 8515 (2000).
[7] Q. Li, K. E. Gray, J. F. Mitchell, Phys. Rev. **B 59**, 9357 (1999).
[8] U. Welp, A. Berger, D. J. Miller, V. K. Vlasko-Vlasov, K. E. Gray, J. F. Mitchell, J. Appl. Phys. **87**, 5043 (2000).
[9] Y. Moritomo, A. Asamitsu, H. Kuwahara, and Y. Tokura, Nature (London) **380**, 141 (1996).
[10] T. Kimura, Y. Tomioka, H. Kuwahara, A. Asamitsu, M. Tamura, and Y. Tokura, Science **274**, 1698 (1996).
[11] H. Asano, J. Hayakawa, and M. Matsui, Appl. Phys. Lett. **70**, 2303 (1997).
[12] R. Kleiner, F. Steinmeyer, G. Kunkel, and P. Müller, Phys. Rev. Lett. **68**, 2394 (1992).
[13] J. B. Philipp, J. Klein, C. Recher, T. Walther, W. Mader, M. Schmid, R. Suryanarayanan, L. Alff, and R. Gross, submitted to Phys. Rev. B.
[14] J. B. Philipp, J. Klein, C. Recher, L. Alff, and R. Gross, to appear in phys. stat. sol. (a) **189** (2002).

Spin Dependent Transport in the Double Perovskite A_2CrWO_6 (A=Ca,Sr,Ba)

A. Erb, J.B. Philipp, R. Gross

Over the past years ferromagnetic tunnel junctions have been studied intensively due to their potential application in magnetoelectronic devices as for example nonvolatile magnetic random access memories. For such devices, materials with high spin polarization at room temperature are required. Here, we present structural, magnetic, and transport properties of both A_2CrWO_6 (A = Ba, Ca, Sr) bulk polycrystalline samples and high-quality thin films. It was found already in 1963 that this double perovskite compound A_2CrWO_6 has a Curie temperature T_C as high as 453 K [1]. We now re-investigated this material and the isostructural compounds Ba_2CrWO_6 and Ca_2CrWO_6 as a possible candidates for room-temperature magnetoelectronic devices.

Sample Preparation and X-ray Analysis

The polycrystalline samples were prepared from stoichiometric mixtures of $SrCO_3$, $BaCO_3$, $CaCO_3$, Cr_2O_3 and WO_3. The carefully mixed starting materials were first fired at 950°C in air. Successive firings were performed in an atmosphere of 5% H_2 in N_2 at a temperature of 1300°C with intermediate grinding. In a last step the powders were pressed into bars of $2 \times 1.5 \times 10\,mm^3$ and sintered between 1300°C and 1600°C for 1 to 4 hours. The differential thermal analysis indicates that the phase formation starts at 900°C in the reducing atmosphere. Increasing the sintering temperature from 1300°C to 1580°C reduces the amount of parasitic phases such as $ACrO_4$ and AWO_4 (A = Sr, Ba, Ca) as found by x-ray analysis. As shown in Fig. 1(b), samples fired at 1580°C and 1600°C are nearly phase pure, however, the 1600°C sample is partially molten. The crystal structure of Sr_2CrWO_6 is cubic with a lattice parameter of 7.832 Å. The almost phase pure samples show a (111) (19.6°) and a (311) (38.5°) peak indicating ordering of the Cr and W positions [2, 3].

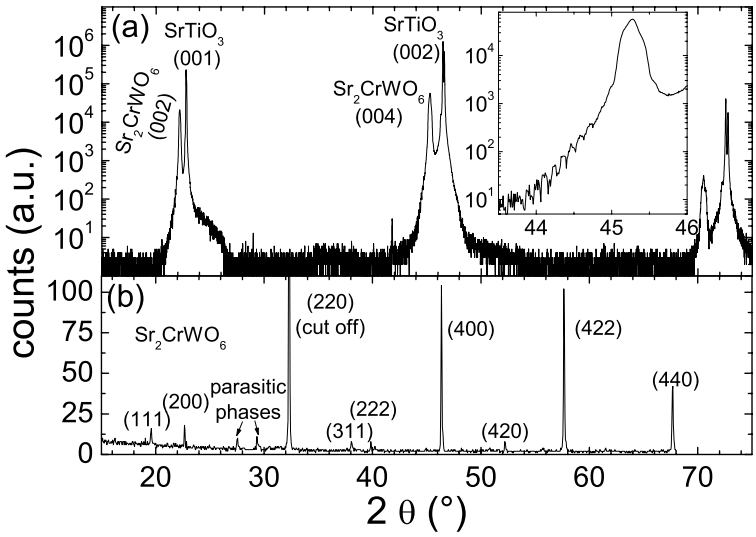

Figure 1: (a) X-ray diffraction pattern for a 100 nm thick Sr_2CrWO_6 thin film on a $SrTiO_3$ substrate. Only (00l) peaks are observed. The inset shows Laue oscillations of the (004) peak. (b) Powder x-ray diffraction of a Sr_2CrWO_6 ceramic sample sintered at 1600°C.

Sr_2CrWO_6 thin films were deposited from stoichiometric polycrystalline targets on (001) $SrTiO_3$ substrates by pulsed laser deposition using a 248 nm KrF excimer laser [4]. The substrate temperature was kept at 730°C during deposition. An argon partial pressure of $2 \cdot 10^{-5}$ Torr was used. The laser energy density on the target surface was about $2\,J/cm^2$, and the laser was operated at a repetition rate of 2 Hz. 2000 pulses yielded films with a thickness of about 100 nm. As found by *in situ* atomic force microscopy, the root mean square roughness of a typical 100 nm thick film is only 6Å. As shown in Fig. 1(a), within the resolution of our four circle x-ray diffractometer only (00l) peaks ($l = 2, 4, 6...$) could be detected.

Rocking curves of the (004) peak had a full width at half maximum (FWHM) of only 0.025° which is very close to the FWHM of the substrate peaks. The fact that Laue oscillations were detected around the film diffraction peaks (see inset of Fig. 1(a)) indicates that the compressive strain due to lattice mismatch between film and substrate (0.3% for $SrTiO_3$) is not relaxed, i.e. the films grow coherently strained [5].

Transport properties and magnetization

The temperature dependence of the resistivity, $\rho(T)$, of the samples was measured with a standard four-probe method using silver epoxyd contacts for the ceramic samples (10 mm × 2 mm × 1.5 mm) and gold contact pads for the thin films.

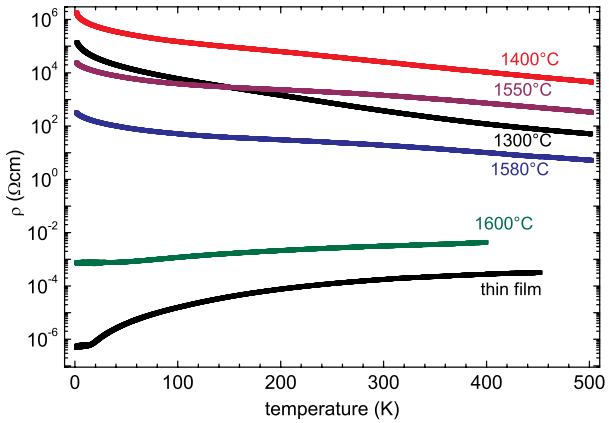

Figure 2: Temperature dependence of the resistivity of ceramic samples prepared under different sintering temperatures and of one epitaxial thin film.

As shown in Fig. 2, the polycrystalline samples with sintering temperatures below 1580°C show a semiconductor-like behavior and a high resistivity. In contrast, the partially molten 1600°C ceramic sample and the thin film show a metallic $\rho(T)$ dependence. The resistivity of the thin film is comparable to that of good metals. Fig. 2 shows that for ceramic samples the increase of the sintering temperature leads to a reduced resistivity and a less pronounced increase of $\rho(T)$ with decreasing T. It is most likely that the high resistivity values of the ceramic samples with sintering temperatures below 1580°C are due to grain boundaries and possible residual parasitic phases at these grain boundaries. Due to the partial melting of the 1600°C sample the amount of grain boundaries is strongly reduced resulting in a metallic $\rho(T)$ dependence. Accordingly, the epitaxial thin film also displays a metallic $\rho(T)$ curve. Scanning electron microscopy showed that the samples sintered at 1400°C to 1580°C have grain sizes between 0.1 and 2 μm, while the 1600°C sample has larger grain sizes between 0.5 and 4 μm.

Fig. 3 shows the magnetoresistance $MR = [R(H) - R(0\mathrm{T})]/R(H)$. The samples with high resistivity show a large negative MR exceeding 100% at 8 T and 5 K. The low-field MR is still above 60% at 1.5 T and 5 K. This value is comparable to that of good Sr_2FeMo_6 samples [3, 6]. The considerable low field MR can be understood in terms of spin polarized tunneling between ferromagnetic domains separated by an insulating barrier at the grain boundary. According to the Jullière model [7] the MR depends on the spin polarization P of the electrodes as $MR = 2P/(1-P^2)$. That is, within this simple model the lower limit for the spin polarization in Sr_2CrWO_6 is estimated to $P = 30\%$. The disappearance of a negative low-field MR both in the partially molten ceramic sample and the epitaxial film provide clear

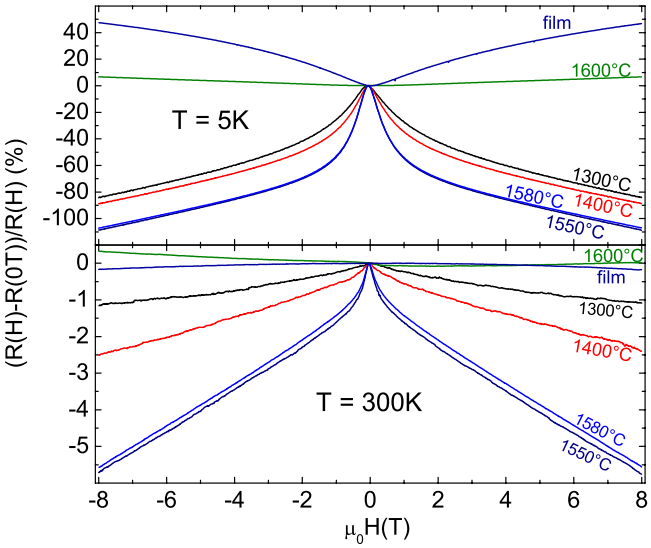

Figure 3: Magnetoresistance of Sr_2CrWO_6 ceramic samples prepared at different sintering temperatures as well as of an epitaxial film at 5 K and 300 K.

evidence for our interpretation that the low-field *MR* is caused by spin polarized tunneling across grain boundaries. Interestingly, the thin film shows an unusual *positive* MR-effect at low T which may be attributed to antiferromagnetic interactions. We note that a high positive MR effect at low T was also observed in Sr_2FeMo_6 thin films with low resistivity [8].

On increasing T, the low-field *MR* is strongly reduced to about 2% at 1.5 T and 300 K. This can be attributed to the reduced magnetization at 300 K as shown in Fig. 4. The measured saturation magnetization is about 1 μ_B/ f.u. at low T. Assuming the configuration Cr^{3+} ($3d^3$) and W^{5+} ($5d^1$), and a ferrimagnetic order [1] a saturation magnetization of 2 μ_B/ f.u is expected. This difference is probably related to Cr/W disorder.

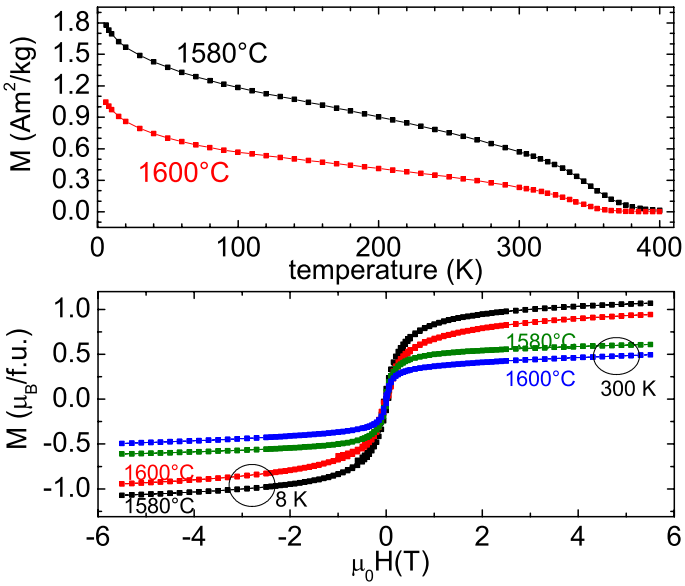

Figure 4: (a) Magnetization vs. temperature of ceramic samples prepared at sintering temperatures of 1580°C and 1600°C. The data are taken on increasing T at a field of 2.3 Oe after field cooling in 6 T. (b) $M(H)$ curves at 8 K and 300 K for the same samples as in (a)

The isostructural compounds A_2CrWO_6 (A = Ca, Ba)

We note, that the origin of magnetism in the double perovskite compounds is still under discussion. To investigate the origin of the magnetism in Sr_2CrWO_6 we also produced the isostructural compounds Ba_2CrWO_6 and Ca_2CrWO_6 as well as partially substituted compounds $CaSrCrWO_6$ and $BaSrCrWO_6$.

It has been found that for the isostructural compounds the lattice constant is modified according to the bigger or smaller ionic sizes of the Ba or Ca ions respectively. The T_c of the isostructural compounds vary strongly with the determined lattice constant as it is shown in Fig. 5.

In summary, we have fabricated both ceramics and epitaxial thin films of the double perovskite Sr_2CrWO_6 with a T_C of about 450°C. The epitaxial films can be fabricated in high quality by pulsed laser deposition at relatively low substrate temperatures. For polycrystalline samples a large low-field *MR* above 100% at 5 K was measured which is reduced to 2% at room temperature. Sr_2CrWO_6 samples without grain boundaries were found to have low resistivity values comparable to those of good metals. Comparing Sr_2CrWO_6 to other double perovskite materials suggests that this material is an interesting candidate for applications in magnetoelectronics due to its high Curie temperature, low resistivity and high degree of spin polarization.

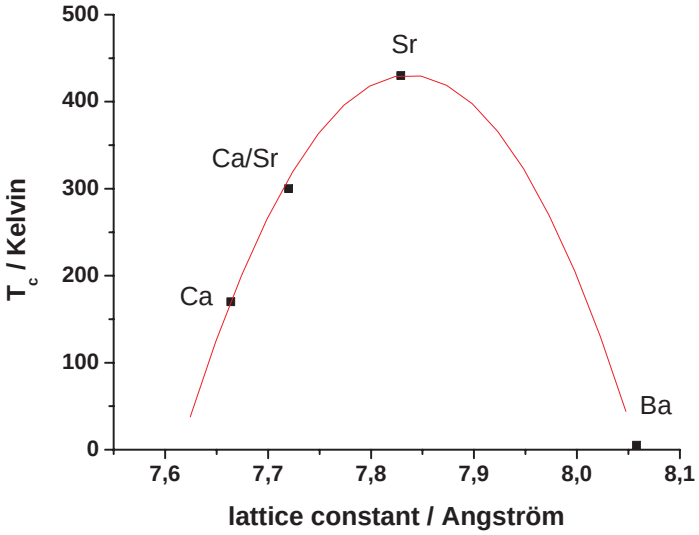

Figure 5: Curie temperature versus lattice constant for the different A_2CrWO_6 compounds with A = Ca, Sr, Ba

References

[1] F. K. Patterson, C. W. Moeller, and R. Ward, Inorg. Chem. **2**, 196 (1963).
[2] Y. Tomioka, T. Okuda, Y. Okimoto, R. Kumai, K.-I. Kobayashi, and Y. Tokura, Phys. Rev. B **61**, 422 (2000).
[3] D. D. Sarma, E. V. Sampathkumaran, Sugata Ray, R. Nagarajan, Subham Majumdar, Ashwani Kumar, G. Nalini, and T. N. Guru Row, Sol. State Com. **114**, 465 (2000).
[4] R. Gross, J. Klein, B. Wiedenhorst, C. Höfener, U. Schoop, J. B. Philipp, M. Schonecke, F. Herbstritt, L. Alff, Yafeng Lu, A. Marx, S. Schymon, S. Thienhaus, and W. Mader, in *Superconducting and Related Oxides: Physics and Nanoengineering IV*, D. Pavuna and I. Bosovic eds., SPIE Conf. Proc. **Vol. 4058** (2000), pp. 278–294.
[5] J. B. Philipp, J. Klein, D. Reisinger, M. Schonecke, A. Marx, A. Erb, L. Alff, and R. Gross, Appl. Phys. Lett. **79**, 3654 (2001).
[6] M. Garcíía-Hernández, J. L. Martínez, M. J. Martínez-Lope, M. T. Casais, and J. A. Alonso, Phys. Rev. Lett. **86**, 2443 (2001).
[7] M. Jullière, Phys. Lett. **A 54**, 225 (1975).
[8] H. Asano, S. B. Ogale, J. Garrison, A. Orozco, Y. H. Li, E. Li, V. Smolyaninova, C. Galley, M. Downes, M. Rajeswari, R. Ramesh, and T. Venkatesan, Appl. Phys. Lett. **74**, 3696 (1999).

Laser Ablation of Oxide Thin Films for Magnetoelectronics

D. Reisinger, J. B. Philipp, B. Blass, A. Erb, A. Marx, L. Alff, R. Gross [1]

Magnetoelectronics or spintronics is a new field of solid state physics where the spin of the electron is brought into play. In conventional electronics the spin degrees of freedom do not play a significant role and the electronic transport properties are mainly dominated by the charge degrees of freedom. In spintronics, in contrast, both spin and charge degrees of freedoms are used for the design of new magnetoelectronic devices with new functionality. Since most of our today's electronics is based on semiconducting materials, intense research activities are focused on the combination of magnetic materials with semiconductors. The goal is to have compatible ferromagnetic materials with high spin-polarization of the charge carriers at the Fermi level at room-temperatures allowing for the injection of spin polarized charge carriers into semiconductors. The first step in this direction is the selection of suitable materials that, of course, have to be compatible with semiconductor processing. In this context, our studies are focusing on ferromagnetic oxides. While the doped manganites provide high spin polarization, they lack of high enough Curie temperatures. A new interesting class of materials that have high critical temperatures well above room temperature are the double perovskites [1, 2, 3]. The second material we are starting to work on is magnetite, which is well known for its low-temperature behavior (Verwey-transition) but only recently has attracted renewed interest in the context of spintronics.

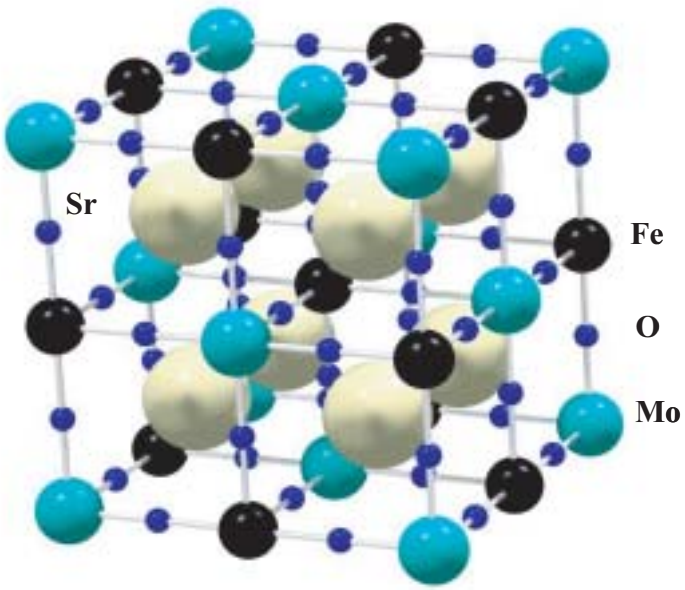

Figure 1: Crystal structure of the double perovskite Sr_2FeMoO_6.

Double perovskites

In Fig. 1 we show the crystal structure of the double perovskite Sr_2FeMoO_6. Thin films of this material have been grown by laser ablation [4, 5]. We have shown that it is possible to grow this material in a layer-by-layer growth mode. We have observed the corresponding RHEED (reflection high energy electron diffraction) intensity oscillations during film growth [6]. We note that Sr_2FeMoO_6 is very sensitive to variations of the growth parameters leading to a transition from a layer-by-layer growth mode to a three dimensional island growth mode. In Fig. 2 an image of the surface of a Sr_2FeMoO_6 thin film obtained by atomic force microscopy (AFM) is shown. It is evident that the surface topology of a thin film, which is grown in the layer-by-layer (Volmer-Weber) mode, is very smooth. A root mean square roughness of only 0.7 nm is found.

In order to obtain information on the spin polarisation in Sr_2FeMoO_6 we have performed Andreev reflexion spectroscopy. In this method, a point contact between superconducting (Nb) tip and the ferromagnetic film is used to probe the spin dependent density of states in the ferromagnetic material. This technique relies on the fact that Andreev reflexion occuring in usual superconductor - normal

[1] This work is supported by the Deutsche Forschungsgemeinschaft.

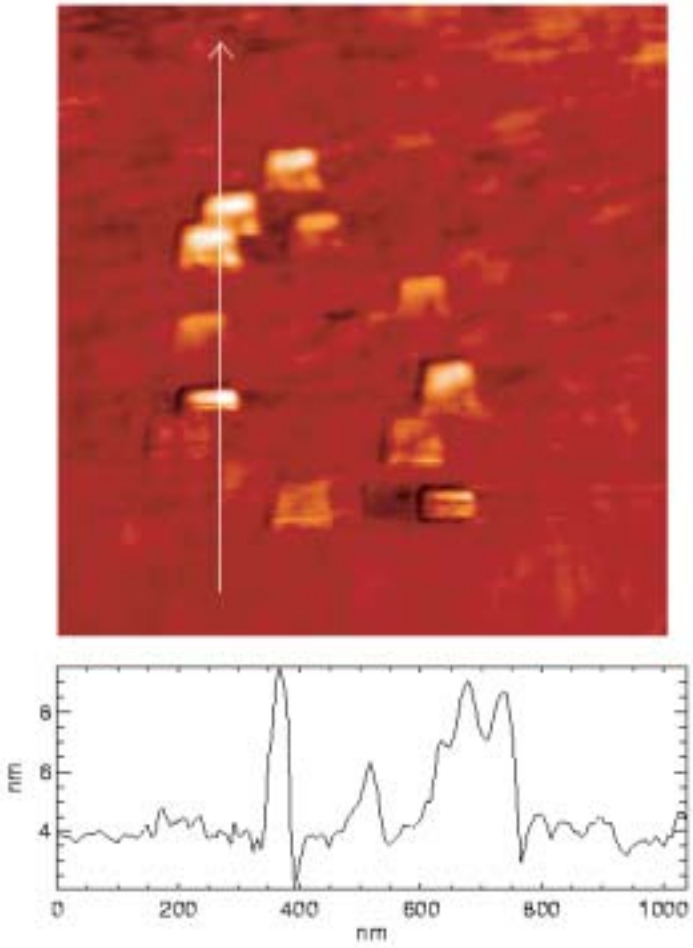

Figure 2: Surface structure of the double perovskite Sr_2FeMoO_6 as grown in the layer-by-layer mode.

to be experimentally confirmed.

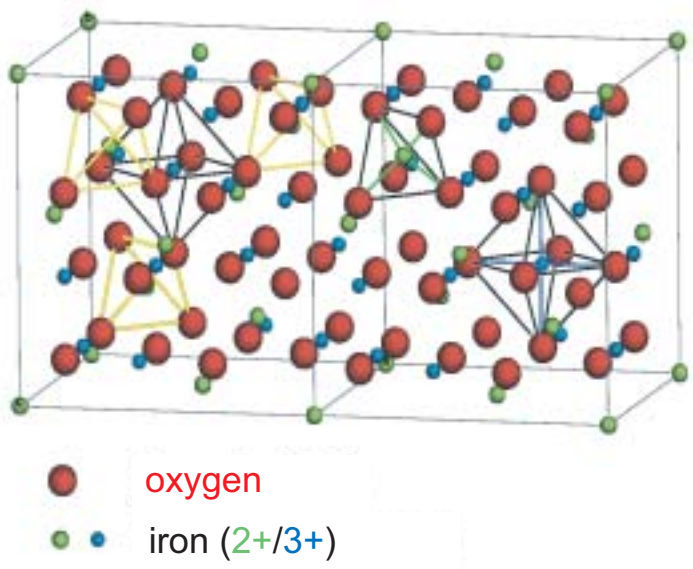

Figure 3: Crystal structure of magnetite (Fe_3O_4).

metal junctions is strongly suppressed in superconductor - ferromagnet junctions. This is caused by the fact that a spin-up electron from the ferromagnet is Andreev retro-reflected as a spin-down hole, for which no or a strongly reduced density of states is available in the ferromagnetic material. The degree of suppression can be directly related to the degree of spin polarization at the Fermi level. Preliminary results yield a spin polarization in Sr_2FeMoO_6 larger than 50% at 4.2 K. This low value (well below the expected 100% predicted by band structure calculations) is most likely due to our experimental setup and interfacial effects. Systematic experiments are required to clarify this issue.

We also have studied other double perovskites which are supposed to have higher critical temperatures such as Sr_2CrWO_6. Surprisingly, first growth studies of Sr_2CrWO_6 thin films show that they also can be grown in a layer-by-layer mode [7]. Interestingly, we have observed a *positive* magnetoresistance effect in Sr_2CrWO_6 for which up to now no theoretical explanation has been found. The influence of doping and lattice strain is currently investigated. Furthermore, the high degree of spin polarization at room temperature has still

Magnetite

We have started to fabricate thin films of the well-known material Fe_3O_4 (magnetite). While it was in the center of active research activities due to its low-temperature Verwey-transition, we now focus on the room temperature properties of this material such as the expected high spin polarization. The material itself has the advantage that it can be grown as epitaxial thin film at considerably lower temperatures than the perovskite type oxides (e.g. the double perovskites). Preliminary results show that smooth thin films can be grown on MgO at temperatures between 350°C and 400°C. This deposition temperature is compatible with the processing requirements for semiconductors. Therefore, magnetite may be

a possible candidate for hybrid structures consisting of semiconductors and ferromagnetic oxides.

References

[1] K.-I.Kobayashi, T. Kimura, H. Sawada, K. Terakura, and Y. Tokura, Nature **395**, 677 (1998).
[2] K.-I. Kobayashi, T. Kimura, Y. Tomioka, H. Sawada, K. Terakura, and Y. Tokura, Phys. Rev.B **59**, 11159 (1999).
[3] F. K. Patterson, C.W. Moeller, and R.Ward, Inorg. Chem. **2**, 196 (1963).
[4] T. Manako, M. Izumi, Y. Konishi, K.-I. Kobayashi,M. Kawasaki, and Y. Tokura, Appl. Phys. Lett. **74**, 2215 (1999).
[5] W. Westerburg, D. Reisinger, and G. Jakob, Phys. Rev. B **62** R767 (2000).
[6] J. Klein, C. Höfener, L. Alff, and R. Gross, J. Magn. Magn. Mater. **211**, 9 (2000); see also Supercond. Sci. Technol. **12**, 1023 (1999).
[7] J. B. Philipp, J. Klein, D. Reisinger, M. Schonecke, A. Marx, A. Erb, L. Alff, and R. Gross, Appl. Phys. Lett. **79**, 3654 (2001).

^{3}He/^{4}He Dilution Refrigerator with Pulse-tube Refrigerator Precooling

K. Uhlig

Just a few weeks before the time of this writing our new dilution refrigerator (DR) which is precooled by a two-stage pulse tube refrigerator (PTR) has been operated for the first time. Actually, this is the first time ever that a DR has been combined with a two-stage PTR. The aim of the project is to build and optimize an easy-to-use multiple purpose DR which operates without cooling liquids. The PTR is the best suited closed-cycle refrigerator (CCR) for precooling a DR because it has no cyclically moving displacer and therefore the most quiet running of all CCRs. Besides, it is expected to have a long mean time between maintenance as there are no cold displacer seals in the cooler which would have to be replaced from time to time like in other CCRs. The compressor needs maintenance only every 20.000 hours.

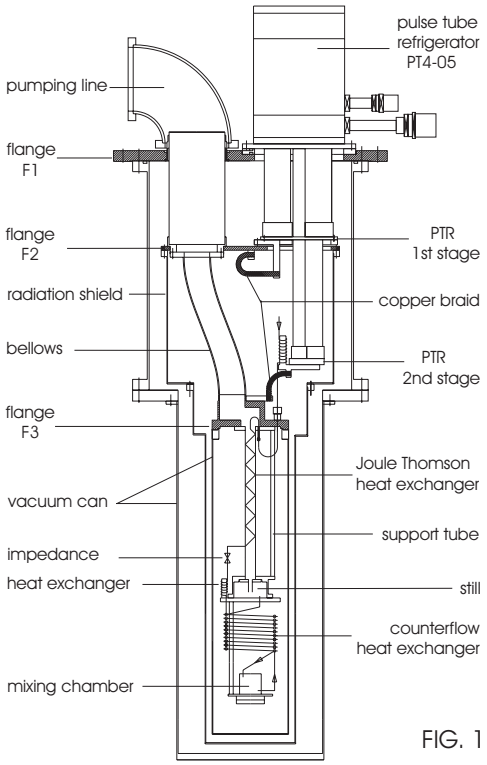

FIG. 1

Our refrigerator is still in a scaled-down status as the ^{3}He was circulated only with a rotary pump; a roots pump or a turbodrag pump will be added to the ^{3}He circuit as soon as the construction activities at the WMI permit. Due to the small pumping speed of the rotary pump the DR could be run only with a small ^{3}He throughput, whereas the full cooling power would be available at maximum throughput. Still, all major components of the DR could be tested, the cryostat, the dilution unit, the rebuilt gas handling system, the newly designed charcoal trap and new pumping lines.

After entering the cryostat the circulating ^{3}He is cooled and purified in a charcoal trap which is thermally connected to the 1^{st} stage of the PTR (T = 43 K). Next the ^{3}He is cooled to the temperature of the 2^{nd} stage (3.0 K) and then in a JT heat exchanger to 2.4 K (Figure 1). After precooling the ^{3}He is expanded

and partially liquefied in a flow impedance; in a heat exchanger which is mounted to the still the gas part of the ^{3}He is liquefied and all of the ^{3}He cooled to about 0.9 K. In a counterflow heat exchanger the ^{3}He is further cooled and finally dissolved into the dilute phase of the mixing chamber where the lowest temperature reached was 15 mK (Figure 2).

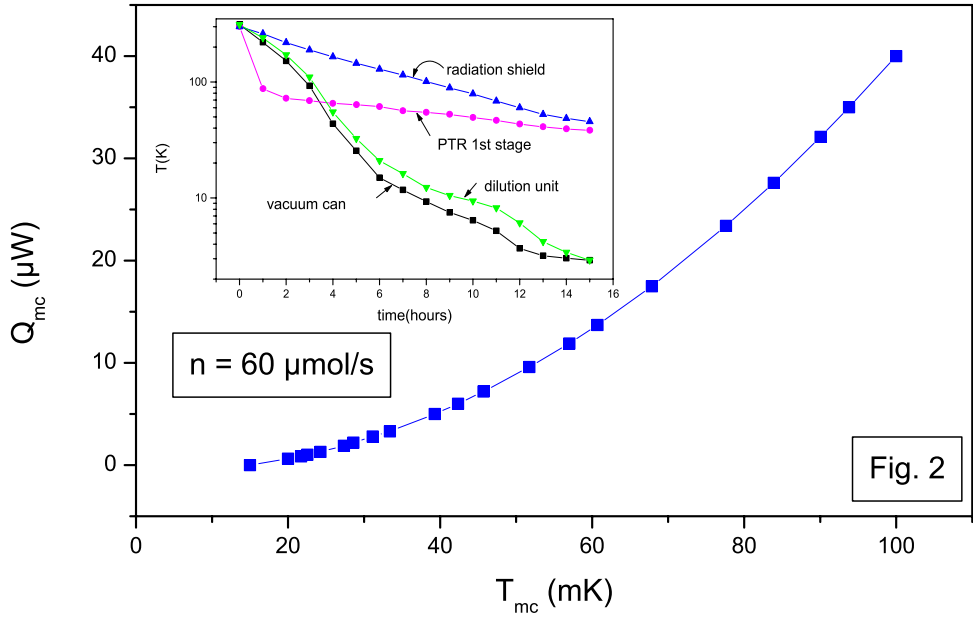

The cool-down of the cryostat takes about 14 hours from room temperature to $T = 4$ K (insert of Figure 2); this can conveniently be done overnight. For the condensation of the ^{3}He/^{4}He mash the DR can be operated like a little liquefier: The rotary pump is run at its maximum backing pressure of 2 bar, and the liquid fraction of the mash which results from JT expansion in the flow impedance accumulates in the dilution unit, whereas the gas part is returned to the rotary pump and thereby precools the helium gas flowing into the DR. The liquefied gas is continuously replaced by helium mash from the storage tank. Using a little compressor with the rotary pump raises the rate of liquefaction (26 std.l/h) by about 20%.

We expect to increase the ^{3}He throughput by about a factor of 3 to 4 once the roots pump can be installed in the dilution circuit, and the cooling power of the DR should be increased accordingly.

Mössbauer Spectroscopic Investigation of Redox Reactions in Vermiculites from Santa Olalla (Huelva, Spain)

A. Lerf [1]

Natural clay minerals of the 2:1 type very often contain Fe ions in the octahedral and/or tetrahedral layers. It has been known for fifty years that at least the octahedral iron ions are easily accessible to redox reactions; a striking example for this are the colour reactions of some amines intercalated into smectites. Oxidation of the octahedral structural iron ions has also been considered as an important step in the weathering of micas to vermiculite. To evaluate the extent of redox reactions one needs to know the Fe^{2+}/Fe^{3+} ratio before and after the reaction. However, it is notoriously difficult to determine this ratio in natural and modified clay minerals by wet chemical methods. The most suitable method to derive reliable Fe^{2+}/Fe^{3+} ratios is Mössbauer spectroscopy.

We report here the Mössbauer parameters measured mainly at room temperature for the vermiculite of Santa Olalla and of Ojen, and some chemically modified samples. As shown previously the spectra can be interpreted by a superposition of three quadrupole doublets and a broad background arising from slow relaxation of paramagnetic Fe^{3+}. One of these is attributable to Fe^{3+}, the other two to Fe^{2+}, all of them in octahedral positions. In agreement with the chemical formula we could not identify Fe^{3+} in tetrahedral sites. The isomer shift (IS) and the quadrupole splitting (QS) of all iron sites in the samples under investigation vary only in small ranges of values: IS of Fe^{3+} 0.26-0.27 mm/s, IS of Fe^{2+} 1.00-1.04 mm/s ; QS of Fe^{3+} 0.89-1.05 mm/s, QS of Fe^{2+} 2.50-2.64 mm/s and 2.16-2.41 mm/s, respectively. These values are in excellent agreement with the parameters found previously for di- and trioctahedral micas and vermiculites.

To get reasonable values of the Fe^{2+}/Fe^{3+} ratio, the parameter which shows the largest variations due to the chemical modifications, one has to be sure about the amount of the different iron sites. To evaluate this parameter properly, one should have in mind the following points. First, the distribution of the hyperfine parameters on the two Fe^{2+} sites should be considered with caution because the fitted values of the areas of the components and of the quadrupole splitting are strongly correlated. The total amount of Fe^{2+}, however, is not affected by this ambiguity of the data analysis. Secondly, in all spectra one observes a broad unresolved component that is assumed to result mainly from slow paramagnetic relaxation of Fe^{3+}. In the 4.2 K spectra the relaxing part is strongly enhanced and in addition a sextet appears for the starting material as well as for the reduced samples. It cannot be ruled out that part of the Fe^{2+} also undergoes a magnetic splitting at low temperatures. Therefore the accuracy in determination of the amount of Fe^{2+} sites cannot be improved by 4.2 K data.

In addition, the amount of the relaxation background (difference of the sum of the relative areas of the resolved components to 100 %) depends on the velocity range in which the spectrum has been recorded; at least for the vermiculite from Santa Olalla the area increases from about 30 % at $\pm$ 5 mm/s to 40 % at $\pm$ 20 mm/s. In case of the Ojén vermiculite the area of the broad background does not change significantly if the velocity has been increased from $\pm$ 5 mm/s to $\pm$ 20 mm/s (it amounts to about 16 %). A comparison of both compounds leads to the conclusion that there is an inverse relation between the area of the broad background and the area of the Fe^{2+} sites. Preliminary results indicate that the amount of the broad background can be changed by chemical manipulations leading to a variation of the Fe^{3+} content.

Since the slow relaxation can occur only if there are no nearest Fe neighbours in the surrounding of Fe^{3+} sites, the question arises what does this broad background mean for the iron distribution in the

[1] In collaboration with F.E. Wagner, Physik Department, TU München and J. Poyato, Sevilla

octahedral layer. Therefore we will try to find a correlation between our Mössbauer data and the OH-vibration frequencies (determined by IR) which are also sensitive to the metal distribution.

Apart from these studies we were successful in the preparation of a methylene blue intercalation compound of a vermiculite. The x-ray data show clearly a homogeneous distribution of the dye molecular cations on the interlayer spaces. However, there is no change of the Fe^{2+}/Fe^{3+} ratio as shown by the Mössbauer spectra although the methylene blue is a redox system which could be reduced by Fe^{2+}. That this process does not occur may be related with the fact the Fe^{3+} formation is accompanied with a proton release which is in conflict with the proton release of the methylene blue due to reduction.

In addition we started to investigate the thermal decomposition of the ammonium vermiculite. At high temperature this compound looses its ammonia and is thus transferred to a protonated form of the vermiculite which can be used for the preparation of new organic intercalation compounds. We also expected to get insight in the bonding strength of the ammonium ions to the negatively charged vermiculite layers, and perhaps in differences in this bonding strength due to inhomogeneous charge distribution within the vermiculite layers. We investigated the thermal decomposition by TG/DSC, EGA (Emanation gas analsysis), IR and Mössbauer spectroscopy. The ammonium compound is exceptionally stable up to about 600 ^{o}C. With the exception of the EGA measurements all of the studies has been carried out first in air. However, this should lead to a complete oxidation of Fe^{2+} to Fe^{3+} as a side reaction. This could be verified by the Mössbauer spectroscopy. To proof the influence of this side reaction on the decomposition behaviour we have carried out TG/DSC and Mössbauer measurements under Ar. Whereas the TG/DSC data do not show a significant difference the Mössbauer spectra indicate a strong change of the Fe^{2+}/Fe^{3+} ratio (see Fig. 1). We have the highest degree of reduction ever observed in our experiments of chemical reduction. In addition one of the two Fe^{2+} shows a strong decrease in the quadrupole splitting to a value of 1.75 mm/s. Such a low value could be due to the formation of oxygen vacancies at the iron sites. The only present reducing agent is the ammonia molecule.

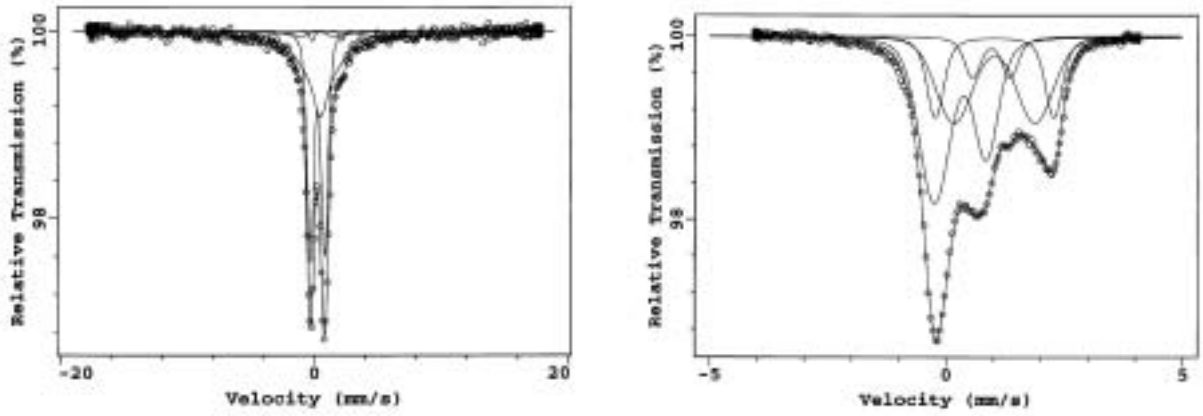

Figure 1: Mössbauer-spectra of Amonium-Vermikulits after heat treatment at 750°C: left under ambient air and right under Argon.

Molecular Simulations in Structure analysis of Tantalum Sulfide intercalated with Methylene Blue

A. Lerf [1]

Structure analysis of tantalum sulfide 2H-TaS_2 intercalated with Methylene Blue $[C_{16}H_{18}N_3S]^+$ (MB-cation) has been carried out using molecular mechanics and molecular dynamics simulations and compared to published experimental data obtained by X-ray powder diffraction [1, 2]. Intercalated compound MB-TaS_2 exhibits three different phases with different concentration of guest species: (1) phase I-MB-TaS_2 with one MB-cation per 15 TaS_2 formula units, (2) phase II-MB-TaS_2 with two MB-cations per 15 TaS_2 formula units and (3) phase III-MB-TaS_2 with three MB cations per 15 TaS_2 formula units. The detailed structure investigation included the analysis of positions and orientation of guest species in the interlayer space, the way of layer stacking, the analysis of charges and the sublimation energy. The basal spacing calculated for all three phases was in a good agreement with the experimental values.

Using molecular simulations we could find reasonable arrangements of MB molecules in all three experimentally observed MB-TaS_2 phases. Fig. 1 shows the arrangement of the MB-cations in the I-MB-TaS_2 phase. The sublimation energy per one MB-cation is highest for the phase I-MB-TaS_2 confirming the experimentally discovered fact that this phase is the most stable one. The agreement between the calculated and experimental basal spacing for the I-MB-TaS_2 and III-MB-TaS_2 phases shows the correct choice of the force field in the present modelling. The modelling gives the clear evidence that the sample prepared as II-MB-TaS_2 is not a pure phase, but an interstratified mixture of phases I-MB-TaS_2 and II-MB-TaS_2.

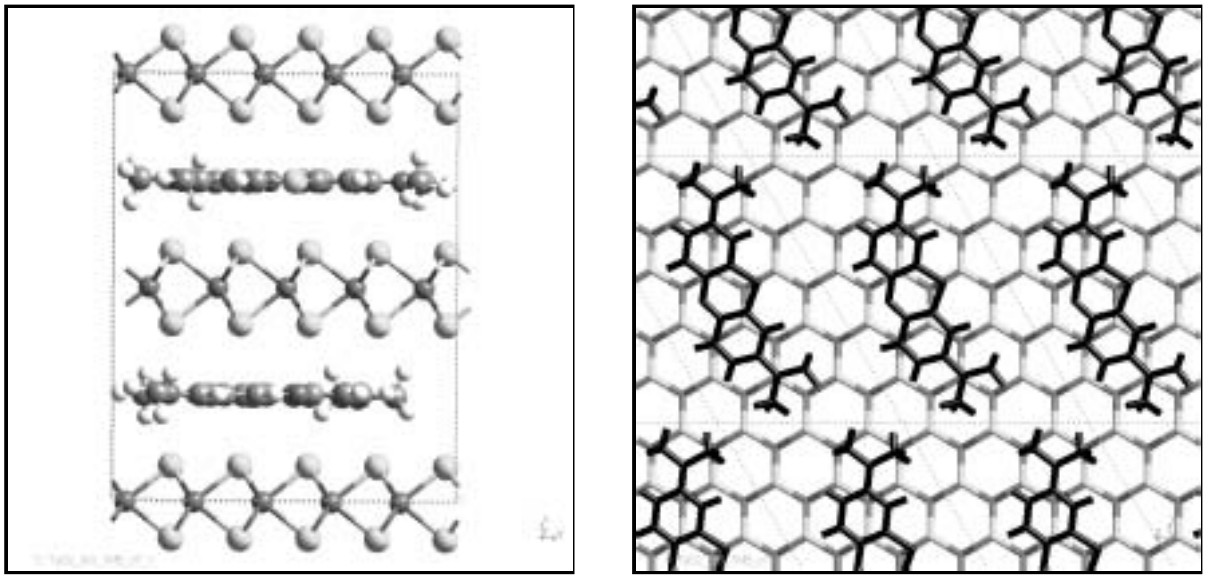

Figure 1: Simulated arrangement of the Methylene Blue cations in the I-MB-TaS_2 phase: left view parallel to the sulfide layers and right perpendicular to the layers.

Comparison of charges shows that the phase III-MB-TaS_2 with the highest concentration of guests exhibits the highest TaS_2 layer charge, i.e. the highest guest-host charge transfer. The increase of the guest concentration is accompanied with the increasing average negative charge on sulphur atoms in host layer and decreasing positive charge on tantalum atoms. This charge redistribution is in excellent agreement with the corresponding finding of a self-consistent linearized augmented plane wave (LAPW) energy

[1] In collaboration with Pavla Čapková and Miroslav Pospíšil, Faculty of Mathematics and Physics, Charles University Prague, Ke Karlovu 3, CZ-12116 Prague, Czech Republic

band structure calculation for some metal intercalation compounds of 2H-TaS_2 [3]. The charges on sulphur atoms in MB-cation exhibit strong changes in dependence on guest concentration. However, the most pronounced changes as a function of the guest concentration can be observed for the total charge of the MB cations. Comparing this result with the slightly increasing total charge of the host layers we have to conclude that the charge transfer during preparation is used mainly for the reduction of MB cations. This is not surprising since the electrochemical potential of MB reduction is quite close to the electrochemical potential of the intercalation compound.

[1] Hauptmann A., Lerf A., Biberacher W., Z. Naturforsch. 51 b (1996) 1571.

[2] Schlicht A., Thesis TU Muenchen 1999.

[3] P. Blaha, J. Phys C 3 (1991) 9381.

Experimental Facilities

Within the last year, several new experimental facilities have been installed at the Walther-Meissner-Institute. On the following pages a brief overview is given on the main equipment and techniques that are available at the Walther-Meissner-Institute at present.

UHV-Laser-MBE

During 2001, a UHV-Laser-Molecular Beam Epitaxy (L-MBE) system for the growth of complex oxide heterostructures has been installed at the WMI. The system has been designed to meet the special requirements of oxide epitaxy. The UHV cluster tool consists of the following main components:

- central transfer chamber.
- load-lock chamber with heater system for substrate annealing.
- laser deposition chamber with in-situ reflection high energy electron diffraction (RHEED) system and atomic oxygen source. The RHEED system has been modified to allow for the operation at high oxygen partial pressure up to 0.5 mbar.
- surface characterization chamber with UHV scanning force microscope (Omikron).
- metallization chamber with four heart electron gun system and liquid nitrogen cooled sample stage. The sample holder can be tilt for shadow evaporation.
- KrF excimer laser.

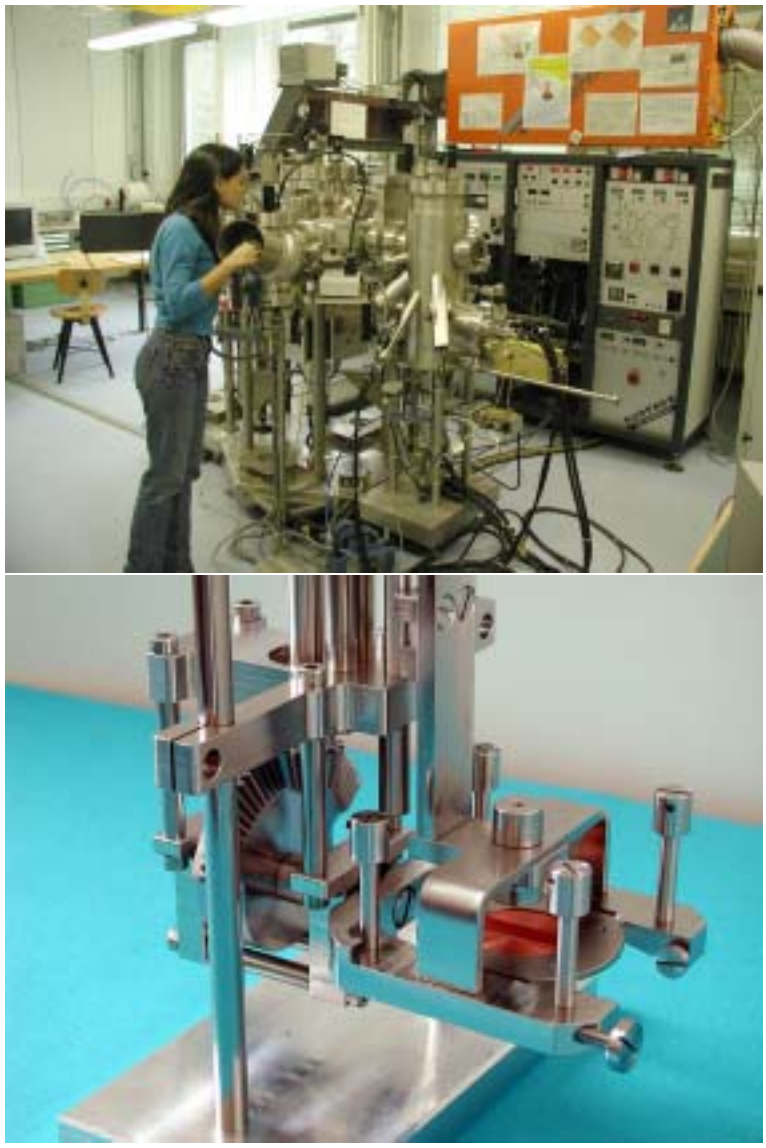

Figure 1: Top: UHV-Laser-Molecular Beam Epitaxy System. Bottom: Sample holder for metallization chamber allowing for evaporation under different angles.

The system is used for the deposition of complex oxide heterostructures consisting of superconducting, magnetic and dielectric materials such as the high-temperature superconductors, the doped manganites, or the double perovskites.

X-ray diffraction system

We have installed two X-ray diffractometers (Bruker D8 Advance and D8 Discover). The two-circle systems is used for powder diffraction. In this system the samples can be heated in oxygen atmosphere up to 1600°C. It is equipped with a Göbel mirror and an area detector to save measuring time. The second system is a high resolution four-circle diffractometer that can be used for reciprocal space mappings. It is equipped with a Göbel mirror and an asymmetric two-fold monochromator and allows for the texture analysis of thin film superlattices and single crystalline materials. In both systems measurements can be carried out fully computer controlled.

Figure 2: Two-circle X-ray difractometer Bruker D8 Advance.

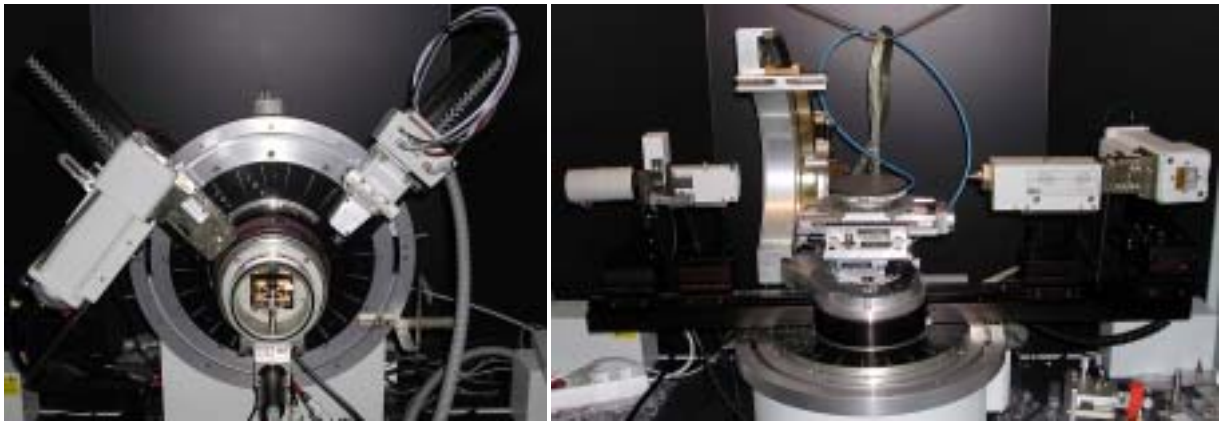

Figure 3: Left: High temperature sample holder for the D8 Advance system. Right: Four-circle high resolution X-ray diffractometer Bruker D8 Discover.

Figure 4: Quantum Design SQUID magnetometer.

SQUID-magnetometer

In 2001, a Quantum Design SQUID magnetometer system as shown in Fig. 4 has been put into operation. The SQUID magnetometer allows for measurements in the temperature regime from 1.5 to 400 K and provides excellent sensitivity particularly in the low field regime. Due to the excellent sensitivity of the system, thin film samples with a very small sample volume can be analyzed. In a special inset, samples can be measured up to temperatures well above room temperature (up to 700° C). For this option the sample volume has to be reduced. The SQUID magnetometer is equipped with a superconducting solenoid allowing for a maximum field of 7 T. At present, the magnetometer is used for the characterization magnetic materials (both in bulk and thin film form). Examples are the doped manganites, magnetite, the double perovskites or magnetic semiconductors.

High Field Laboratory

A high magnetic field laboratory with a 8/10 and 15/17 Tesla magnet system was set up in the basement of the WMI. The larger field values require the use of a λ-stage. The magnet systems are lowered below the ground level to facilitate the access to the top flange and the change of the sample sticks. The magnet systems are decoupled from the building to avoid noise due to vibrations of the building. A variety of sample holders can be mounted allowing for e.g. sample rotation during the measurement. For standard sample holders the accessible temperature regime is $1.5\,\mathrm{K} < T < 300\,\mathrm{K}$. However, also ^{3}He/^{4}He dilution refrigerator units ($T > 20$ mK) or high temperature units ($T < 700$ K) can be mounted. All measurements are fully computer controlled (by the use of the LabView software tool) allowing for remote control and almost continuous measurements.

Figure 5: High field laboratory with Oxford 17 T magnet system.

Figure 6: Top: Part of the clean room facility with optical lithography equipment and clean room benches. Bottom: Resist coater and hot plates.

Clean Room Facility

Within 2001 a class 1000 clean room facility with an area of about 50 m^2 has been put into operation at the Walther-Meissner-Institute.
The clean room is subdivided into two parts for optical lithography and electron beam lithography, respectively. The clean room facility is equiped with the standard tools for optical lithography such as resists coaters, hot plates, wet benches, a mask aligner and an optical projection lithography system. The technical infrastructure for the clean room is located in the basement of the institute directly below the clean room area.

Electron Beam Lithography

The Electron Beam Lithography System is installed in the clean room facility. It consists of a Philips XL 30 SFEG scanning electron microscope (SEM) with a Raith Elphy Plus electron beam lithography system and a laser stage. The SEM is equipped with a hot field emitter and typically provides a beam diameter of less the 2 nm at 25 keV or about 3.5 nm at 5 keV. The lithography unit allows the fabrication of nanostructures down to about 10 nm. We have realized the controlled fabrication of metallic strip patterns with a strip width of about 20 nm. The electron beam lithography is used for the fabrication of nanostructures in metallic and oxide systems used for the study of quantum effects in mesoscopic samples.

Figure 7: Top: Philips XL 30 SFEG Scanning Electron Microscope with Raith Elphy Plus Lithography System. Bottom: Raith Laser Stage.

Optical Lithography

For optical lithography a Süss MJB 3 maskaligner or a optical microscope based projection system are used. The maskaligner is operating in the 1 : 1 soft or hard contact mode and is using chromium metal masks. In the projection system the mask pattern is demagnified by a factor of 5 to 100. Therefore, cheap foil masks can be used. With both systems microstructure with a lateral width down to 1 μm can be fabricated.

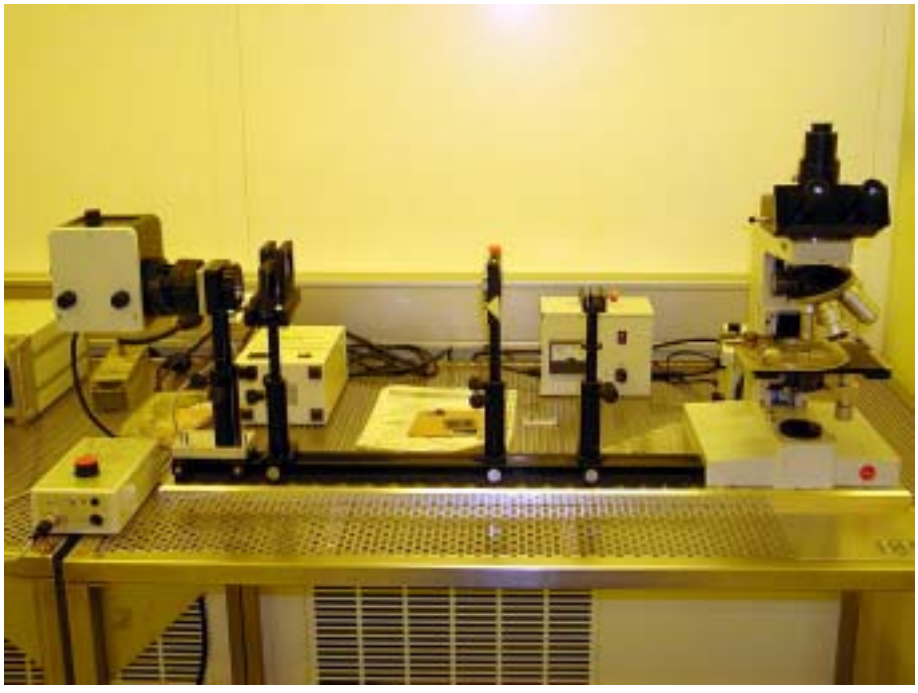

Figure 8: Top: Süss MJB 3 maskaligner for optical lithography. Bottom: Optical projection lithography based on an optical microscope.

Publications

1. **κ–(BETS)$_2$C(CN)$_3$: studies of SdH and dHvA oscillations under ambient and high pressures**
   T.G. Togonidze,M.V. Kartsovnik, J.A.A.J. Perenboom, N.D. Kushch, H. Kobayashi,
   Physica **B 294–295**, 435–438 (2001).
2. **The phase diagram of α–(BEDT–TTF)$_2$KHg(SCN)$_4$ for magnetic fields almost parallel to the layers**
   P. Christ, W. Biberacher, D. Andres, M.V. Kartsovnik, E. Balthes, H. Weiss, H. Müller,
   Synthetic Metals **120**, 1019–1020 (2001).
3. **Magneto–quantum oscillations in κ–(BEDT–TTF)$_2$Cu[N(CN)$_2$]Br**
   H. Weiss, M.V. Kartsovnik, W. Biberacher, E. Balthes, A.G.M. Jansen, N.D. Kushch,
   Synthetic Metals**120**, 837–838 (2001).
4. **A Light–Scattering Study of Dynamical Carrier Properties in Cuprate Systems**
   M. Opel, R. Nemetschek, F. Venturini, R. Hackl, I. Tüttö, H. Berger, L. Forró, A. Erb, B. Revaz, E. Walker,
   Ferroelectrics **249**, 155–164 (2001).
5. **B–T–P phase diagram of α–(BEDT–TTF)$_2$KHg(SCN)$_4$**
   M.V. Kartsovnik, D. Andres, W. Biberacher, P. Christ, E. Steep, E. Balthes, H. Weiss, H. Müller, N.D. Kushch,
   Synthetic Metals **120**, 687–690 (2001).
6. **Mössbauer spectroscopic investigation of redox reactions in vermiculites from Santa Olalla (Huelva, Spain)**
   A. Lerf, F.E. Wagner, J. Poyato,
   Solid State Ionics **141–142**, 479–486 (2001).
7. **Magnetoresistance studies of α–(BEDT–TTF)$_2$KHg(SCN)$_4$ under pressure**
   D. Andres, M.V. Kartsovnik, W. Biberacher, T. Togonidze, H. Weiss, E. Balthes, N.D. Kushch,
   Synthetic Metals **120**, 841–842 (2001).
8. **Voltage–Flux–Characteristics of Asymmetric dc SQUIDs**
   J. Müller, S. Weiss, R. Gross, R. Kleiner, D. Koelle
   IEEE Trans. Appl. Supercond. **11**, 912–915 (2001).
9. **Heteroepitaxial growth of high–temperature superconductors and doped manganites in ramp type geometry**
   U. Schoop, M. Schonecke, S. Thienhaus, J. Klein, L. Alff, R. Gross
   Physica **C 350**, 237 (2001).
10. **Phase sensitive measurements of the superconducting order parameter in hole and electron doped HTS**
    L. Alff, B. Welter, S. Kleefisch, A. Marx, R. Gross
    Physica **C 357–360**, 309 (2001).
11. **Role of ion beam etching in the fabrication of ramp–type junctions**
    U. Schoop, M. Schonecke, S. Thienhaus, S. Schymon, L. Alff, and R. Gross
    Physica **C 351**, 200 (2001).
12. **Transport and Noise Characteristics of Submicron High Temperature Superconductor Grain Boundary Junctions**
    F. Herbstritt, T. Kemen, A. Marx, R. Gross
    Appl. Phys. Lett. **78**, 955 (2001).
13. **Thermal Conductivity and Thermal Hall Effect in Bi– and Y–based High–T$_c$ Superconductors**
    B. Zeini, A. Freimuth, B. Büchner, M. Galffy, R. Gross, A. P. Kampf, M. Gläser, G. Müller–Vogt, L. Winkler
    European Phys. J. **B 20**, 189 (2001).

14. **Comparison of Josephson vortex flow transistors with different gate line configurations**
J. Schuler, S. Weiss, T. Bauch, A. Marx, D. Koelle, and R. Gross
Appl. Phys. Lett. **78**, 1095 (2001).
15. **Possible Pseudogap Behavior of Electron Doped High–Temperature Superconductors**
S. Kleefisch, B. Welter, M. Naito, A. Marx, L. Alff, R. Gross,
Phys. Rev. **B 63**, Rapid Com. 100507 (2001).
16. **Canted Antiferromagnetism in $La_{0.94}Sr_{0.06}MnO_3$**
J. Geck, M. Hücker, B. Büchner, R. Gross, L. Pinsard–Gaudart, A. Revcolevschi,
Phys. Rev. **B 64**, 144430 (2001).
17. **Pseudo gap like tunneling spectra in electron doped HTS**
L. Alff, S. Kleefisch, B. Welter, A. Marx, R. Gross, M. Naito
Physica **C 357–360**, 134 (2001).
18. **Magnetotransport studies and mechanism of Ho and Y doped $La_{0.7}Ca_{0.3}MnO_3$**
V. Ravindranath, M. S. Ramachandra Rao, G. Rangarajan, Yafeng Lu, J. Klein, R. Klingeler, S. Uhlenbruck, B. Büchner, R. Gross
Phys. Rev. **B 63**, 184434 (2001).
19. **Spin dependent transport in the double perovskite Sr_2CrWO_6**
J. B. Philipp, J. Klein, D. Reisinger, M. Schonecke, A. Marx, A. Erb, L. Alff, R. Gross
Appl. Phys. Lett. **79**, 3654–3656 (2001).
20. **Direct observation and anisotropy of the contribution of gap nodes in the low–temperature specific heat of** $YBa_2Cu_3O_7$
Y. Wang, B. Revaz, A. Erb, A. Junod,
Phys. Rev. **B 63**, 094508 (2001).
21. **Onset of dielectric modes at 110 K and 60 K due to local lattice distortions in nonsuperconducting** $YBa_2Cu_3O_{6.0}$ **crystals**
Z. Zhai, P.V. Parimi, J.B. Sokoloff, S. Sridhar, A. Erb,
Phys. Rev. **B 63**, 092508 (2001).
22. **Nonlinear conductivity in the ground state of α–$(BEDT–TTF)_2KHg(SCN)_4$**
M. Basletic, B. Korin–Hamzic, M.V. Kartsovnik, H. Müller,
Synthetic Metals **120**, 1021–1022 (2001).
23. **Orbital effect of a magnetic field on the low–temperature state in the organic metal α–$(BEDT–TTF)_2KHg(SCN)_4$**
D. Andres, M.V. Kartsovnik, W. Biberacher, H. Weiss, E. Balthes, H. Müller N. Kushch,
Phys. Rev. **B 64**, 161104 (2001).
24. **Dynamics of individual traps in submicron high–temperature superconductor grain boundary junctions**
A. Marx, T. Kemen, L. Alff, R. Gross
Proceedings of the *16th International Conference on Noise in Physical Systems and 1/f Fluctuations ICNF 2001*, Gainesville, Florida, G. Bosman (ed.) World Scientific 2001, pp. 47–50.
25. **Magnetic origin of the charge order transition in lightly doped $La_{1-x}Sr_xMnO_3$**
R. Klingeler, J. Geck, R. Gross, L. Pinsard–Gaudart, A. Revcolevschi, S. Uhlenbruck, B. Büchner,
Phys. Rev. **B**, submitted for publication (01/2001).
26. **Microstructure and magnetoresistance of epitaxial films of the layered perovskite $La_{2-2x}Sr_{1+2x}Mn_2O_7$ ($x = 0.3$ and 0.4)**
J. B. Philipp, J. Klein, Ch. Recher, T. Walter, W. Mader, M. Schmid, R. Suryanarayanan,L. Alff, R. Gross,
Phys. Rev. **B**, submitted for publication (03/2001).
27. **Structure and Transport Properties of Coherently Strained $La_{2/3}Ca_{1/3}MnO_3$/$SrTiO_3$ Superlattices**
Yafeng Lu, J. Klein, F. Herbstritt, L. Alff, R. Gross

Europ. Phys. J. **B**, submitted for publication (04/2001).

28. **Anisotropic transport properties of biaxially strained thin films of doped manganites**
J. Klein, J. B. Philipp, G. Carbone, A. Vigliante, L. Alff, R. Gross
Phys. Rev. Lett., submitted for publication (07/2001).
29. **Local magnetic order in manganite thin films studied by 1/f noise measurements**
A. Marx, J. B. Philipp, P. Reutler, A. Bensaid, F. Herbstritt, C. Höfener, R. Gross
Proceedings of the *16th International Conference on Noise in Physical Systems and 1/f Fluctuations ICNF 2001*, Gainesville, Florida, G. Bosman (ed.) World Scientific 2001, pp. 31–34.
30. **Growth and magnetotransport properties of epitaxial films of the layered perovskite $La_{2-2x}Sr_{1+2x}Mn_2O_7$**
J. B. Philipp, J. Klein, Ch. Recher, L. Alff, R. Gross
Phys. Stat. Sol., accepted for publication (2001).
31. **Growth and structure of coherently strained films of doped manganites**
J. Klein, J. B. Philipp, D. Reisinger, L. Alff, R. Gross
Phys. Stat. Sol., accepted for publication (2001).
32. **Ultra violet light assisted oxygenation process for sub–micron $YBa_2Cu_3O_{7-\delta}$ thin film devices**
F. Herbstritt, Th. Kemen, A. Marx, R. Gross
J. Appl. Phys., submitted for publication (10/2001).
33. **Anisotropy of the low–field critical point of the melting line in twinned YBCO single crystals**
J. Figueras, T. Puig, X. Obradors, A. Erb, E. Walker,
Phys. Rev. **B**, submitted for publication (2001).
34. **Anisotropic behaviour of the melting line and the low critical field in YBCO**
J. Figueras, T. Puig, X. Obradors A. Erb, E. Walker,
Physica **C**, accepted for publication (2001).
35. **The oxygen isotope effect in the a–b–plane reflectance of underdoped** $YBa_2Cu_3O_7$
N.L. Wang, T. Timusk, J.P. Franck, P. Schweiss, M. Bradon, A. Erb,
Phys. Rev. Lett., submitted for publication (2001).
36. **Resistivity and Magnetization of Ho and Y Doped $La_{0.7}Ca_{0.3}MnO_3$**
M. S. Ramachandra Rao, V. Ravindranath, Yafeng Lu, J. Klein, R. Klingeler, S. Uhlenbruck, B. Büchner, R. Gross
J. Magn. Magn. Mat., submitted for publication (2001).

Completed and ongoing Diploma and Ph.D. Theses

Ph.D. Theses

1. **Strained Superlattices and Magnetic Tunnel Junctions Based on Doped Manganites**
   Yafeng Lu, July 2001.
2. **Epitaktische Heterostrukturen aus dotierten Manganaten**
   Jürgen Klein, October 2001.
3. **Mesoskopische Normalleiter–Supraleiter Systeme**
   Thomas Kemen, December 2001.
4. **Ladungstransport und Rauschen in submikrometer-strukturierten Korngrenzenkontakten aus $YBa_2Cu_3O_{7-\delta}$**
   Frank Herbstritt, December 2001.
5. **Ramp Junctions Based on Superconducting and Magnetic Transition Metal Oxides**
   Mitja Schonecke, since December 1998.
6. **Spin–dependent Transport in Mesoscopic Metallic Systems**
   Jürgen Schuler, since December 1998.
7. **Electronic Raman Scattering on High Temperature Superconductors**
   Francesca Venturini, since October 1998.
8. **Spin Electronics Based on Ferromagnetic Oxides**
   Jan Boris Philipp, since April 2000.
9. **Symmetry of the Order Parameter and Pseudo–gap Behavior of High Temperature Superconductors**
   Bettina Welter, since August 2000.
10. **Electronic and Magnetic Properties of Organic Metals and Superconductors**
    Dieter Andres, since September 2000.
11. **Physics and Growth Mechanisms of Heteroepitaxial Layer Structures Based on Oxid Materials**
    Daniel Reisinger, since October 2000.
12. **Nuclear Magnetic Resonance and Magnetization Measurements on Solid ^{3}He**
    Carmen Millan–Chacarteou, since November 2001.

Diploma Theses

1. **NMR–Experiments on Solid ^{3}He**
   Frank Deppe, since February 2001.
2. **Tunneling Spectroscopy on Electron–doped High Temperature Superconductors**
   Yoshiharu Krockenberger, since July 2001.
3. **Electrical Transport Measurements on Coupled Quantum Dots**
   Jan Weber, since September 2001.
4. **Magnetotransport Properties of Epitaxial Manganite Thin Films**
   Barbara Blass, since October 2001.

Research Projects and Cooperations

Many of our research projects have benefited from the collaboration with external groups via joint research projects, individual collaborations, exchange programs and visitors. Several collaborations are based on joint projects which are financially supported by different organizations (see list below). A large number of collaborations also exist with several universities and other research institutions without direct financial support. These are also listed below.

Funded Projects

Deutsche Forschungsgemeinschaft (DFG)

1. Elektronenmikroskopische Analyse von Defektstrukturen, lokalen strukturellen Eigenschaften und Ladungsordnungsphänomenen in dotierten Manganaten
   (R. Gross, Az. GR 1132/3-1)
   Partner: Universität Bonn

2. Untersuchung des niederfrequenten $1/f$ Rauschens in Josephson–Kontakten aus Hochtemperatur–Supraleitern zur Charakterisierung elementarer Rauschzentren und Klärung der Transportmechanismen
   (A. Marx und R. Gross, Az. Ma 1953/1-1+2)

3. Vortex–Antidot–Wechselwirkung in dünnen Schichten aus Hochtemperatur–Supraleitern
   (R. Wördenweber, R. Gross und R. P. Hübener, Az. GR 1132/11-1, -2)

4. Heteroepitaxie von Übergangsmetalloxiden
   (L. Alff und R. Gross, Az. Al 560/1-1+2)

5. Kristalline organische Metalle und Supraleiter: Synthese und elektronische Eigenschaften, gefördert von der DFG und der russischen Stiftung für Grundlagenforschung (RFFI)
   (W. Biberacher, WMI, und N. Kushch, Institut für Probleme der chemischen Physik, Cernogolovka)

6. Untersuchung des Wechselwirkungspotentials in Kuprat–Supraleitern durch Vergleich verschiedener spektroskopischer Methoden
   (R. Hackl, Az. HA 2071/2-1+2)

Bundesminister für Bildung, Wissenschaft, Forschung und Technologie (BMBF)

1. Verbundprojekt: Ultra–schnelle und ultra–verlustarme Informationstechnik–Komponenten
   Teilvorhaben: Transport– und Rauscheigenschaften von Nano–SiGe–Bauelementen
   (R. Gross und A. Marx, Förderkennzeichen: 13N7902)
   Partner: DaimlerChrysler AG, AMO GmbH.

2. Wissenschaftlich–Technologische Zusammenarbeit mit Indien (Indian Institute of Technology, Madras)
   (R. Gross, Projektkennzeichen: IND 01/009)
   Partner: M. S. R. Rao, Indian Institute of Technology, Madras, India.

3. Verbundprojekt: Spinelektronik und Spinoptoelektronik in Halbleitern
   Teilprojekt: Ferromagnetische metallische Oxide mit hoher Spinpolarisation für die Spinelektronik
   (R. Gross, Förderkennzeichen: 13010259)
   Partners: Universities of Würzburg, Hamburg, Regensburg, Hannover and Marburg, Max–Planck–Institute Halle, Siemens AG, Infineon Technologies, Aixtron GmbH.

European Union

1. Research and Training of Young Researchers on the Magnetic Properties of ^{3}He by Means of Neutron Diffraction
   (E. Schuberth; coordination: Dr. Konrad Siemensmeyer, Hahn–Meitner Institut Berlin GmbH)
   Partners: Hahn–Meitner Institut, Berlin, Univ. of Florida, Royal Holloway College, London, Univ. Liverpool, CNRS, Grenoble and Univ. Paris, Saclay.

2. European Science Foundation Network *"Vortex Matter at Extreme Scales and Conditions"*
   (R. Gross; coordination: Prof. Moshchalkov, Univ. Leuven)
   Partners: several european Universities and research facilities.

3. High Field Infrastructure Cooperative Network
   (W. Biberacher)
   Partners: in total 31 participants, coordination: CNRS Grenoble.

Deutscher Akademischer Austauschdienst (DAAD)

1. Projektbezogener Personenaustausch mit Ungarn
   (R. Hackl)
   Ungarische Akademie der Wissenschaften, Institut für Festkörperphysik und Optik, Prof. Istvan Tüttö

2. Projektbezogener Personenaustausch mit Italien, Vigoni–Programm
   (R. Hackl)
   Universita di Roma La Sapienza, Instituto Nazionale di Fisica della Materia, Prof. Paolo Calvani

3. Projektbezogener Personenaustausch mit Spanien, Aciones Integradas Hispano–Alemanas
   (A. Lerf)
   Centro de Investigaciones Cientificas "Isla de Cartuja", Universidad de Sevilla, Prof. Dr. Jose Luis Perez Rodriguez

Collaborations

Other collaborations without direct project funding involve:

- Technion, Israel (Prof. G. Koren, Dr. E. Polturak)
- NTT, Japan (Prof. Takayanagi, Dr. M. Naito)
- Tokyo Institute of Technology, Japan (Prof. M. Kawasaki, Prof. K. Koinuma)
- Materials Physics Laboratory, Helsinki University of Technology (Dr. Tero Heikkilä)

- Department of Condensed Matter Physics, The Weizmann Institute of Science, Israel (Dr. Moshe Schechter)
- Chalmers University of Technology, Gothenburg, Sweden (Dr. Z. Ivanov, Dr. P. Delsing)
- Ludwig–Maximilians–University Munich, Germany (Dr. F. Wilhelm)
- University of Tübingen, Germany (Prof. R. Kleiner, Prof. D. Kölle)
- Max–Planck Institut für Metallforschung, Stuttgart (Dr. P. Wochner, Dr. A. Vigliante)
- University of Leuven, Belgium (Dr. P. Wagner, Prof. V.V. Moshchalkov)
- Hungarian Academy of Sciences, Technische Universität Budapest, Budapest, Hungary (Prof. Dr. K. Kamaras, Dr. Attila Virosztek, Prof. Dr. A. Zawadowski)
- Eötvös Lorand University, Budapest, Hungary (Dr. I. Tüttö)
- Universitá di Roma ”La Sapienza”, Roma, Italy (Prof. Dr. Paolo Calvani)
- Institut für Experimentelle Physik, Slowakische Akademie der Wissenschaften, Kosice (Prof. K. Flachbart)
- Northwestern University Evanston, Illinois
- University of Florida
- Institute of Solid State Physics, Chernogolovka, Russia (Dr. R.P. Shibaeva, Prof. Dr. V. Ryazanov, Prof. Dr. Lev Vinnikov)
- Institute of Problems of Chemical Physics, Chernogolovka, Russia (Prof. Dr. O.A. Dyachenko)
- High–Magnetic–Field Laboratory, Grenoble, France (Dr. A.G.M. Jansen)
- National Pulsed–Magnetic–Field Facility, Toulouse, France (Dr. L. Brossard)
- B. Verkin Institute for Low Temperature Research and Engineering, Kharkov, Ukraine (Prof. V.G. Peschansky)
- Institute for Material Science, Barcelona, Spain (Prof. E. Canadell)
- Department of Chemistry, University of Cambridge, UK (Dr. Jacek Klinowski)
- Institut für Technologie Anorganischer Stoffe der TU Graz, Austria (Prof. Besenhard)
- University of Nantes, France (Prof. M. Danot)

Invited Conference Talks and Seminar Lectures

Lambert Alff

1. **Doping dependence of the symmetry of the superconducting order parameter in electron–doped high–temperature superconductors**
   21. – 24. 05, 2001
   Invited talk at the Minerva Workshop on „Advances in High Temperature Superconductivity, Ramat Gan, Israel.
2. **Tunneling effects in oxide grain boundary junctions: high–temperature superconductors and doped manganites**
   05. 09. 2001
   Seminar lecture, Chalmers University, Gothenburg, Sweden.
3. **Tunneling effects in oxide grain boundary junctions: high–temperature superconductors and doped manganites**
   06. 11. 2001
   Seminar lecture, University of Augsburg, Germany.
4. **Widerstand zwecklos: Hochtemperatur–Supraleiter im Kommen?!**
   07. 11. 2001
   Schülertag der Technischen Universität München.

Dieter Andres

1. **Einfluss von Magnetfeld und Druck auf den Ladungsdichtewellenzustand des organischen Metalls $\alpha - (\mathbf{BEDT-TTF})_2\mathbf{KHg(SCN)_4}$**
   29. 03. 2001
   65. Frühjahrstagung der DPG, Hamburg.
2. **Effect of high magnetic field and pressure on the charge density wave state of the organic metal $\alpha - (\mathbf{BEDT-TTF})_2\mathbf{KHg(SCN)_4}$**
   30. 04. – 14. 05. 2001
   School on "Trends in high magnetic field science", Institut d'Etudes Scientifiques de Cargese, Corse.

Werner Biberacher

1. **Magnetic torque studies on $\alpha - (\mathbf{BEDT-TTF})_2\mathbf{KHg(SCN)_4}$**
   05. 07. 2001
   Institute for Problems of Chemical Physics in Chernogolovka, Russia.
2. **Organic metals in high magnetic fields**
   07. 09. 2001
   Annual meeting of the High Field Infrastructure Cooperative Network (EU).

Dietrich Einzel

1. **Zur Strömung von flüssigem ^{3}He in Aerogel**
   29. 03. 2001
   invited talk at the 65. Frühjahrstagung der DPG, Hamburg.
2. **Liquid ^{3}He Aerogel: a Dirty Fermi Liquid**
   20. 06. 2001
   Ginzburg–Seminar/Journal Club der TUM.

Andreas Erb

1. **MgB_2 – a 39 K superconductor from the chemistry shelf**
   06. 06. 2001
   Ginzburg–Seminar/Journal Club der TUM.

Rudolf Gross

1. **Metallische Nanostrukturen – von den quantenmechanischen Grundlagen zur Nanoelektronik**
   12. 01. 2001
   Oberseminar des Center for Nanoscience der Ludwig–Maximilians–Universität München, Germany.
2. **Von der Elektronik zur Spintronik – können Spins unsere heutige Elektronik revolutionieren ?**
   13. 06. 2001
   Physikalisches Kolloquium der Fakultät für Physik, Universität Tübingen, Germany.
3. **Von der Elektronik zur Spintronik: Revolutionieren magnetische Materialien unsere heutige Elektronik ?**
   13. 06. 2001
   Physikalisches Kolloquium des Fachbereichs Physik und Geowissenschaften, Technische Universität Braunschweig, Germany.
4. **Von der Elektronik zur Spintronik – können Spins unsere heutige Elektronik revolutionieren ?**
   16. 07. 2001
   Kolloquium der Münchener Physiker, Ludwig–Maximilians–Universität München, Germany.
5. **Biaxial Strain Effects in Doped Manganites**
   R. Gross
   17. – 19. 09. 2001,
   Workshop on the Present and Future of Research in Manganites, Granada, Spain.
6. **Anisotropic Transport Properties in Biaxially Strained Thin Films of the Doped Perovskite Manganites**
   R. Gross
   27. – 28. 09. 2001
   8^{th} International Workshop on Oxide Electronics, Osaka, Japan.
7. **Manganite based thin films and heterostructures: strain effects, interfaces and magnetoelectronic devices**
   01. 10. 2001
   Correlated Electron Research Center, National Institute of Advanced Industrial Science and Technology (AIST), Tsukuba, Japan.
8. **Oxide Engineering using Laser Molecular Beam Epitaxy**
   02. 10. 2001
   NTT Basic Research Laboratories, Atsugi, Japan.
9. **Interface and Strain Effects in Doped Manganites**
   R. Gross
   07. – 10. 10. 2001,
   International Workshop 2001 on “Ordering Phenomena in Transition Metal Oxides”, Kloster Irsee, Germany.
10. **“Von der Elektronik zur Spintronik” oder “Als die Elektronen spinnen lernten”**
    17. 10. 2001
    Deutsches Museum, München, im Rahmen der Vortragsserie “Wissenschaft für Jedermann”

Rudolf Hackl

1. **Carrier dynamics in differently doped cuprates as observed by inelastic light scattering**
   14. – 17. 2. 2001
   Korrelationstage 2001, Max–Planck–Institut für die Physik komplexer Systeme Dresden, Germany.

2. **Raman–Untersuchung der verschiedenen Arten von Energielücken in Kupferoxid–Systemen**
   05. 02. 2001
   Max–Born–Institut, Berlin.
3. **Electronic anisotropies in cuprates: Raman results for a wide range of doping**
   23. 04. 2001
   Katholische Universität Leuven.
4. **Electronic anisotropies in cuprates: Raman results for a wide range of doping**
   28. 06. 2001
   Technische Universität Braunschweig.

Mark Kartsovnik

1. **Interlayer magnetoresistance in layered organic conductors**
   01. – 05. 09. 2001
   NATO Advanced Research Workshop "Molecular Low–Dimensional and Nanostructured Materials for Advanced Applications" (MMAA), Poznan, Poland.

Anton Lerf

1. **Feste Stoffe mit einstellbarer Dicke**
   09. 01. 2001
   Seniorenstudium an der Ludwig–Maximillians–Universität, München.
2. **Intercalation chemistry: history, topics and perspectives**
   17. 04. 2001
   Centro de ciencia de materiales de Sevilla, centro mixto CSIC–Universidad de Sevilla, Spain.
3. **Dye molecule intercalation compounds of 2H–TaS_2: electrointercalation and superconducting properties**
   05. 07. 2001
   Institute of Problems of Physical Chemistry, Russian Academy of Sciences, Chernogolovka, Russia.
4. **Mössbauer spectroscopic investigation of vermiculites from Andalusia (Spain)**
   24. – 26. 10. 2001
   XVI Reunión Científica de la Sociedad Espanola de Arcillas, SEA 2001, Beaza (Jaén).

Achim Marx

1. **Transport and Noise in Nanostructures**
   13. 01. 2001
   Sitzung der Kommission für Tieftemperaturforschung der Bayerischen Akademie der Wissenschaften, Garching.
2. **Transport and Noise in HTS Nanojunctions**
   01. 10. 2001
   Tagung *Kryoelektronische Bauelemente 2001*, Kerkrade, The Netherlands.
3. **Local magnetic ordering in manganite thin films studied by 1/f noise measurements**
   22. 10. 2001
   16th International Conference on Noise in Physical Systems and 1/f Fluctuations (ICNF) 2001, Gainesville, USA.
4. **Dynamics of individual traps in submicron high–temperature grain boundary junctions**
   22. 10. 2001
   16th International Conference on Noise in Physical Systems and 1/f Fluctuations (ICNF) 2001, Gainesville, USA

Karl Neumaier

1. **Spezifische–Wärme–Messungen an $YbRh_2(Si_{1-x}Ge_x)_2$ unter 100 mK – Probleme und Resultate**
   04. 12. 2001
   Max–Planck–Institut für Physik fester Stoffe, Dresden, Germany.

Matthias Opel

1. **Electronic and Phononic Properties in Superconducting and Antiferromagnetic Cuprates**
   25. 06. 2001
   Karl–Franzens–Universität, Graz, Austria.
2. **Electronic and Phononic Raman Scattering in Superconducting and Antiferromagnetic Cuprates**
   07. 09. 2001
   Max–Planck–Institut für Festkörperforschung, Stuttgart, Germany.

Erwin Schuberth

1. **Novel Magnetism in ^{3}He Nano–Clusters**
   08. 03. 2001
   Kolloqiumsvortrag am Max–Planck–Institut für die Chemie fester Stoffe, Dresden, Germany.

Kurt Uhlig

1. **^{3}He/^{4}He–Mischkühler mit closed–cycle–refrigerator–Vorkühlung**
   13. 01. 2001
   Kommissionssitzung, Walther–Meissner–Institut.

Francesca Venturini

1. **A wide–range doping study of Bi2212 in the superconducting state**
   11. 01. 2001
   Università di Roma ”La Sapienza”, Italia.

Seminars, Courses, Lectures and other Scientific Activities

Walther–Meissner Seminars

The Friday Seminar

1. **Ursprung der Pseudolücke in unterdotiertem YBaCuO: supraleitende Phasenfluktuationen**
   Dr. Christoph Meingast, IFP, Forschungszentrum Karlsruhe
   19. 01. 2001
2. **Kristallographische Ordnung: ein neuer Tuning–Parameter im Nicht–Fermi–Flüssigkeitssystem $UCu_{5-x}Pd_x$**
   Dr. Ernst–Wilhelm Scheidt, Institut f. Physik, Universität Augsburg
   05. 02. 2001
3. **Elementanalytik an Dünnschichtsystemen**
   Dr. Andreas Bergmaier, Beschleuniger–Labor, TU München
   09. 02. 2001
4. **Thermodynamic analysis of MBE growth of InGaAsN**
   Vladimir A. Odnoblyudov, Ioffe Institut, St. Petersburg, Russia
   22. 02. 2001
5. **EKG–Analyse bei Kammerflimmern: eine wertvolle Informationshilfe für den Notarzt?**
   Prof. Dr. Anton Amann, Institut für Allgemeine Anorganische und Theoretische Chemie und der Univ.–Klinik für Anaesthesie der Leopold–Franzens–Universität, Innsbruck, Austria
   27. 04. 2001
6. **Theoretische Beschreibung "hochkorrelierter" Systeme mittels LDA+U Rechnungen (Kuprate, FeAl, UX–Verbindungen)**
   Dr. Peter Blaha, Institut für Physikalische und Theoretische Chemie, Technische Universität, Wien, Austria
   04. 05. 2001
7. **Rauschen und Ladungstransport in Korngrenzenkontakten aus $YBa_2Cu_3O_{7-\delta}$ mit sub-μm–Abmessungen**
   Frank Herbstritt, II. Physikalisches Institut, Lehrstuhl Angewandte Physik, Universität zu Köln
   18. 05. 2001
8. **Dynamics of Nanostructured HTS Grain Boundary Josephson Junctions**
   Dr. Boris Chesca, Physikalisches Institut, Universität Tübingen
   18. 05. 2001
9. **Rauschexperimente mit mesoskopischen Leitern**
   Prof. Christoph Strunk, Institut für Experimentelle und Angewandte Physik, Univerisität Regensburg
   21. 05. 2001
10. **$Bi_2Sr_2CaCu_2O_{8+x}$ bicrystal c–axis twist Josephson junctions: A new phase–sensitive test of order–parameter symmetry**
    Prof. Richard A. Klemm, MPI für Physik komplexer Systeme, Dresden
    22. 05. 2001
11. **Magnetic Anisotropy of Layered Manganites $La_{2-2x}Sr_{1+2x}Mn_2O_7$ (x = 0.35, 0.45)**
    Dr. S. J. Oh, Korean Basic Science Institute, Taejeon, Korea.
    25. 05. 2001
12. **Josephson pi–junctions and their applications in digital and quantum logics**
    Prof. V. Ryazanov, Institute of Solid State Physics, Chernogolovka, Russia
    22. 06. 2001
13. **Teilchen–Loch–Kohärenz in unkonventionellen Supraleitern**
    Prof. Dr. Dierk Rainer, Universität, Bayreuth
    29. 06. 2001
14. **Flux–Flow Widerstand in Supraleitern: Was ist neu in den Kupraten?**
    Prof. Dr. Rudolf P. Hübener, Universität Tübingen
    06. 07. 2001
15. **Interplay of superconductivity and magnetism in the borocarbide compound $TmNi_2B_2C$**
    Nicolas Luchier, CNRS Grenoble, France
    10. 07. 2001

16. **Compacted metal powders at very low temperatures: superconductivity and magnetic properties**
    PD Dr. Reinhard König, Physikalisches Institut, Universität Bayreuth
    13. 07. 2001
17. **Korrekturen zum orthodoxen Verhalten von Einzelladungstransistoren mit kleinen Tunnelwiderständen**
    Dr. Roland Schäfer, Institut für Festkörperphysik, Forschungszentrum Karlsruhe
    20. 07. 2001
18. **Angle–resolved photoemission spectroscopy in high–temperature superconductors**
    Prof. Zhi–Xun Shen, Departments of Physics and Applied Physics, Stanford University, USA
    20. 07. 2001
19. **Giant Thermoelectric Effect in Superconductors**
    Prof. Dr. G.F. Zharkov, P. N. Lebedev Physical Institute, Russian Academy of Sciences, Russia
    24. 07. 2001
20. **Evidence for an *id* component in the superconducting gap of overdoped $(Y_{1-x}Ca_x)Ba_2Cu_3O_7$ thin films**
    Dr. Eli Faber, School of Physics and Astronomy, Tel Aviv University, Israel
    11. 10. 2001
21. **Transport through superconductor/magnetic dot/superconductor structures**
    Prof. Dr. Mikael Fogelström, Institute for Theoretical Physics, Chalmers and Göteborg University
    12. 10. 2001
22. **Far–infrared ellipsometry on cuprate high–T_c superconductors – new results concerning the in–plane dielectric response**
    Dr. Christian Bernhard, Max–Planck–Institut für Festkörperphysik, Stuttgart
    19. 10. 2001
23. **Ferromagnet/Halbleiter–Hybridstrukturen: Theorie und Experiment**
    Dr. Dirk Grundler, Universität Hamburg
    26. 10. 2001
24. **Flux injection in annular junctions and vortex qubits**
    Prof. Dr. Alexey Ustinov, Physikalisches Institut, Universität Erlangen–Nürnberg
    09. 11. 2001
25. **Unconventional metal–insulator transition in Bi2212**
    Francesca Venturini, Walther–Meissner-Institut
    16. 11. 2001
26. **Pulsrohrkühler, Funktionsweise und Stand der Technik**
    Dr. Albert Hofmann, Institut für Technische Physik, Forschungszentrum Karlsruhe
    23. 11. 2001
27. **Tunnelgekoppelte Quantenpunktsysteme und ihre kapazitive Wechselwirkung**
    Dipl.–Phys. Andreas Klaus Hüttel, Sektion Physik, LMU München
    30. 11. 2001
28. **AC Josephson effect and shot noise in superconducting d–wave junctions**
    Dr. Juan Carlos Cuevas, Institut für Theoretische Festkörperphysik, Universität Karlsruhe
    07. 12. 2001
29. **Superconducting quantum bits: Introduction, coherence properties and the measurement process**
    Dr. Frank Wilhelm, Lehrstuhl für Theoretische Festkörperphysik, Sektion Physik der LMU München
    14. 12. 2001

The Tuesday Seminar

1. **Raman effect in HTc superconductors**
   M. Opel
   24.04. 2001
2. **Transport and Noise in Nanostructures**
   A. Marx
   22.05.2001
3. **Drehmomentmessungen an organischen Metallen**
   W. Biberacher

05.06.2001

4. **Elektrochemische Präparation von Festkörpern**
   A. Lerf
   19.06.2001
5. **Angle–dependent magnetoresistance oscillations in layered metals**
   M. Kartsovnik
   03.07.2001
6. **Growth of Bulk Materials and Single Crystals**
   A. Erb
   17.07.2001
7. **Facilities and applications at millikelvin temperatures**
   E. Schuberth
   31.07.2001
8. **Dünnschichtepitaxie und Transporteigenschaften neuer Materialien für die Magnetoelektronik**
   D. Reisinger
   11.09.2001
9. **Heteroepitaxie von Übergangsmetalloxiden**
   M. Schonecke
   18.09.2001
10. **GUT of unconventional superconductivity**
    D. Einzel
    02.10.2001
11. **Electronic Raman scattering in cuprates**
    F. Venturini
    16.10.2001
12. **Vortex structure in superconductors**
    L. Ya Vinnikov
    23.10.2001
13. **Rückblick und Ausblick der Detektorentwicklung – I**
    E. Umlauf
    30.10.2001
14. **Interlayer conductivity in quasi–2D compounds**
    P. Grigoriev
    06.11.2001
15. **Tunnelmessungen an $Pr_{2-x}Ce_xCuO_4$ im Magnetfeld**
    B. Welter
    13.11.2001
16. **Rückblick und Ausblick der Detektorentwicklung – II**
    E. Umlauf
    20.11.2001
17. **Präparation und erste physikalische Eigenschaften von Sr_2CrWO_6**
    A. Erb, B. Philipp
    27.11.2001
18. **Physical properties resulting from an effective change in space dimensionality for electrons in magnetic fields**
    A. Lebed
    04.12.2001
19. **Herstellung metallischer Nanostrukturen**
    J. Schuler
    11.12.2001
20. **Quanteninformationsverarbeitung mit Festkörpern**
    R. Gross
    18.12.2001

Lectures

Dietrich Einzel

WS 2000/2001	Mathematische Methoden der Physik 1
WS 2000/2001	Übungen zu Mathematische Methoden der Physik 1
WS 2000/2001	Einführung in die Supraleitung (mit E. Schuberth)
SS 2001	Mathematische Methoden der Physik 2
SS 2001	Übungen zu Mathematische Methoden der Physik 2
SS 2001	Ausgewählte Kapitel aus der Tieftemperaturphysik (mit E. Schuberth)
WS 2001/2002	Mathematische Methoden der Physik 1
WS 2001/2002	Übungen zu Mathematische Methoden der Physik 1
WS 2001/2002	Supraleitung und Suprafluidität: Theorie

Rudolf Gross

WS 2000/2001	Magnetoelektronik I (Magnetoelectronics I)
SS 2001	Magnetoelektronik II (Magnetoelectronics II)
WS 2001/2002	Experimentalphysik III – Optik, Quantenphänomene und Aufbau der Atome (Experimental Physics III)
WS 2001/2002	Übungen zu Experimentalphysik III (mit L. Alff)

Anton Lerf

SS 2001	Festkörperchemie (mit K. Köhler)
WS 2001/2002	Angewandte Anorganische Chemie II
WS 2001/2002	Grenzprobleme der Naturwissenschaften

Erwin Schuberth

WS 2000/2001	Experimentalphysik II für Lehrberufe
WS 2000/2001	Übungen zu Experimentalphysik II für Lehrberufe
WS 2000/2001	Einführung in die Supraleitung (mit D. Einzel)
SS 2001	Experimentalphysik I für Lehrberufe
SS 2001	Übungen zu Experimentalphysik I für Lehrberufe
SS 2001	Ausgewählte Kapitel aus der Tieftemperaturphysik (mit D. Einzel)
WS 2001/2002	Experimentalphysik II für Lehrberufe
WS 2001/2002	Übungen zu Experimentalphysik II für Lehrberufe

Organization of Conferences

Summer School on *"Neutron Scattering from Solid ^{3}He"*
Frauenchiemsee, Germany
August 27 – 31, 2001.

Staff of the Walther–Meissner Institut

Director
Prof. Dr. Rudolf Gross

Technical Director
Dr. Karl Neumaier

Administration/Secretary's Office
Jutta Laaser
Emel Dönertas

Scientific Staff
Dr. habil. Lambert Alff
Dr. Werner Biberacher
Dr. habil. Dietrich Einzel
Dr. habil. Andreas Erb
Dr. habil. Rudi Hackl
Dr. Mark Kartsovnik
Dr. habil. Anton Lerf
Dr. Achim Marx
Dr. Matthias Opel
Dr. Christian Probst
Dr. habil. Erwin Schuberth
Dr. Kurt Uhlig
Dr. habil. Edgar Umlauf
Dipl.–Phys. Dieter Andres
Dipl.–Phys. Frank Herbstritt
Dipl.–Phys. Thomas Kemen
Dipl.–Phys. Carmen Millan-Chacarteou
Dipl.–Phys. Boris Philipp
Dipl.–Phys. Daniel Reisinger
Dipl.–Phys. Mitja Schonecke
Dipl.–Phys. Jürgen Schuler
Dipl.–Phys. Francesca Venturini
Dipl.–Phys. Bettina Welter

Technical Staff
Joachim Geismann
Gabrielle Görblich
Ulrich Guggenberger
Dieter Guratzsch
Hermann Hagn
Wolfgang Hehn
Julius Klaus
Robert Müller
Roman Müller
Jan Naundorf
Georg Nitschke
Walter Nitschke
Christian Reichlmeier
Harald Schwaiger
Helmut Thies
Siegfried Wanninger

Assistants
Ingrid Freimuth
Sybilla Plöderl
Gülcay Kursat

Permanent Guests
Prof. Dr. B. S. Chandrasekhar
Dr. Robert Doll
Prof. Dr. Schöllhorn

Guest Researchers

1. Prof. Dr. B.S. Chandrasekhar
   permanent guest
2. Dr. Robert Doll
   permanent guest
3. Prof. Dr. Schöllhorn
   permanent guest
4. Dr. Qing–ming Zhang, Nanjing University, Nanjing, China
   22. 10. 2000 – 31. 12. 2001
5. Dr. Attila Virosztek, Central Research Institute for Solid State Physics and Optics, Hungarian Academy of Sciences, Technische Universität Budapest, Budapest, Hungary
   17. 05. – 25. 05. 2001, 12. 11. – 19. 11. 2001
6. Prof. Dr. K. Kamaras, Central Research Institute for Solid State Physics and Optics, Hungarian Academy of Sciences, Technische Universität Budapest, Budapest, Hungary
   22. 10. – 27. 10. 2001
7. Prof. Dr. A. Zawadowski, Technische Universität Budapest, Budapest, Hungary
   01. 07. – 31. 07. 2001
8. Dr. I. Tüttö, Central Research Institute for Solid State Physics and Optics, Eötvös Lorand University, Budapest, Hungary
   01. 07. – 31. 07. 2001
9. Prof. Dr. Juan Poyato Ferrera, Instituto de Ciencia de Materiales de Sevilla, Sevilla, Spanien
   06. 07. – 07. 09. 2001
10. Prof. Dr. Jose Luis Perez Rodriquez und Prof. Dr. Juan Poyato Ferrera, Instituto de Ciencia de Materiales de Sevilla, Sevilla, Spanien
    02. 12. – 07. 12. 2001
11. Dr. Luis Perez Maqueda, Instituto de Ciencia de Materiales de Sevilla, Sevilla, Spanien
    17. 09. – 12. 10. 2001
12. Dr. F. Borondics, Central Research Institute for Solid State Physics and Optics, Budapest, Hungary
    19. 11. – 30. 11. 2001
13. Pavel Grigoriev, Landau Institute for Theoretical Physics, Chernogolovka, Russia
    19. 03. – 06. 04. 2001
14. Dr. Sergei Pesotskii, Institut für Probleme der Chemischen Physik, Chernogolovka
    07. 11. – 18. 12. 2001
15. Dr. Dirk Manske, Institut für Theoretische Physik, Freie Universität Berlin
    07. 03. – 11. 03. 2001
16. Prof. Dr. Paolo Calvani, Universitá di Roma ”La Sapienza”, Roma, Italy
    29. 11. – 02. 12. 2001
17. Dipl.-Phys. Andrea Lucarelli, Università di Roma La Sapienza, Roma, Italy
    02. 04. – 06. 04. 2001
18. Dipl.-Phys. Michele Ortolani, Università di Roma La Sapienza, Roma, Italy
    29. 11. – 02. 12. 2001
19. Dr. Alexei Kovalev, Institut für Festkörperphysik, Chernogolovka
    02. 04. – 02. 05. 2001
20. Balazs Borda, Technische Universität Budapest, Budapest, Hungary
    01. 07. – 31. 07. 2001

21. Prof. Dr. A. Janossy, Technische Universität Budapest, Budapest, Hungary
    01. 02. – 05. 02. 2001
22. Prof. Dr. P. Capkova, Department of Chemical Physics and Optics, Karls-Universität, Prag
    04. 12. – 09. 12. 2000
23. Dr. A. Lebed, Landau Institute for Theoretical Phycics, Chernogolovka, Russia
    21. 11. 2001 – 21. 12. 2001
24. Prof. Dr. Gely Zharkov, Lebedev Physical Institute, Russian Academy of Sciences, Moscow, Russia
    01. 06. – 31. 07. 2001
25. Prof. Dr. V. Ryazanov, Institute of Solid State Physics, Chernogolovka, Russia
    15. 06. – 30. 06. 2001
26. Prof. Dr. Lev Vinnikov, Institute of Solid State Physics, Chernogolovka, Russia
    01. 10. – 31. 10. 2001
27. Prof. Dr. O.A. Dyachenko, Institute of Problems of Chemical Physics, Chernogolovka, Russia
    03. 08. – 09. 08. 2001

Commission for Low Temperature Physics

Members of the Commission for Low Temperature Physics of the Bavarian Academy of Sciences:

Kaiser, Wolfgang, Leiter (Technische Universität München)
Brenig, Wilhelm, stellv. Leiter (Technische Universität München)
Landwehr, Gottfried (Universität Würzburg)
Hänsch, Theodor (Max-Planck Institut für Quantenoptik, Garching)
Koch, Frederick (Technische Universität München)
Kotthaus, Jörg Peter (Ludwig-Maximilians-Universität München)
Rainer, Dierk (Universität Bayreuth)
Renk, Karl Friedrich (Universität Regensburg)
Schwoerer, Markus (Universität Bayreuth)